DESIGN AND CHARACTERIZATION OF A MICROFLUIDIC FLOW CYTOMETER

Joshua K. Herr

A dissertation submitted to the faculty of the University of North Carolina at Chapel Hill in partial fulfillment of the requirements for the degree of Doctor of Philosophy in the Department of Chemistry.

Chapel Hill
2010

Approved by:

Professor J. Michael Ramsey

Professor James Jorgenson

Professor Mark Schoenfisch

Professor Norman Sharpless

Professor Glenn Walker

© 2010
Joshua K. Herr
ALL RIGHTS RESERVED

ABSTRACT

Joshua K. Herr

DESIGN AND CHARACTERIZATION OF A MICROFLUIDIC FLOW CYTOMETER

(Under the direction of J. Michael Ramsey)

The development and characterization of a microfluidic flow cytometer is described in this dissertation for rapid, inexpensive fluorescence and scatter based cellular enumeration for biomedical diagnostic and monitoring applications. Microfluidic cytometry enables a portable, economical platform for performing point-of-care cellular assays that are impractical with large conventional flow cytometry systems. Microchips were fabricated from glass using standard photolithography and wet chemical etching techniques. These chips were used in conjunction with static optical and electronic components to construct a robust instrument capable of accepting disposable microchips.

Flow cytometry measurements on-chip have demonstrated cellular analysis at rates greater than 2 kHz using vacuum driven flow, and positive pressure driven flow cytometry has been performed to measure cells at 12 kHz. Measurement precision has been investigated using commercially available calibration beads, and results demonstrate that the precision of chip based cytometry measurements is close to that seen using conventional instrumentation.

Cell discrimination based on immunophenotyping has been demonstrated in mixtures of cultured cells, peripheral blood mononuclear cells, and whole blood to

demonstrate the applicability of this instrument for clinical cellular diagnostic and monitoring applications. Comparison studies have been performed using conventional cytometry instrumentation to assess the accuracy of our microfluidic system for immunophenotyping applications.

Efforts have also been made to incorporate erythrocyte lysis on-chip in order to rapidly analyze whole blood in an automated fashion. Chemical erythrocyte lysis followed by leukocyte cytometry has been integrated on a single monolithic device to demonstrate the ability to accurately measure cell subtype ratios from a whole blood sample while reducing off-chip sample processing steps. Further, applications in blood dosimetry are described to reveal potential advantages of performing rapid blood cell counts for therapeutic monitoring and bioterrorism applications using only a fingerstick of whole blood.

The technology described in this dissertation may be applied to numerous applications requiring the measurement of relative cell populations from biological fluids. Further development and optimization of this instrument has the potential to increase the accessibility of clinical cellular analyses in resource poor settings by providing rapid, low-volume, inexpensive clinical testing at the point-of-care.

For Mom, Dad, Nat, and Sandy and Philip Weissman

ACKNOWLEDGEMENTS

I cannot begin to express how grateful I feel for having the help, advice, and support from so many people who have influenced me over the years and helped me to get to this point. I first would like to acknowledge Dr. Ramsey who has been very supportive of my work while allowing me to independently pursue my experimental curiosities throughout my graduate school career. The advice and guidance I have received from him over the past 5 years have helped me greatly both in my graduate studies and in the alignment of my professional goals. I have also received a great deal of help from Jean Alarie over the years, and I greatly appreciate his support and admire his dedication to helping everyone in our group with their issues while maintaining our smoothly running research lab. Others in the Ramsey group including Dr. Kevin Braun, Dr. Scott Mellors, and Dr. Hamp Henley have been great assets throughout my graduate career, and I appreciate both their friendship and their willingness to assist me whenever I asked. I am also very appreciative of the help I have received by Jeff SooHoo and Soren Johnson in the design, preparation, and execution of our specific projects.

My time at the University of Florida was very influential in my decision to pursue a graduate degree in chemistry. I first would like to acknowledge my Instrumental Analysis instructor Dr. Kathryn Williams whose grueling course quickly drew me to analytical chemistry, and whose kindness and useful discussions helped me to determine

my path towards a graduate degree in chemistry. I also had the opportunity to perform undergraduate research in the group of Professor Weihong Tan. Dr. Tan provided me with an excellent opportunity to make an impact in his group in a short amount of time, and I am grateful for the opportunity to work for him. Two members of the Tan group, Dr. James Yang and Dr. Steven Suljak were particularly helpful during my time as an undergraduate researcher. Both James and Steve had a significant impact on my development as a scientist, and I am glad to have had the opportunity to work with them as I learned a great deal about designing experiments from them.

I am most grateful for the love and support given to me by my family. My mom has always been my biggest supporter, and her kindness, tireless work ethic, and eternal motivation to help others has by far been my biggest inspiration. I am also grateful for the help and advice provided by my dad over the years, who is always equipped with a practical solution for any occasion. I must also thank my grandmother Sandy and late grandfather Philip for their role in forming the man I am today, and whose love and support drive me to succeed in all of my pursuits. Lastly I want to thank the love of my life, my wife Natalie, who has supported me as both my biggest fan and my best friend. There is no way I could have done this without her, and I cannot begin to explain how much it means to have her by my side.

TABLE OF CONTENTS

Page

LIST OF FIGURES

LIST OF ABBREVIATIONS

ADC	analog/digital converter
AF488	AlexaFluor 488
CCD	charge coupled device
CD	cluster of differentiation
CFD	computational fluid dynamic
cm	centimeter
Cs	Cesium
CV	coefficient of variation
DNA	deoxyribonucleic acid
EDTA	etethylenediaminetetraacetic acid
FACS	fluorescence activated cell sorting
FADU	fluorometric analysis of DNA unwinding
FISH	fluorescence in-situ hybridization
FITC	fluorescein isothiocyanate
fsc	forward scatter
Gy	grey
HIV	human immunodeficiency virus
Hz	hertz
kHz	kilohertz
LED	light emitting diode

m	meter
mm	millimeter
MHz	megahertz
min	minute
mL	milliliter
mm	millimeter
mW	milliwatt
MW	molecular weight
NA	numerical aperture
nm	nanometer
PBM	peripheral blood mononuclear
PBMC	peripheral blood mononuclear cell
PBS	phosphate buffered saline
PDMS	polydimethylsiloxane
PE	phycoerythrin
PEEK	poly ether ether ketone
PEG	polyethylene glycol
PMT	photomultiplier tube
psi	pounds per square inch
QD	quantum dot
RNA	ribonucleic acid
s	second
SB	sheath buffer port

SC	sample cell port
ssc	side scatter
SW	sample waste port
TBI	total body irradiation
TDT	terminal deoxynucleotidyl transferase
µm	micrometers
UV	ultravoilet

LIST OF SYMBOLS

a	channel radius
d	channel depth
∇	gradient
E	electric field vector
f	focal length
η	viscosity
g	acceleration due to gravity
L	channel length
λ	wavelength
M^2	quality factor
p	pressure
Q	volumetric flow rate
Q_C	cell solution flow rate
Q_S	sheath buffer flow rate
ρ	fluid density
v	velocity
w	channel width
w_F	focused beam radius
w_L	radius of the beam at the laser output

CHAPTER 1:

FOUNDATIONS FOR FLOW CYTOMETRY BASED ON MICROFLUIDIC TECHNOLOGY

1.1 Introduction

Efforts to develop and commercialize miniaturized instrumentation for medical diagnostics have steadily increased over the past decade. The aim is to produce devices that have similar performance features (sensitivity, accuracy, and reproducibility) as their full-scale laboratory counterparts but, in addition to providing rapid results, are more economical and robust. The efforts are driven in part by trends toward personalized medicine where timely results are desired at the point of care for disease state or therapeutic regime monitoring. Small, relatively inexpensive devices that may be used outside standard laboratory settings also have the potential to increase diagnostic and screening capabilities in rural and underdeveloped areas, greatly enhancing healthcare in those regions. Furthermore, if rapid, inexpensive assays were available as alternatives to expensive screening methods they would be more widely employed, leading perhaps to more favorable medical outcomes.

Accessibly priced personal assay kits that test for pregnancy, fertility, blood glucose, HIV, illicit drugs, and other disorders have been readily adopted and

incorporated into standard practice throughout the world. Point-of-care devices for simple blood chemistry testing and immunoassays have also been commercialized.[1,2] Similar devices for diagnosis and monitoring of more complex diseases such as autoimmune disorders and specific cancers are needed. Assays for these diseases typically require the measurement of multiple parameters to obtain useful clinical information[3] and consequently are more challenging to develop as point-of-care tests. Trained pathologists commonly perform these complex assays, but there are a few examples of simple, inexpensive, multi-parameter assays for the diagnosis and monitoring of disease states that can be performed easily by nonprofessionals. Continued focus on the development of these assays will escalate the drive towards personalized medicine and greatly improve accessibility to these types of medical tests in resource-limited regions.

One of the first steps in the development of a point-of-care, multi-parameter diagnostic device is to establish the type of sample that will be tested and the analytes within the sample that will be detected. Next, the signal transduction and detection mechanisms need to be defined. To develop an automated device, sample processing steps such as dilution, rinsing, or separation may be required. The materials necessary to fabricate the device must be selected based on cost, durability, sample compatibility, and constraints imposed by the detector. The device needs to be designed to minimize its overall dimensions to reduce costs and enhance portability. It should accommodate minimum sample volumes required for accurate analysis in consideration of the patient supplying the biological sample and discomfort resulting from invasive sampling

techniques. Depending on the detector chosen for the assay, analog to digital signal conversion may be necessary, as well as appropriate software to process acquired data.

Following the design and fabrication of the device, initial testing and characterization are necessary. Biological samples derived from animal models or willing donors must be tested repeatedly and results compared to conventional screening assays. The device should function as well as current technology but preferably with superior performance (higher sensitivity, lower cost per assay, greater speed, increased portability). Finally, if the device will be commercialized as a medical diagnostic tool, it must pass through a stringent regulatory approval process to ensure accuracy and safety.[4,5]

The development (design, fabrication, initial characterization and testing) of an inexpensive multifunctional microfluidic device for rapid clinical diagnosis and disease state monitoring is described in this dissertation. Whole human blood was chosen as the sample since many disorders can be detected or monitored through blood analysis. Intact white blood cells are of specific interest due to their diagnostic significance in autoimmune disorders,[6-9] HIV,[10,11] and hematologic cancers.[12-14] Fluorescence from dye-labeled antibody probes bound to cells and laser light scattering were used to detect cells in a microfluidic flow cytometer. Microfluidic chips were fabricated from glass, which is relatively robust and amenable to optical based detection. Since whole human blood is a very complex fluid, efforts were taken to reduce its complexity and enable selective analysis of white blood cells without significant interference from the other components. Contrived cultured cell mixtures, human blood, and murine blood samples were analyzed on-chip to simulate diagnostic assays typically performed on patient samples. Results

from the microfluidic system were compared to those obtained on conventional instrumentation in order to assess the accuracy of the assays performed.

The remainder of this chapter will provide a background review of the fundamental concepts in microfluidics and flow cytometry, as well as a review of cell based microfluidic applications to date. In addition, this chapter will attempt to substantiate the need for an automated, portable microfluidic cytometry system for blood cell analysis. The following chapter will discuss the design and fabrication of the microfluidic device, and the construction of the optical detection setup. Chapter 3 will describe initial characterization experiments performed using the microfluidic device to assess the critical design properties and ultimate limitations of the device. Chapter 4 will discuss the results from immunophenotypic analysis of cells from cell mixtures. Finally, chapters 5-7 will cover the investigation of multiple biological applications using the microfluidic flow cytometer.

1.2 Microfluidics Background

The origin of microfluidics can be linked to advancements in the microelectronics industry since many fabrication processes were borrowed or adapted to develop the technology. Since the invention of the transistor in 1947 at Bell Laboratories,[15] and the continued development of new integrated circuit technologies, the capabilities of electronic circuit manufacturing have continued to advance. Consequently, efforts have focused on reducing the size of integrated circuits to develop small, powerful electronic devices primarily for the manipulation of encoded information, i.e., information

technology. The result of these efforts is the vast microelectronics industry in existence today.

Some of the techniques commonly employed for silicon-based circuit fabrication in the microelectronics industry have been adapted to develop advanced microfabricated chemical and biochemical sensors. The intrinsic reproducibility of these techniques makes them ideal for the fabrication of microfluidic devices intended for commercialization. Additionally, the spatial resolution afforded by these processes, which were perfected for producing small electronic chips, allows for the accurate fabrication of very small sensors. The first example of a microfabricated chemical measurement device was a hybridized gas chromatograph where the separation column and thermal detector were machined on Si wafers.[16] Further developments by Manz et al. and others were critical in advancing chemical separation-based microsystems by demonstrating the increased separation performance achievable by decreasing separation column dimensions.[17-21] The field has since grown significantly to include a variety of separation techniques, chemical synthesis procedures, biological assays, and cell based assays.[22-27] Additionally, microfluidic pumps, valves, detectors, and sensors have been developed for these systems.[23,24,28-33]

Recent trends in the development of microfluidic devices have focused on integrating functional elements to create "lab-on-a chip" or total analysis systems.[34-40] The efforts to incorporate entire experimental protocols on microfabricated devices are directed towards minimizing the cost per analysis, increasing overall sample throughput, and enabling fully automated operation. Advanced synthetic procedures, multidimensional chemical separations, biomedical diagnostic assays, and chemical

sensors have all been developed and commercialized in some cases.[23,24] Parallel processing has also been demonstrated to increase analysis throughput.[41]

Microfluidic devices have been fabricated from quartz,[42] glass,[43-48] and many polymeric materials.[33,49-54] More complex multilayer devices have been produced using primarily soft lithography.[30,31,33] A combination of photolithography, wet chemical etching and bonding techniques are typically used to fabricate devices from glass.[19] Starting with a patterned photomask, photolithography is commonly employed to pattern specific designs on substrates for microfluidic devices. This procedure typically utilizes a thin layer of photoresist material spun on to the substrate surface that changes its chemical properties when exposed to radiation—typically ultraviolet light—to leave a pattern on the substrate after chemically developing and washing away exposed photoresist. For devices fabricated from glass or quartz, a buffered solution of hydrofluoric acid is typically used to chemically etch the photolithographically patterned substrates to make channels. Chemical etching of glass or quartz is an isotropic process, removing material uniformly in all directions, thereby limiting the maximum achievable aspect ratio (depth/width). Channels in etched substrates can be enclosed by thermally bonding a flat piece of glass or quartz on top of the etched material. Via holes are typically drilled through the substrate or coverplate to permit access to channels where necessary. These holes are typically drilled using ultrasonic milling or powder blasting techniques.[55]

General advantages of performing chemical analysis on microfluidic systems include the ability to precisely control the movement of small volumes of fluid, low reagent consumption compared to conventional systems, and overall reduced size and

cost of instrumentation.[45,56-59] Additionally, the ability to inexpensively fabricate these devices makes them disposable, which is especially important when considering analyzing potentially infectious clinical samples on-chip.[57]

1.3 Microfluidics Theory

To describe a fluid traveling through a microfluidic channel, one can assume that there is a conservation of mass. In addition, when describing an incompressible fluid—meaning that the fluid density (ρ) is constant—there is also conservation of volume. Therefore, the continuity equation can be written as follows to describe the situation where fluid flow velocities (v) are much smaller than the velocity of pressure waves in the fluid.[60]

$$\nabla \cdot \mathrm{v} = 0 \tag{1.1}$$

Additionally, the Navier-Stokes equation can be written as follows to describe the motion of an incompressible fluid.

$$\rho[\partial_t \mathrm{v} + (\mathrm{v} \cdot \nabla)\mathrm{v}] = -\nabla \mathrm{p} + \eta \nabla^2 \mathrm{v} + \rho \mathrm{g} + \rho_{\mathrm{el}} \mathrm{E} \tag{1.2}$$

This expresses the conservation of momentum with relation to the viscous and body forces acting on the fluid at any arbitrary location in the flow field at any instant of time,[55] where $-\nabla \mathrm{p}$ describes the force per unit volume on a fluid due to pressure, $\eta \nabla^2 \mathrm{v}$ describes the force per unit volume due to viscous forces, $\rho \mathrm{g}$ describes the force per unit volume due to gravitational forces, and $\rho_{\mathrm{el}} \mathrm{E}$ describes the force per unit volume due to electrical forces. The Navier-Stokes equation for the situation where Poiseuille flow

dominates fluid flow in a circular cross-section channel can be solved to determine the velocity vector field across the tube area. The velocity distribution relationship is as follows.

$$v_x(r) = \frac{\Delta p}{4\eta L}(a^2 - r^2) \tag{1.3}$$

The velocity distribution can then be integrated across the tube area to give the equation describing the volumetric flow rate Q.

$$Q = \frac{\pi a^4}{8\eta L}\Delta p \tag{1.4}$$

Where a is the channel radius, η is the solution viscosity, L is the channel length, and Δp is the magnitude of the pressure drop. This is just a single example of a reduced form of the Navier-Stokes relationship. When performing computational fluid dynamics (CFD) simulations for prospective microfluidic device designs, it is the Navier-Stokes relationship that is solved for with specific conditions defined based on the materials, fluids, and forces involved.

1.4 Flow Cytometry Background

Flow cytometry is a technology that is used for the simultaneous measurement of many characteristics of individual cells as they flow in a solution through a beam of light. This technology has been used for over 50 years, and has advanced over that time to incorporate numerous capabilities and advanced functionalities for characterizing cell populations that were not possible in an automated fashion previously. Before the

development of flow cytometry, cell samples were characterized manually using microscopy techniques. This practice is still common today for specific applications where the trained eye of a pathologist is needed for accurate assessment. However, the high-throughput and multiplexing capabilities of conventional flow cytometry make it the widespread choice for complex cell sample characterization. The development of the Coulter Counter also set the foundation for modern cytometry.

Wallace Coulter developed an instrument in 1956 that passed a flowing cell suspension through a small aperture while simultaneously measuring ionic conductance.[61] This principle worked on the basis that the electrical conductivity of cells is lower than that of a buffer solution, resulting in increased impedance across the aperture when containing a cell. This instrument allowed for counting and sizing of mixed cell samples, including complex mixtures of cells such as whole blood. This is done by correlating cell size with measured changes in impedance. This development in conjunction with the need for more advanced, higher-throughput microscopy techniques led to the development of modern flow cytometry.

Many basic examples, as early as the mid 1940's through the early 1970's, describe the detection and sorting of colloidal particles and cells. The work of F.T. Gucker and colleagues was based on the photoelectronic detection of colloidal particles in a laminar sheath stream of air for the detection of anthrax spores and other biowarfare agents, and was built for the U.S. Army during World War II.[62] Louis A. Kamentsky developed spectrophotometric flow cytometry instruments and the first cell sorting instrumentation at IBM in the early 1960's.[63-65] However, the fluorescence based cytometry instruments developed commercially by Partec in 1968 and development of

the Fluorescence Activated Cell Sorter (FACS) by Herzenberg at Stanford can be credited with the basic framework for modern flow cytometry and cell sorting technology.[66,67] These instruments established the capability for cellular differentiation and separation based on cells stained with fluorescent antibodies. Another major development leading to the advanced utility of flow cytometry was the discovery of methods to produce monoclonal antibodies and other molecular recognition elements for extracellular, intracellular, and nuclear molecular targeting.[68] The availability of monoclonal antibodies developed for specific cell surface proteins allowed for the facile discrimination of distinct cell subsets, greatly increasing the significance of immunofluorescence based cellular characterization by flow cytometry.

Since the 1970's, many advancements have been made to help develop state-of-the-art flow cytometry instrumentation.[69] Fluidic, optical, hardware, and software improvements have all assisted the evolution of modern flow cytometry. These improvements have allowed for higher precision measurements at faster analysis rates. Also, significantly more physiochemical information can be obtained on a per-cell basis using modern instrumentation due to the incorporation of multiple lasers, and the continued development of fluorescent dyes and tandem-dye conjugates providing fluorescent markers that span nearly the entire range of the visible spectrum. Current state-of-the-art instrumentation makes use of 2 or 3 lasers, allowing for the simultaneous detection of 12-18 different cellular parameters at throughputs surpassing 90,000 cells per second.[69]

Information obtained by flow cytometry can be classified into two categories; intrinsic structural characteristics and extrinsic properties. Intrinsic properties such as

cell size and granularity can be obtained using forward and side elastic light scatter based detection, which is incorporated in most modern cytometry instrumentation. These properties allow for the separation of cell subsets from complex mixtures without fluorescent tags. Many extrinsic properties can also be measured with the addition of targeted labeling reagents such as monoclonal antibodies conjugated to fluorescent dyes. Structural information such as DNA and RNA content and base ratios can be measured using specific nucleic acid stains. Additionally, immunofluorescence measurements can be used to determine the presence and abundance of both surface and intracellular receptors. Some other functional measurements commonly determined are cytoplasmic calcium levels, DNA degradation/ apoptosis, and enzyme activity.[69]

1.5 Flow Cytometry Instrumentation

A modern flow cytometer has three main components; a fluidic system for cell transport, an optical system for detection, and a signal processing unit.[69] Precise coordination of all three elements is necessary for accurate, reproducible high-speed measurements. The major fluidic component is a flow chamber (shown in Figure 1.1). The purpose of the flow chamber is to align the cells in solution into single file within a narrow stream. Hydrodynamic focusing is used to align the cells by forcing another stream of fluid—known as the sheath fluid—to envelop the cell sample stream as it exits the nozzle tip. The sheath and cell streams are forced into a narrow tube after they combine, causing the cross-sectional area of the inner cell stream to narrow. The cells remain within the narrowed stream and are aligned in single file. The extent to which the

cell stream is narrowed, and consequently the cell alignment, can be adjusted for specific applications by varying the ratio of pressures applied to the cell sample and sheath solutions. Flow velocities for cell sample solutions can exceed 10 meters per second with applied pressures ranging from 10 – 100 psi.

The purpose of hydrodynamically narrowing the cell stream is to ensure that all cells pass through a small optical detection volume in a single file. The detection volume is ideally similar to the volume of the cell so as to limit background signal from the buffer solution and maximizing optical signals from the cell. As cells flow through this region, they pass through one or more focused laser spots. These lasers are used to induce both light scattering and fluorescence from the cells. A schematic of a simple flow cytometry optical configuration is shown in Figure 1.2. An incident laser beam is passed through 2 cylindrical lenses in order to shape the beam into an elliptical profile. This elliptically focused beam is aligned so that the long axis is orthogonal to the cell stream flow, providing more uniform illumination of cells, independent of small deviations in the cell stream position as compared to a circular beam profile.[70] The focused laser beam is directed through the hydrodynamically focused cells in the flow chamber.

As cells pass through the focused laser beam, elastically scattered light and fluorescence are emitted from each cell or from dye molecules attached to the cell. Optical components are aligned around the flow chamber to collect these signals. The scattered light is typically collected from two directions; at a small angle from the incident beam and at a 90º angle from the incident beam. Small angle scatter—also called forward scatter or FSC—is collected at angles < 10º from the incident beam with a

photodiode detector. A beam stop may be placed in line with the incident beam in front of the photodiode so that the scattered light can be detected without saturating the detector. Fluorescence and 90º scattered light (known as side scatter – SSC) detectors are placed orthogonal to the incident beam and forward scatter detector. Side scatter signatures are used to reveal differences in cell surface roughness and granularity. As shown in 1.2, the fluorescence and side scatter signals are passed through a series of dichroic mirrors that direct the different signals to individual photomultiplier tubes (PMT's). This enables the spectral separation of multiple fluorescence signals from each cell. The first PMT can be used to detect the side scatter signal, while the remaining detectors are for the detection of fluorescence from different dye molecules conjugated to specific types of antibodies. In front of each detector is a band pass filter to reduce the detection of light other than from the specific dye fluorescence corresponding to that channel.

The output signals from each detector are amplified by passing through a current to voltage amplifier. The signals are digitized and then immediately analyzed to extract peak intensities or areas from detected events. A defined channel (normally FSC) is used to trigger data acquisition from all other detectors when a cell is present. The values obtained from the channels of interest are loaded into a user defined software interface where results can be plotted to monitor the cell solution characteristics in real time. When more than one laser is used, there are multiple interrogation spots. As a result, the signals from each laser interrogation point must be synchronized to ensure that the correct signals from each cell are properly correlated.

1.6 Microfluidics for Cellular Applications

The inherent advantages of microfluidic devices have led to numerous applications incorporating cells. Channel features on the micron scale allow for facile manipulation and interrogation of cells. Examples of microfluidic cellular applications range from miniaturized examples of bulk processes, to complex, integrated analyses of cells not possible using conventional instrumentation.[71,72] While numerous cellular applications have been demonstrated on microfluidic devices, this introduction will focus on previous demonstrations and advancements of microfluidic flow cytometry.

Previous reports on microfluidic flow cytometry devices has predominately focused on strategies for fluid manipulation, cell focusing, integrating optical components, or demonstration of applications.[58,73] Fluid manipulation on microfluidic devices for flow cytometry applications has been most commonly demonstrated using off-chip pumping methods.[44,48,52,74-81] However, there are some examples where pumping and valves have been integrated on-chip.[48,54,82] For example, electrokinetic pumping has been employed for fluid manipulation and hydrodynamic focusing of cells on chip.[45,83,84] Additionally, dielectrophoresis has been used for fluid manipulation for on-chip cytometry applications.[85]

Strategies for microfluidic cytometry have been demonstrated using narrow channels that force cells through a detection region without any hydrodynamic focusing.[86-90] Issues with this strategy include the increased shear stress experienced by cells as they pass through the narrow channel, as well as the increased probability for channel clogging as compared to examples employing hydrodynamic focusing.

Numerous examples of hydrodynamic focusing in a single dimension (i.e. in only one plane) on-chip have been demonstrated.[45,47,49,53,58,74,77,84,91-94] This focusing strategy is commonly employed due to a simple microchip design and ease of fabrication. One example is based on a simple cross-channel intersection first described by Jacobson et. al.[83] While one-dimensional focusing is most common, issues with this strategy still exist including shear effects in the dimension not being focused, and variations in the location of cells as they pass by the detection region. Two-dimensional hydrodynamic focusing strategies have also been developed for flow cytometry applications on-chip.[51,52,95-99] Although this focusing approach most closely resembles the focused sample stream profile obtained in conventional capillary based cytometry systems, fabrication of these devices can be complex and multiple layers of patterned material must be properly aligned and bonded in order to successfully obtain the desired hydrodynamic focusing effect.

Efforts to integrate optical components into microfluidic cytometry devices have been demonstrated in order to reduce the amount of large-scale external components necessary for optical measurements. Optical fibers or materials such as SU-8, PDMS, and other polymers have been incorporated on-chip to act as optical waveguides.[48,88,92-94,100] These waveguides are used to direct and focus the excitation light to the cells on-chip. Another approach has been to incorporate a low power dye laser on-chip with integrated waveguides and photodiodes for optical fluorescence measurements in fluids.[101,102] Negative aspects to these integrated designs are the added complexity in fabrication and the increased cost associated with producing devices containing different

materials. These drawbacks could prohibit the ability to inexpensively mass-produce these devices for commercial applications.

Many biological applications have been demonstrated using microfluidic flow cytometry devices in order to demonstrate efficacy, and in some cases, reveal distinct advantages over analysis by conventional flow cytometry. Microfluidic cytometry has been used for cellular phenotyping,[103] bacterial analysis,[45,75,104] rare cell detection,[77] monitoring cellular transfection[105] and apoptosis,[106] and cell cycle analysis.[78] Some of these applications have also incorporated other processing steps such as automated fluorescence staining,[105,106] cell culture,[74] integrated cell lysis for the analysis of intracellular components,[44,107] and cell sorting.[74,76,77,82,108-110]

1.7 Concluding Remarks

Significant progress has been made over the past few decades in the development of highly specific targeting reagents, sample processing protocols, and multiplexed cytometry instrumentation to perform numerous complex analyses for various clinical diagnostic and monitoring applications. Modern commercial flow cytometry instruments are costly and require large sample volumes such that the development of small, disposable devices based on this technology would have a profound impact on the cost and accessibility of diagnostic and monitoring assays. Microfabrication technologies allowing for the inexpensive, reproducible production of small, disposable devices provide an ideal platform for the development of a point-of-care diagnostic device. Microfluidics allow for the integration of sample processing steps, presenting the

opportunity for automated "sample-in answer-out" analysis not currently possible with conventional instrumentation. Automated sample processing and analysis is critical for applications in resource-limited settings where pathologists or trained technicians are not present.

Flow cytometry is a rapid technique for analyzing clinical samples and characterizing complex cellular solutions. It is used as the basis for numerous clinical diagnostic and monitoring applications that can in many instances be successfully implemented on substantially simpler platforms than typically employed. For example, the microfabricated flow cytometer with the 2-color detection scheme described in this dissertation can be used for detecting leukocyte malignancies, applications in blood dosimetry, and HIV monitoring. The strategy employed here was to devise a simple microfluidic cytometer to preserve the ability to inexpensively fabricate disposable devices. One-dimensional focusing was employed to simplify the fabrication process. In addition, off-chip pumping and optics were utilized for the development of a stable, robust instrument with inexpensive, disposable microfluidic chips for point-of-care applications.

1.8 Figures

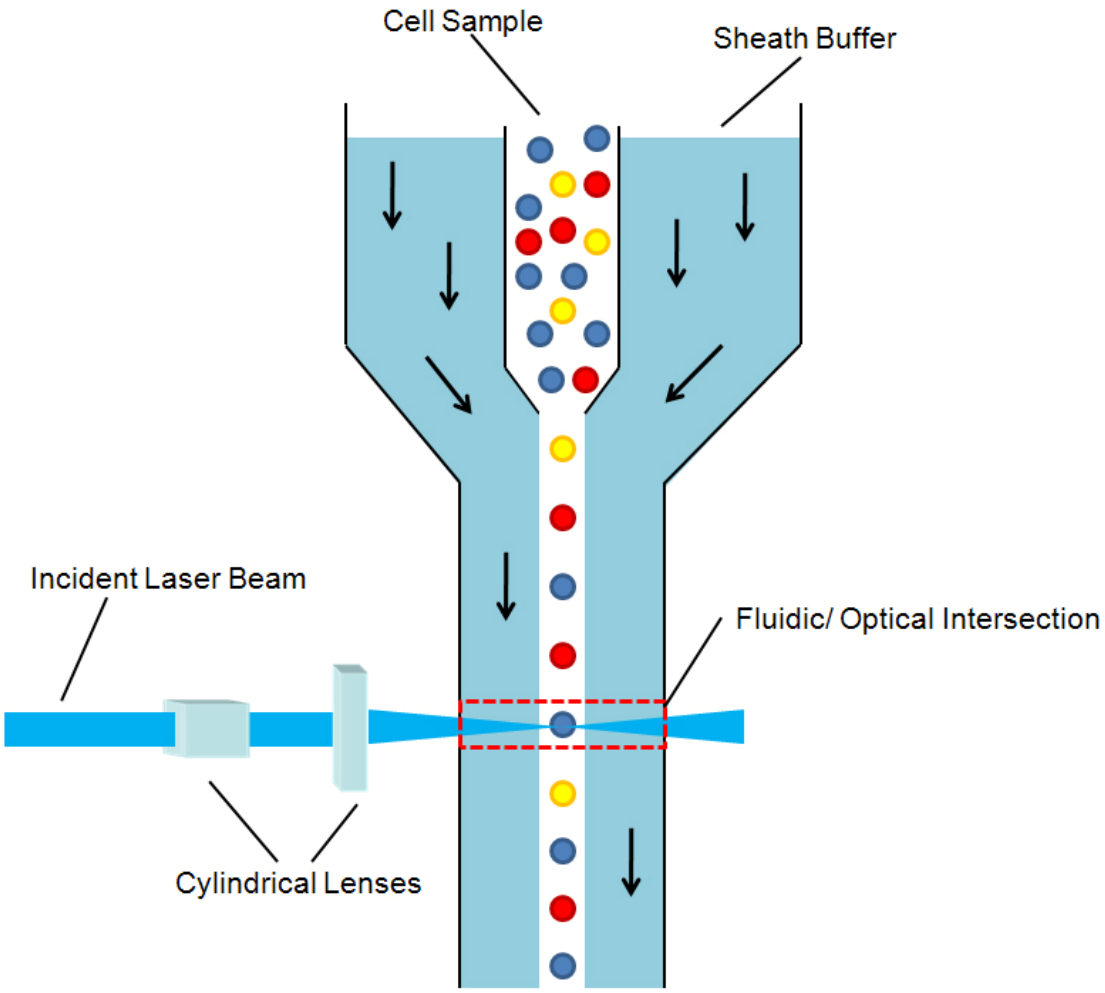

Figure 1.1 Schematic of a typical flow chamber in a conventional flow cytometry system, illustrating the principle of hydrodynamic focusing that ensures proper cell alignment for passage through a fluidic/ optical intersection.

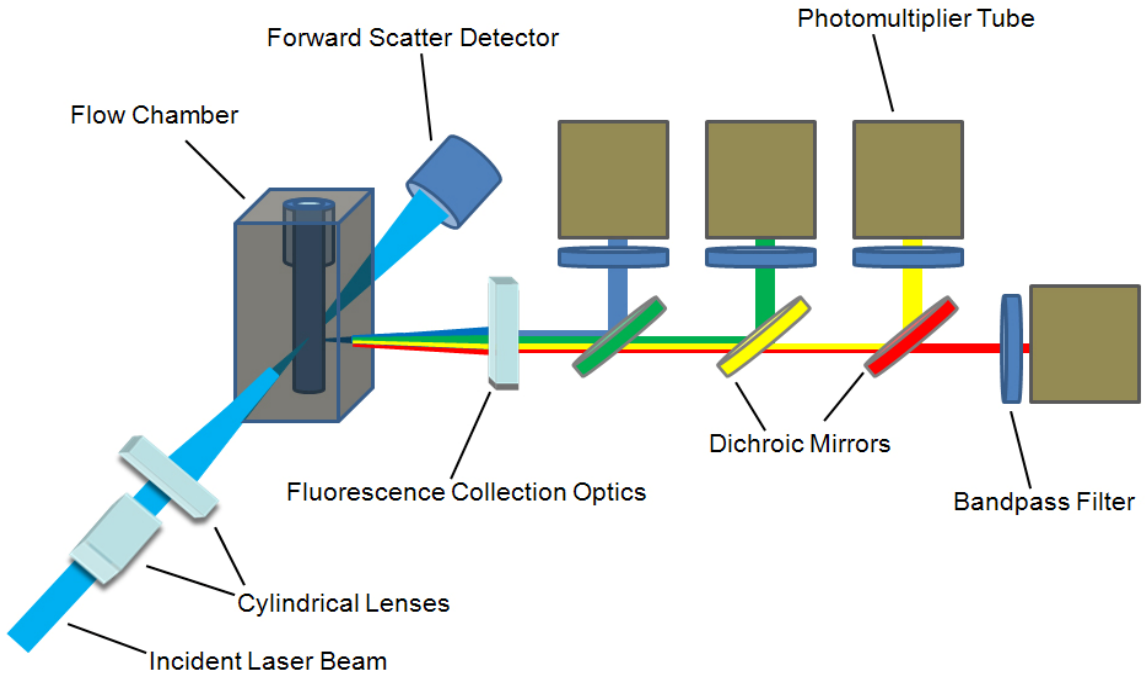

Figure 1.2 Schematic of a common optical configuration for a commercial cytometry system.

1.9 References

(1) Erickson, K. A.; Wilding, P. *Clinical Chemistry* **1993**, *39*, 283-287.

(2) Baskin, L. B.; Morgan, D. L.; Parupia, J. Y. *Laboratory Medicine* **1996**, *27*, 193-197.

(3) Salas, V. M.; Edwards, B. S.; Sklar, L. A. *Adv Clin Chem* **2008**, *45*, 47-74.

(4) Abdel-aleem, S. *Design, execution, and management of medical device clinical trials*; John Wiley & Sons: Hoboken, N.J., 2009.

(5) Cheng, M.; World Health Organization. *Medical device regulations : global overview and guiding principles*; World Health Organization: Geneva, 2003.

(6) Baecher-Allan, C.; Brown, J. A.; Freeman, G. J.; Hafler, D. A. *Novartis Found Symp* **2003**, *252*, 67-88; discussion 88-91, 106-114.

(7) Baecher-Allan, C.; Viglietta, V.; Hafler, D. A. *Semin Immunol* **2004**, *16*, 89-98.

(8) Roncador, G.; Brown, P. J.; Maestre, L.; Hue, S.; Martinez-Torrecuadrada, J. L.; Ling, K. L.; Pratap, S.; Toms, C.; Fox, B. C.; Cerundolo, V.; Powrie, F.; Banham, A. H. *European Journal of Immunology* **2005**, *35*, 1681-1691.

(9) Sakaguchi, S. *Annu Rev Immunol* **2004**, *22*, 531-562.

(10) Douek, D. C.; Picker, L. J.; Koup, R. A. *Annual Review of Immunology* **2003**, *21*, 265-304.

(11) Stein, D. S.; Korvick, J. A.; Vermund, S. H. *Journal of Infectious Diseases* **1992**, *165*, 352-363.

(12) Lacombe, F.; Durrieu, F.; Briais, A.; Dumain, P.; Belloc, F.; Bascans, E.; Reiffers, J.; Boisseau, M. R.; Bernard, P. *Leukemia* **1997**, *11*, 1878-1886.

(13) Paredes-Aguilera, R.; Romero-Guzman, L.; Lopez-Santiago, N.; Burbano-Ceron, L.; Camacho-Del Monte, O.; Nieto-Martinez, S. *American Journal of Hematology* **2001**, *68*, 69-74.

(14) Swat, W.; Ignatowicz, L.; Kisielow, P. *Journal of Immunological Methods* **1991**, *137*, 79-87.

(15) Riordan, M.; Hoddeson, L. *Crystal fire : the birth of the information age*, 1st ed.; Norton: New York, 1997.

(16) Terry, S. C.; Jerman, J. H.; Angell, J. B. *Ieee Transactions on Electron Devices* **1979**, *26*, 1880-1886.

(17) Jacobson, S. C.; Hergenroder, R.; Koutny, L. B.; Ramsey, J. M. *Analytical Chemistry* **1994**, *66*, 1114-1118.

(18) Jacobson, S. C.; Hergenroder, R.; Koutny, L. B.; Ramsey, J. M. *Analytical Chemistry* **1994**, *66*, 2369-2373.

(19) Jacobson, S. C.; Hergenroder, R.; Koutny, L. B.; Warmack, R. J.; Ramsey, J. M. *Analytical Chemistry* **1994**, *66*, 1107-1113.

(20) Manz, A.; Miyahara, Y.; Miura, J.; Watanabe, Y.; Miyagi, H.; Sato, K. *Sensors and Actuators B-Chemical* **1990**, *1*, 249-255.

(21) Manz, A.; Harrison, D. J.; Verpoorte, E. M. J.; Fettinger, J. C.; Paulus, A.; Ludi, H.; Widmer, H. M. *Journal of Chromatography* **1992**, *593*, 253-258.

(22) Fiorini, G. S.; Jeffries, G. D. M.; Lim, D. S. W.; Kuyper, C. L.; Chiu, D. T. *Lab on a Chip* **2003**, *3*, 158-163.

(23) Dittrich, P. S.; Tachikawa, K.; Manz, A. *Analytical Chemistry* **2006**, *78*, 3887-3907.

(24) West, J.; Becker, M.; Tombrink, S.; Manz, A. *Analytical Chemistry* **2008**, *80*, 4403-4419.

(25) Golden, A. P.; Tien, J. *Lab on a Chip* **2007**, *7*, 720-725.

(26) Li, S.; Freidhoff, C. B.; Young, R. M.; Ghodssi, R. *Journal of Micromechanics and Microengineering* **2003**, *13*, 732-738.

(27) Mair, D. A.; Rolandi, M.; Snauko, M.; Noroski, R.; Svec, F.; Frechet, J. M. J. *Analytical Chemistry* **2007**, *79*, 5097-5102.

(28) Mela, P.; Tas, N. R.; Berenschot, E. J. W.; van Nieuwkasteele, J.; van den Berg, A. *Electrophoresis* **2004**, *25*, 3687-3693.

(29) Nam, S. W.; Van Noort, D.; Yang, Y.; Park, S. *Lab on a Chip* **2007**, *7*, 638-640.

(30) Unger, M. A.; Chou, H. P.; Thorsen, T.; Scherer, A.; Quake, S. R. *Science* **2000**, *288*, 113-116.

(31) Groisman, A.; Enzelberger, M.; Quake, S. R. *Science* **2003**, *300*, 955-958.

(32) Thorsen, T.; Maerkl, S. J.; Quake, S. R. *Science* **2002**, *298*, 580-584.

(33) Quake, S. R.; Scherer, A. *Science* **2000**, *290*, 1536-1540.

(34) Weigl, B. H.; Bardell, R. L.; Cabrera, C. R. *Advanced Drug Delivery Reviews* **2003**, *55*, 349-377.

(35) Haeberle, S.; Zengerle, R. *Lab on a Chip* **2007**, *7*, 1094-1110.

(36) Tanaka, Y.; Sato, K.; Shimizu, T.; Yamato, M.; Okano, T.; Kitamori, T. *Biosensors & Bioelectronics* **2007**, *23*, 449-458.

(37) Ohno, K.; Tachikawa, K.; Manz, A. *Electrophoresis* **2008**, *29*, 4443-4453.

(38) Zhang, Y. H.; Ozdemir, P. *Analytica Chimica Acta* **2009**, *638*, 115-125.

(39) Mark, D.; Haeberle, S.; Roth, G.; von Stetten, F.; Zengerle, R. *Chemical Society Reviews* **2010**, *39*, 1153-1182.

(40) Manz, A.; Graber, N.; Widmer, H. M. *Sensors and Actuators B-Chemical* **1990**, *1*, 244-248.

(41) Mckenna, B. K.; Selim, A. A.; Bringhurst, F. R.; Ehrlich, D. J. *Lab on a Chip* **2009**, *9*, 305-310.

(42) Sobek, D., ; Young, A.M.; Gray, M.L.; and Senturia, S.D. *Proc. IEEE* **1993**, *2*, 219-224.

(43) Jacobson, S. C.; Ramsey, J. M. *Anal Chem* **1997**, *69*, 3212-3217.

(44) McClain, M. A.; Culbertson, C. T.; Jacobson, S. C.; Allbritton, N. L.; Sims, C. E.; Ramsey, J. M. *Anal Chem* **2003**, *75*, 5646-5655.

(45) McClain, M. A.; Culbertson, C. T.; Jacobson, S. C.; Ramsey, J. M. *Anal Chem* **2001**, *73*, 5334-5338.

(46) Poulsen, C. R.; Culbertson, C. T.; Jacobson, S. C.; Ramsey, J. M. *Analytical Chemistry* **2005**, *77*, 667.

(47) Schrum, D. P.; Culbertson, C. T. *Analytical Chemistry* **1999**, *71*, 4173.

(48) Wang, Z.; El-Ali, J.; Engelund, M.; Gotsaed, T.; Perch-Nielsen, I. R.; Mogensen, K. B.; Snakenborg, D.; Kutter, J. P.; Wolff, A. *Lab Chip* **2004**, *4*, 372-377.

(49) Chung, S.; Park, S. J.; Kim, J. K.; Chung, C.; Han, D. C.; Chang, J. K. *Microsystem Technologies-Micro-and Nanosystems-Information Storage and Processing Systems* **2003**, *9*, 525-533.

(50) Hung, C. I.; Ke, B. J.; Huang, G. R.; Hwei, B. H.; Lai, H. F.; Lee, G. B. *Journal of Fluids Engineering-Transactions of the Asme* **2001**, *123*, 672-679.

(51) Simonnet, C.; Groisman, A. *Applied Physics Letters* **2005**, *87*, -.

(52) Simonnet, C.; Groisman, A. *Anal Chem* **2006**, *78*, 5653-5663.

(53) Tung, Y. C.; Zhang, M.; Lin, C. T.; Kurabayashi, K.; Skerlos, S. J. *Sensors and Actuators B-Chemical* **2004**, *98*, 356-367.

(54) Yang, R.; Feeback, D. L.; Wang, W. J. *Sensors and Actuators a-Physical* **2005**, *118*, 259-267.

(55) Madou, M. J. *Fundamentals of microfabrication : the science of miniaturization*, 2nd ed.; CRC Press: Boca Raton, 2002.

(56) Andersson, H.; van den Berg, A. *Sensors and Actuators B-Chemical* **2003**, *92*, 315-325.

(57) Chung, T. D.; Kim, H. C. *Electrophoresis* **2007**, *28*, 4511-4520.

(58) Huh, D.; Gu, W.; Kamotani, Y.; Grotberg, J. B.; Takayama, S. *Physiological Measurement* **2005**, *26*, R73-R98.

(59) Ramsey, J. M. *Nat Biotechnol* **1999**, *17*, 1061-1062.

(60) Bruus, H. *Theoretical microfluidics*; Oxford University Press: Oxford ; New York, 2008.

(61) Coulter, W. H. *Proc.Natl.Electronics Conf.* **1956**, *12*, 1034-1042.

(62) Gucker, F. T., O'Konski, C.T., Pickard, H.B., Pitts, J.N. *J Am Chem Soc* **1947**, *69*, 2422-2431.

(63) Kamentsky, L. A., Derman, H., Melamed, M.R *Science* **1963**, *142*, 1577-1580.

(64) Kamentsky, M., M.R, Derman, H. *Science* **1965**, *150*, 630-631.

(65) Kamentsky, M., M.R. *Science* **1967**, *156*, 1364-1365.

(66) Bonner, W. A., Hulett, H. R., Sweet, R. G. and Herzenberg, L. A. *Review of Scientific Instruments* **1972**, *43*, 404-409

(67) Hulett, H. R., Bonner, W. A., Sweet, R. G. and Herzenberg, L. A. *Clinical Chemistry* **1973**, *19*, 813-816.

(68) Kohler, G., Milstein, C. *Nature* **1975**, *256*, 495-497.

(69) Shapiro, H. M. *Practical flow cytometry*, 4th ed.; Wiley-Liss: New York, 2003.

(70) Watson, J. V. *Cytometry* **1981**, *2*, 14-19.

(71) El-Ali, J.; Sorger, P. K.; Jensen, K. F. *Nature* **2006**, *442*, 403-411.

(72) Sims, C. E.; Allbritton, N. L. *Lab on a Chip* **2007**, *7*, 423-440.

(73) Ateya, D. A.; Erickson, J. S.; Howell, P. B.; Hilliard, L. R.; Golden, J. P.; Ligler, F. S. *Analytical and Bioanalytical Chemistry* **2008**, *391*, 1485-1498.

(74) Wolff, A.; Perch-Nielsen, I. R.; Larsen, U. D.; Friis, P.; Goranovic, G.; Poulsen, C. R.; Kutter, J. P.; Telleman, P. *Lab Chip* **2003**, *3*, 22-27.

(75) Inatomi, K. I.; Izuo, S. I.; Lee, S. S. *Letters in Applied Microbiology* **2006**, *43*, 296-300.

(76) Kruger, J.; Singh, K.; O'Neill, A.; Jackson, C.; Morrison, A.; O'Brien, P. *Journal of Micromechanics and Microengineering* **2002**, *12*, 486-494.

(77) Lancaster, C.; Kokoris, A.; Nabavi, M.; Clemmens, J.; Maloney, P.; Capadanno, J.; Gerdes, J.; Battrell, C. F. *Methods* **2005**, *37*, 120-127.

(78) Bernini, R.; De Nuccio, E.; Brescia, F.; Minardo, A.; Zeni, L.; Sarro, P. M.; Palumbo, R.; Scarfi, M. R. *Anal Bioanal Chem* **2006**, *386*, 1267-1272.

(79) Stiles, T.; Fallon, R.; Vestad, T.; Oakey, J.; Marr, D. W. M.; Squier, J.; Jimenez, R. *Microfluidics and Nanofluidics* **2005**, *1*, 280-283.

(80) Sun, Y.; Yin, X. F. *Journal of Chromatography A* **2006**, *1117*, 228-233.

(81) Yao, B.; Luo, G. A.; Feng, X.; Wang, W.; Chen, L. X.; Wang, Y. M. *Lab Chip* **2004**, *4*, 603-607.

(82) Fu, A. Y.; Chou, H. P.; Spence, C.; Arnold, F. H.; Quake, S. R. *Anal Chem* **2002**, *74*, 2451-2457.

(83) Jacobson, S. C.; Ramsey, J. M. *Analytical Chemistry* **1997**, *69*, 3212-3217.

(84) Lee, G. B.; Chang, C. C.; Huang, S. B.; Yang, R. J. *Journal of Micromechanics and Microengineering* **2006**, *16*, 1024-1032.

(85) Holmes, D.; Morgan, H.; Green, N. G. *Biosensors & Bioelectronics* **2006**, *21*, 1621-1630.

(86) Eyal, S.; Quake, S. R. *Electrophoresis* **2002**, *23*, 2653-2657.

(87) Fu, A. Y.; Spence, C.; Scherer, A.; Arnold, F. H.; Quake, S. R. *Nature Biotechnology* **1999**, *17*, 1109-1111.

(88) Lien, V.; Zhao, K.; Berdichevsky, Y.; Lo, Y. H. *Ieee Journal of Selected Topics in Quantum Electronics* **2005**, *11*, 827-834.

(89) Perry, H.; Greiner, C.; Georgakoudi, I.; Cronin-Golomb, M.; Omenetto, F. G. *Rev Sci Instrum* **2007**, *78*, 044302.

(90) Stavis, S. M.; Edel, J. B.; Samiee, K. T.; Craighead, H. G. *Lab Chip* **2005**, *5*, 337-343.

(91) Blankenstein, G.; Larsen, U. D. *Biosensors & Bioelectronics* **1998**, *13*, 427-438.

(92) Fu, L. M.; Yang, R. J.; Lin, C. H.; Pan, Y. J.; Lee, G. B. *Analytica Chimica Acta* **2004**, *507*, 163-169.

(93) Lee, G. B.; Lin, C. H.; Chang, G. L. *Sensors and Actuators a-Physical* **2003**, *103*, 165-170.

(94) Pamme, N.; Koyama, R.; Manz, A. *Lab Chip* **2003**, *3*, 187-192.

(95) Sundararajan, N.; Pio, M. S.; Lee, L. P.; Berlin, A. A. *Journal of Microelectromechanical Systems* **2004**, *13*, 559-567.

(96) Chang, C. C.; Huang, Z. X.; Yang, R. J. *Journal of Micromechanics and Microengineering* **2007**, *17*, 1479-1486.

(97) Peter B. Howell Jr, J. P. G., Lisa R. Hilliard, Jeffrey S. Erickson, David R. Mottb and Frances S. Ligler *Lab on a Chip* **2008**, *8*, 1097-1103.

(98) Miyake, R.; Ohki, H.; Yamazaki, I.; Takagi, T. *Jsme International Journal Series B-Fluids and Thermal Engineering* **1997**, *40*, 106-113.

(99) Mao, X.; Lin, S. C.; Dong, C.; Huang, T. J. *Lab Chip* **2009**, *9*, 1583-1589.

(100) Xiang, Q.; Xuan, X. C.; Xu, B.; Li, D. Q. *Instrumentation Science & Technology* **2005**, *33*, 597-607.

(101) Balslev, S.; Jorgensen, A. M.; Bilenberg, B.; Mogensen, K. B.; Snakenborg, D.; Geschke, O.; Kutter, J. P.; Kristensen, A. *Lab on a Chip* **2006**, *6*, 213-217.

(102) Novak, L.; Neuzil, P.; Pipper, J.; Zhang, Y.; Lee, S. H. *Lab on a Chip* **2007**, *7*, 27-29.

(103) Chien, C. M.; Cheng, J. L.; Chang, W. T.; Tien, M. H.; Wu, W. Y.; Chang, Y. H.; Chang, H. Y.; Chen, S. T. *J Chromatogr B Analyt Technol Biomed Life Sci* **2003**, *795*, 1-8.

(104) Sakamoto, C.; Yamaguchi, N.; Nasu, M. *Appl Environ Microbiol* **2005**, *71*, 1117-1121.

(105) Buhlmann, C.; Preckel, T.; Chan, S.; Luedke, G.; Valer, M. *J Biomol Tech* **2003**, *14*, 119-127.

(106) Chan, S. D. H.; Luedke, G.; Valer, M.; Buhlmann, C.; Preckel, T. *Cytometry Part A* **2003**, *55A*, 119-125.

(107) Wheeler, A. R.; Throndset, W. R.; Whelan, R. J.; Leach, A. M.; Zare, R. N.; Liao, Y. H.; Farrell, K.; Manger, I. D.; Daridon, A. *Anal Chem* **2003**, *75*, 3581-3586.

(108) Dittrich, P. S.; Schwille, P. *Analytical Chemistry* **2003**, *75*, 5767-5774.

(109) Fu, A. Y.; Spence, C.; Scherer, A.; Arnold, F. H.; Quake, S. R. *Nat Biotechnol* **1999**, *17*, 1109-1111.

(110) Voldman, J.; Gray, M. L.; Toner, M.; Schmidt, M. A. *Analytical Chemistry* **2002**, *74*, 3984-3990.

CHAPTER 2:

DESIGN AND CONSTRUCTION OF THE MICROFLUIDIC FLOW CYTOMETRY SYSTEM

2.1 Introduction

A small, inexpensive flow cytometry system should be designed to simplify manufacturing processes and operational complexity while maintaining the ability to accurately characterize complex cellular mixtures. In order to satisfy these requirements, the microfluidic device described in this dissertation has been designed to simplify fabrication and reduce pumping requirements. The instrument is designed to utilize stationary optical, electronic, and pumping components off-chip and accommodate a disposable microfluidic device that contains the flow chamber. As such, the optical configuration for this instrument is a modified version of that employed in conventional flow cytometers.

The design and construction of the microfabricated flow cytometer, the optical detection system, and the signal processing electronics are described in this chapter. The microfluidic flow chamber was designed with the aid of computational fluid dynamic simulations that predict hydrodynamic focusing. Optical components in the detection setup were configured to collect forward scattered light to allow cells to be detected and

counted independent of fluorescent labels. Two discrete fluorescent signals could also be measured to differentiate cell subsets in complex mixtures via fluorescently labeled cell recognition elements. Hardware and software for real-time signal processing were also incorporated, allowing for rapid instrument alignment using calibration beads and significantly reducing the amount of time necessary to analyze large experimental data sets.

2.2 Theory

2.2.1 Hydrodynamic Focusing

The relative hydraulic resistances of cell sample to sheath fluid channels must be properly designed for a hydrodynamic focusing chamber where fluid flow is driven by a vacuum source. This is necessary to ensure the proper hydrodynamic focusing required for the specific application is achieved. The chip described in this dissertation utilizes a single input reservoir for the sheath buffer solution. This solution is split into two streams that recombine after they intersect the cell sample solution as shown in Figure 2.4a. The proper ratio of hydraulic resistances of the channels was calculated using Equations 2.1 and 2.2 to achieve the desired hydrodynamic focusing effect. Equation 2.1 was set equal to 0.15, which is the desired ratio of cell to sheath channels to obtain cell stream focusing to a width of 10 μm. Since all channel depths are equal on the device, channel lengths and widths were tuned to achieve the proper flow rate ratio.

$$\text{Flow rate ratio} = \frac{Q_C}{Q_C + 2Q_S} \tag{2.1}$$

Q_C is the cell solution flow rate and Q_S is the sheath buffer flow rate. The flow rate Q is defined in Equation 2.2.

$$Q = \frac{\Delta P w d^3}{12 \eta L} \tag{2.2}$$

In this equation, ΔP is the applied pressure drop, w is the channel width, d is the channel depth, η is the solution viscosity, and L is the channel length. Applying Ohm's law to Equation 2.2—substituting the ratio of channel length to area for hydraulic resistance—and cancelling out constant terms such as channel depth and solution viscosity allows the flow rate ratio to be expressed in terms of channel lengths (L) and widths (w) as shown in Equation 2.3.

$$\frac{Q_B}{Q_C} = \frac{L_C w_B}{L_B w_C} \tag{2.3}$$

For the device described here, the flow rate ratio $\frac{Q_B}{Q_C}$ in Equation 2.3 was set equal to 3 based on the desired flow rate, and channel lengths and widths determined.

2.2.2 Laser Beam Shaping

The incident laser beam was shaped into an elliptical profile with the long axis orthogonal to the cell flow direction to increase the reproducibility of the time each cell spends in the excitation beam. Beam shaping was accomplished using a pair of crossed cylindrical lenses, where each cylindrical lens is used to focus the beam in one direction.[1]

The properties of the lens pair required for this setup was calculated using Equation 2.4 based on the desired final focused elliptical beam profile,

$$w_{\mathrm{F}} = \frac{\lambda f M^2}{\pi w_{\mathrm{L}}} \tag{2.4}$$

where w_{F} is the desired radius of the focused beam, λ is the laser wavelength, f is the focal length of the cylindrical lens, M^2 is the quality factor of the incident beam (assumed to be 1.0), and w_{L} is the radius of the beam at the laser output. A final focused beam profile of 15 μm by 100 μm was chosen to ensure that cells experience minimal variation in excitation time due to small deviations in their location relative to the center of the beam. Uniformity of measurements is ensured by aligning the long axis of the focused beam over the entire width of the center cell stream channel. In addition, the focused beam profile was chosen to reduce the probability of having more than one cell in the excitation beam simultaneously.

2.3 Microchip Design

The microfluidic device was intended to achieve proper hydrodynamic focusing of the cell solution using a simple design. Glass chips were used due to their relative robustness, optical transparency, and compatibility with low-pressure driven flow. One dimensional focusing is utilized to simplify chip fabrication. In addition, all channels (i.e. the sheath buffer channels and cell solution channels) were etched to the same depth in a single etch step to provide the desired channel dimensions. Further, all fluid flow is driven by applying sub-ambient pressure to a single channel. This eliminates the need for

two pumps that are commonly employed to supply independent control of the cell sample and sheath flow rates using positive pressure.

When manipulating fluid using pressures, it is important to understand the fluid flow profile and consider how it will impact the cells traveling on-chip. The effects from pressure-induced parabolic flow do not need to be considered in the plane focused by the sheath buffer since the sidewall drag forces predominantly act on the outer-sheath fluid stream. In the device described using one-dimensional hydrodynamic focusing, it is however necessary to consider how the parabolic flow profile effects the cell stream solution in the vertical dimension not focused by the sheath flow. Different fluid velocities within this stream caused by the parabolic flow profile can cause the cells to travel at different speeds, increasing the variance in cell excitation and detection times. In order to reduce this effect, the channel depth can be minimized. The cells will then experience the flow profile near the walls where the flow is slower, and in the center of the channel at the maximum fluid velocity. The result is that the cells will travel at a velocity equivalent to the average fluid velocities across the parabolic flow profile. An issue with minimizing the channel depth is that the channels can quickly clog with cells, cell debris, or particulate contaminants, rendering the microfluidic device inoperable. For applications described in this dissertation concerning blood cell solutions, channel depths of 20-25 μm were chosen as a compromise between minimizing the parabolic flow effects and reducing the possibility for channel clogging.

Calculations to determine the optimal ratio of hydraulic resistances of cell solution flow to sheath channel flow along with computational fluid dynamic simulations were employed on prospective flow chamber designs to ensure proper hydrodynamic

focusing. Adequate hydrodynamic focusing for the application was defined by the ability to focus the cell solution to a width close to 10 μm. After calculating the proper ratios of channel hydraulic resistances using Equations 2.1, 2,2, and 2.3, designs incorporating different intersecting angles of sheath buffer channels to cell solution channels were simulated. The results are shown in Figures 2.1-2.3. A 90º angle of intersection as shown in Figure 2.1 has been described previously in the literature for microchip cytometry applications.[2] Figure 2.2 shows a simulation of a 35º angle of intersection, which closely resembles the focusing strategy employed in most commercially available capillary based cytometry systems. Figure 2.3 is the result from a 135º angle intersection simulation. The hydrodynamic focusing properties demonstrated by these simulations led to the selection of the channel layout in Figure 2.3 as the optimal design for the microfluidic cytometry flow chamber. This design has maximum sheath channel widths of 465 μm and a sample cell channel width of 70 μm.

Figure 2.4a shows an image of the final microfluidic cytometry chip design with arrows indicating fluid flow direction. The size of the monolithic glass device is 25.4 mm x 50.8 mm x 1.8 mm. The chip uses a vacuum source applied at a single sample waste port (SW) to control the fluid flow from both the sample cell (SC) and sheath buffer (SB) channels. Using a single vacuum source is advantageous as it reduces off-chip complexity compared to applying positive pressure at both SC and SB to drive flow. Another advantage is that the focused sample cell stream dimensions at the detection region are relatively independent of the fluid velocity—given the diffusion coefficient of a lymphocyte—and will therefore not depend significantly on the magnitude of the applied sub-ambient pressure. This is a result of the constant ratio of sheath to sample

fluid flow, defined by the channel architecture. Consequently, the chip can be run at different analysis rates through control of the single vacuum source without affecting the focused stream profile. A third advantage is that by splitting the sheath buffer flow into identical focusing channels (f1, f2), a symmetrically focused stream at the detection region results since the flow rates in f1 and f2 are identical. Figure 2.4b shows a photograph of the microfluidic device in operational form with glass reservoirs attached for introducing sheath and cell solutions and a threaded nanoport attached for applying vacuum to the device.

2.4 Experimental

2.4.1 Computational Fluid Dynamic Simulations

Microchannel architectures were modeled using Coventorware fluid dynamic simulations software (Coventor, Cary, NC) to allow in silico optimization of the hydrodynamic focusing performance. Simulations were performed for prospective flow chamber designs by modeling the hydrodynamic focusing intersection of a dye solution having a diffusion coefficient of 2.6×10^{-6} cm^2 s^{-1}—instead of a solution containing suspended cells—with water when sub-ambient pressure is applied below the intersection. Simulated fluid flow was achieved through the application of 10^{-3} torr of pressure below the intersection of the cell and sheath solutions.

2.4.2 Microchip Fabrication

Glass microfluidic chips were fabricated using standard wet chemical etching techniques as described previously.[3-5] White crown glass substrates (B270) coated with chromium and positive photoresist (Telic Co., Valencia, CA) were patterned with the chip design by flood UV exposure using a custom photomask (Photoplot Store, Colorado Springs, CO). After photoresist development (MF-319; Microchem, Newton, MA) and removal of exposed chromium (Chromium Etchant; Transene, Danvers, MA), channels were etched into the glass substrate using a dilute HF/NH_4F solution (10:1 Buffered Oxide Etch; Transene). Etching was allowed to proceed until the desired dimensions were obtained as determined by profilometry (P-15; KLA-Tencor, San Jose, CA). The etched substrates were then diced and access holes made by powder blasting (Comco Inc., Burbank, CA). All glass was then thoroughly cleaned by sonication in a 5% solution of Contrad (Fisher, Waltham, MA) for ten minutes, followed by immersion in Nanostrip solution (Cyantek Corp., Fremont, CA) for 30 minutes. Etched glass substrates and glass cover plates were then hydrolyzed in a 2:2:1 solution of $H_2O/NH_4OH/H_2O_2$ for 30 minutes at 70°C, and thermally bonded at 550°C for ten hours. Buffer and cell solution reservoirs were made by attaching glass cloning cylinders (Fisher) over via holes using a two-part epoxy. A poly(etheretherketone) (PEEK) nanoport fitting (Upchurch Scientific, Oak Harbor, WA) was attached to the microchip waste port in order to apply sub-ambient pressure for fluid manipulation. A 10/32 threaded PEEK fitting was used to attach the nanoport to a segment of 0.04'' ID PEEK tubing for connection to a Venturi style vacuum pump (Vaccon, Medfield, MA).

2.4.3 Surface Modification

To reduce cell and cell debris adhesion to the microfluidic channel walls, a thin coating of polyethylene glycol (PEG) was covalently attached to all the channels. A modified procedure from that described by Razunguzwa et al.[6] was employed for the PEG coating. First, 1 N NaOH was drawn through the channels for 30 minutes to hydrolyze the glass surface. The chip was then flushed with Nanopure H_2O for 10 minutes, dried by pulling air through the chip, followed by flushing with dry toluene for 5 minutes. The channels were filled with a solution of N-(triethoxysilylpropyl)-O-polyethylene oxide urethane (MW= 500) (120 mg/mL) (Gelest Inc., Morrisville, PA) in toluene and left to react at room temperature for 8 hours. The chip was then flushed with toluene for 5 minutes and dried at 80 °C for 3 hours.

2.4.4 Optical Instrumentation

Laser excitation was obtained using a 488-nm solid-state laser (40 mW) (Cyan; Newport Corp., Irvine, CA). Fluorescence and scatter signals were collected using a 40x microscope objective (NA=0.45) (Creative Devices Inc., Neshanic Station, NJ). Optical filters including dichroic mirrors, band-pass filters, and long-pass filters were purchased from Semrock (Rochester, NY). The elastic scatter signal was detected using a photodiode detector (Thorlabs Inc., Newton, NJ). Fluorescence signals were spatially filtered using a 400-μm slit (Thorlabs Inc., Newton, NJ), and directed to photomultiplier tubes for detection (PMT) (H6780; Hamamatsu Photonics, Bridgewater, NJ).

A schematic of the optical detection configuration is shown in Figure 2.5, and a photograph of the detection system is shown in Figure 2.6. The 488-nm solid-state laser (40 mW) was focused to an elliptical spot (15 μm x 100 μm) from above the chip using a pair of crossed cylindrical lenses.[1] A photograph of the crossed cylindrical lens pair is shown in Figure 2.7a. A 40x microscope objective (NA=0.45) was positioned under the microchip for the collection of fluorescence and elastic scatter. The elastic scatter signal is separated from the fluorescence by passing the collected light through a 495-nm cutoff dichroic mirror. The reflected scatter signal is then directed to a photodiode for detection. The transmitted fluorescence light is spatially filtered using a 400-μm slit, and then passed through a 493-nm long pass filter to remove any incident laser light.

Common fluorescent markers used in combination with 488-nm laser excitation include FITC, AF488, PE, Calcein, and PerCP as well as tandem dye conjugates such as PE-Texas Red, PE-AF610, PE-Cy5 and PerCP-Cy5.5. This instrument is generally configured to detect FITC with a tandem dye such as PE-Texas Red. For this specific application, a 593 nm cutoff dichroic mirror splits the incident fluorescence into two channels, followed by band-pass filtering before detection with separate PMT's. FITC fluorescence signals are passed through a bandpass filter with a maximum transmittance of 536-nm with a 40-nm bandwidth, while PE-Texas Red fluorescence is passed through a 624-nm maximum transmittance filter also having a 40-nm bandwidth. Figure 2.7b shows a photograph of the fluorescence detection region of the instrument, showing a filter wheel mounted in front of each PMT to easily modify the spectral detection capabilities of the instrument by changing the band-pass filters based on the specific fluorescent molecule pair employed.

2.4.5 Signal Processing

Current outputs from each PMT are amplified through individual low-noise current preamplifiers (SR570; Stanford Research Systems, Sunnyvale, CA), and digitized using a 16-bit multifunction I/O card (PCI-6251 National Instruments, Austin, TX). A 14-bit high speed digitizer (National Instruments PXI-5122) has also been incorporated for experiments where long acquisition times and acquisition rates over 1 MHz are required. Data acquisition and the extraction of cell signal information from raw data was performed using custom LabVIEW (National Instruments) programs.

Current signals output from the PMT's and photodiode detectors were passed through a current to voltage amplifier, and resulting voltage signals were transferred to a data acquisition card. Custom LabVIEW software was used to save data output from each detector, and process raw data signals in order to extract event information. Raw fluorescence and scatter data from each channel was analyzed in LabVIEW to find signals above a defined threshold. The optical signals in each channel were then correlated, and peak intensities and areas are extracted to display as distribution histograms and scatter plots. Screen captures, photographs, and descriptions of the hardware and software programs used are displayed in Appendices.

2.5 Conclusions

Efforts to design and construct the microfluidic cytometry device and optical detection configuration were described in this chapter. To design a flow chamber that is driven solely by applying a sub-ambient pressure, calculations were performed to ensure

the proper ratio of cell to sheath channel hydraulic resistances were achieved to obtain the desired hydrodynamic focusing properties. Computational fluid dynamic simulations were used in combination with these calculations to determine the optimal focusing angle at the intersection of sheath buffer and cell solutions in the flow chamber.

The optical detection system assembled was based on a simplified version of state-of-the-art cytometry optical designs, maintaining the capacity to simultaneously detect forward scattered light and two fluorescence channels from individual cells. Further, the system was constructed to facilitate rapid removal of the microfluidic device for disposable applications. In addition, the instrument was designed to easily vary the fluorescence detection characteristics of the system through the use of filter wheels and cage cube systems from which filters can be quickly substituted.

2.6 Figures

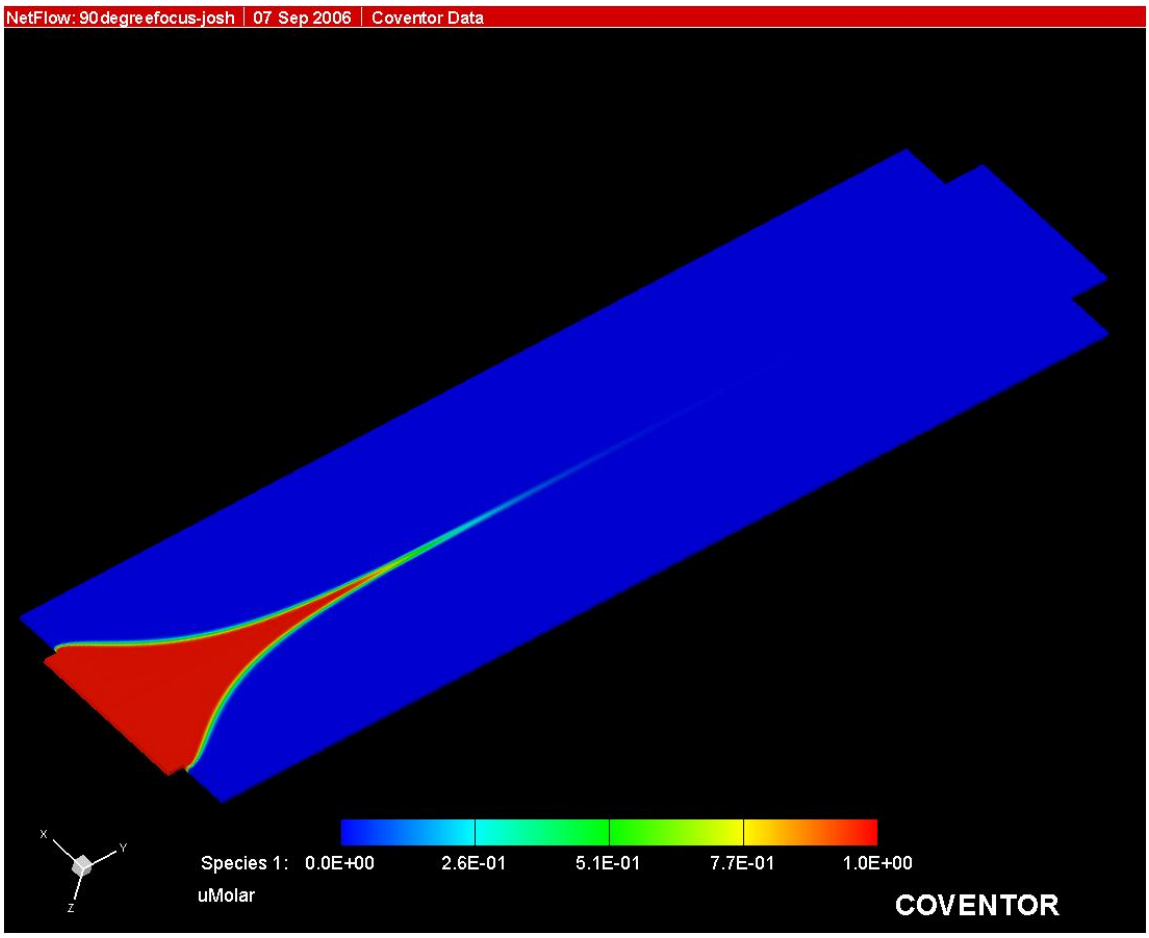

Figure 2.1 Result from a computational fluid dynamic simulation of a prospective microfluidic flow chamber design where the sheath buffer intersects the cell solution at a 90º angle.

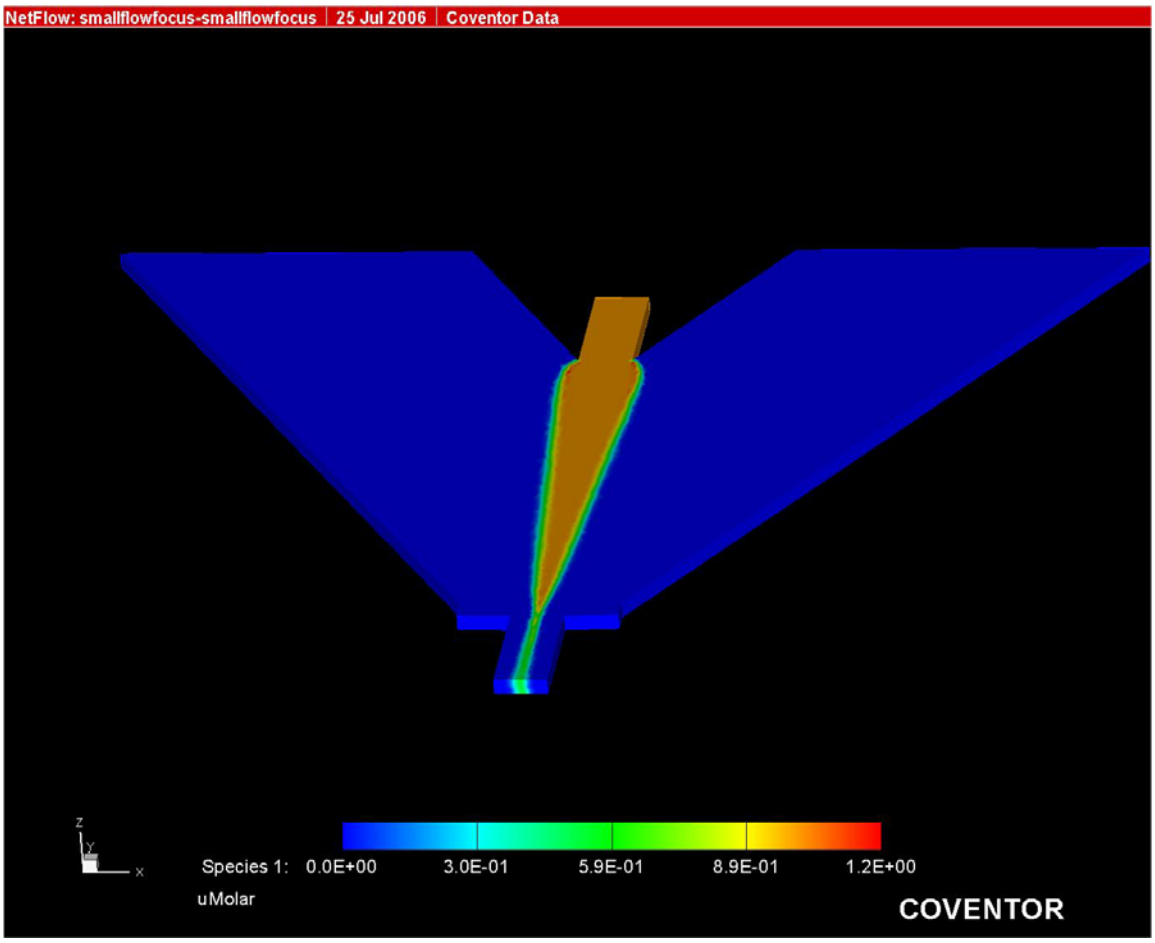

Figure 2.2 Result from a computational fluid dynamic simulation of a prospective microfluidic flow chamber design where the sheath buffer intersects the cell solution at a 35º angle.

A

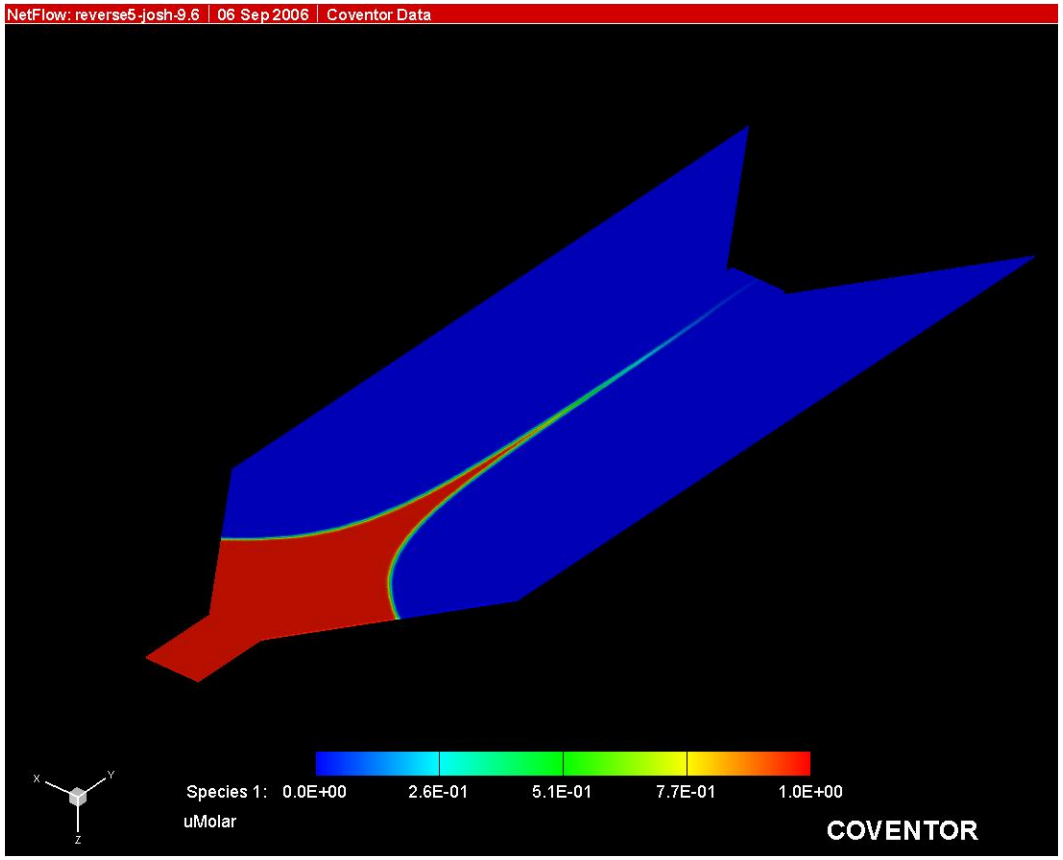

B

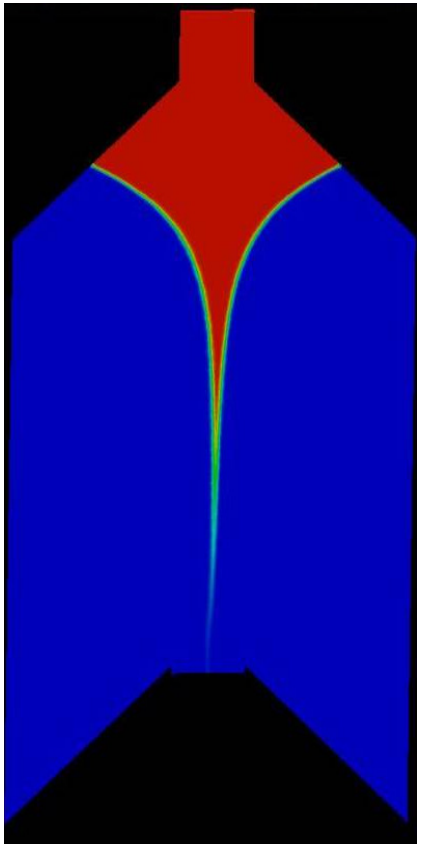

Figure 2.3 Result from computational fluid dynamic simulation of a prospective microfluidic flow chamber design where the sheath buffer intersects the cell solution at a 135º angle.

A

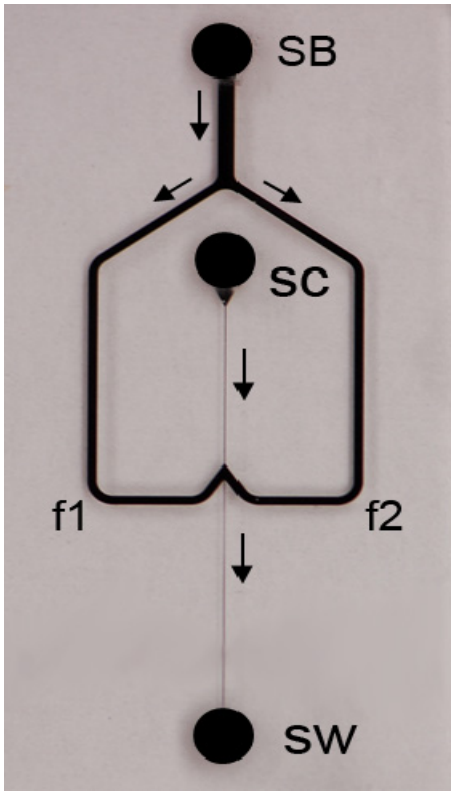

B

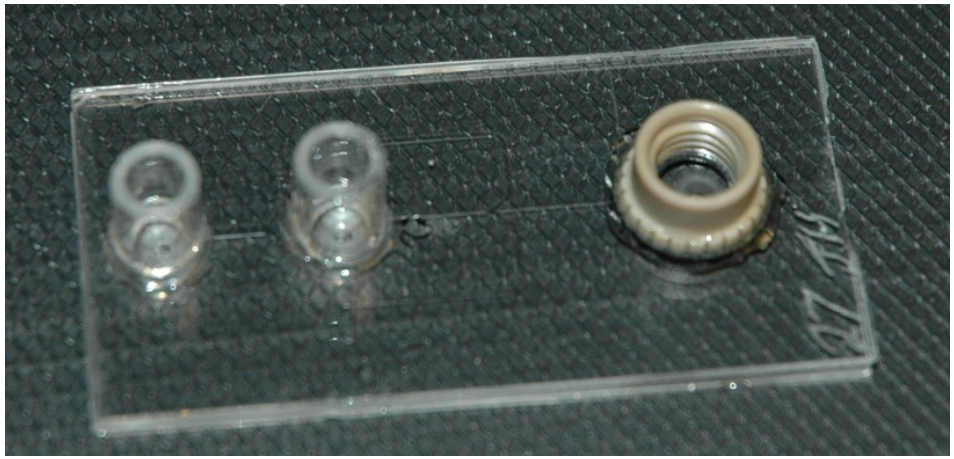

Figure 2.4 (A) Photograph of the glass microfluidic device loaded with dye for better visualization of the channels. **(B)** Photograph of the microfluidic device in operational form with glass cylinders secured to the chip over the sheath buffer (SB) and cell solution (SC) reservoirs, and a threaded PEEK nanoport attached over the sample waste (SW) channel for vacuum connection.

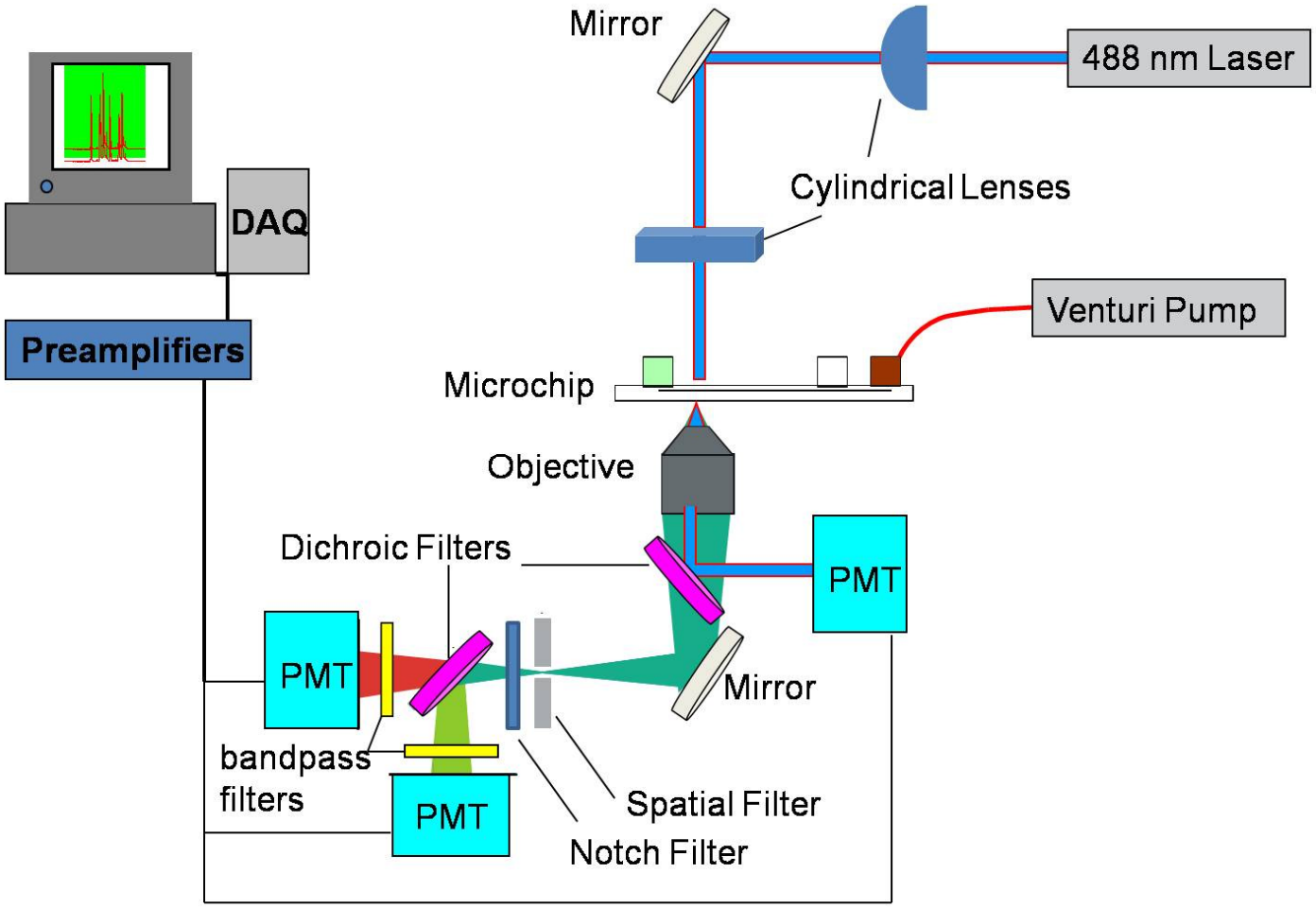

Figure 2.5 Schematic diagram of the optical detection setup of the microfluidic cytometry instrument for the detection of two fluorescence channels and forward-scattered light.

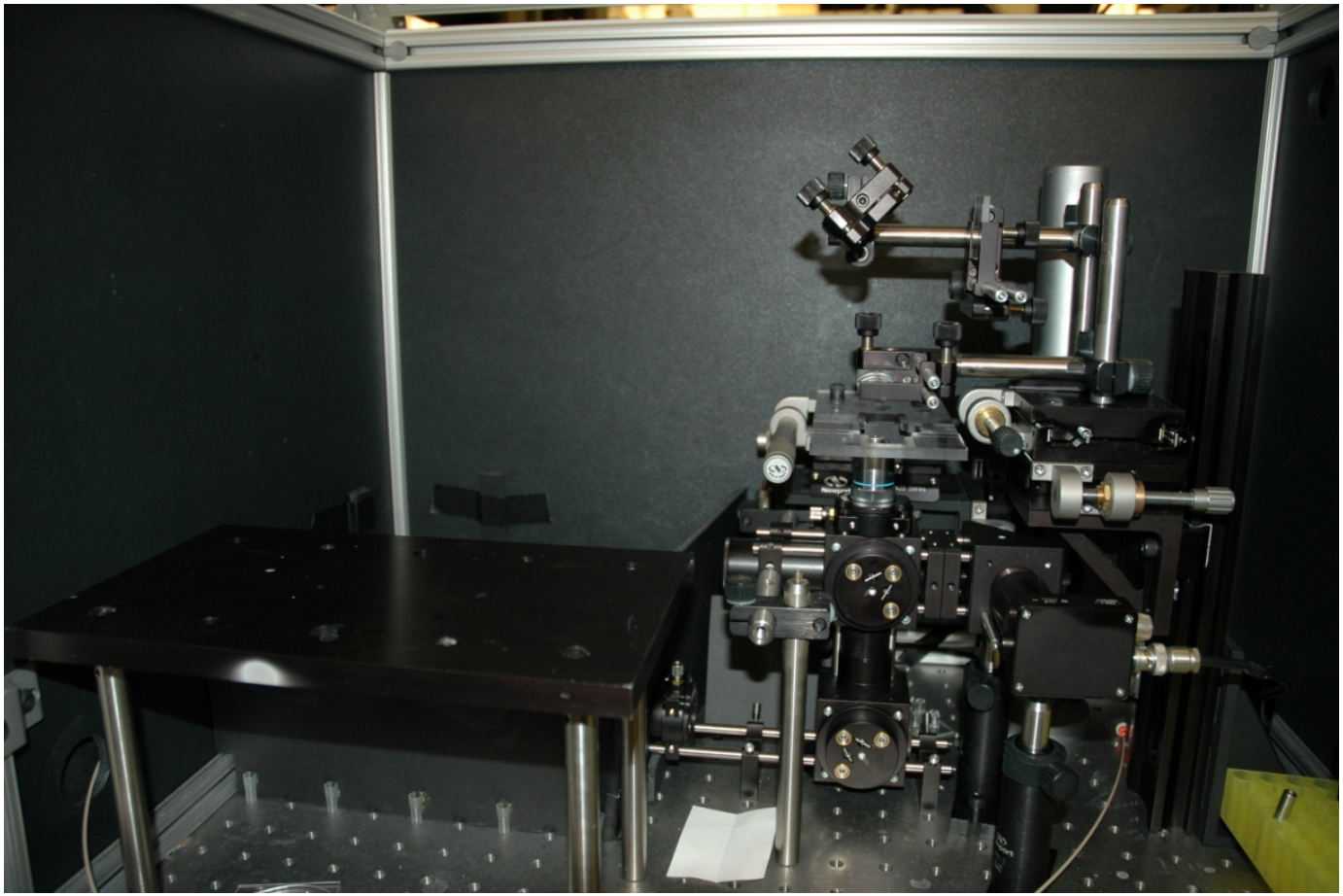

Figure 2.6 Photograph of the microfluidic flow cytometry detection system assembled on an optical table within a dark box.

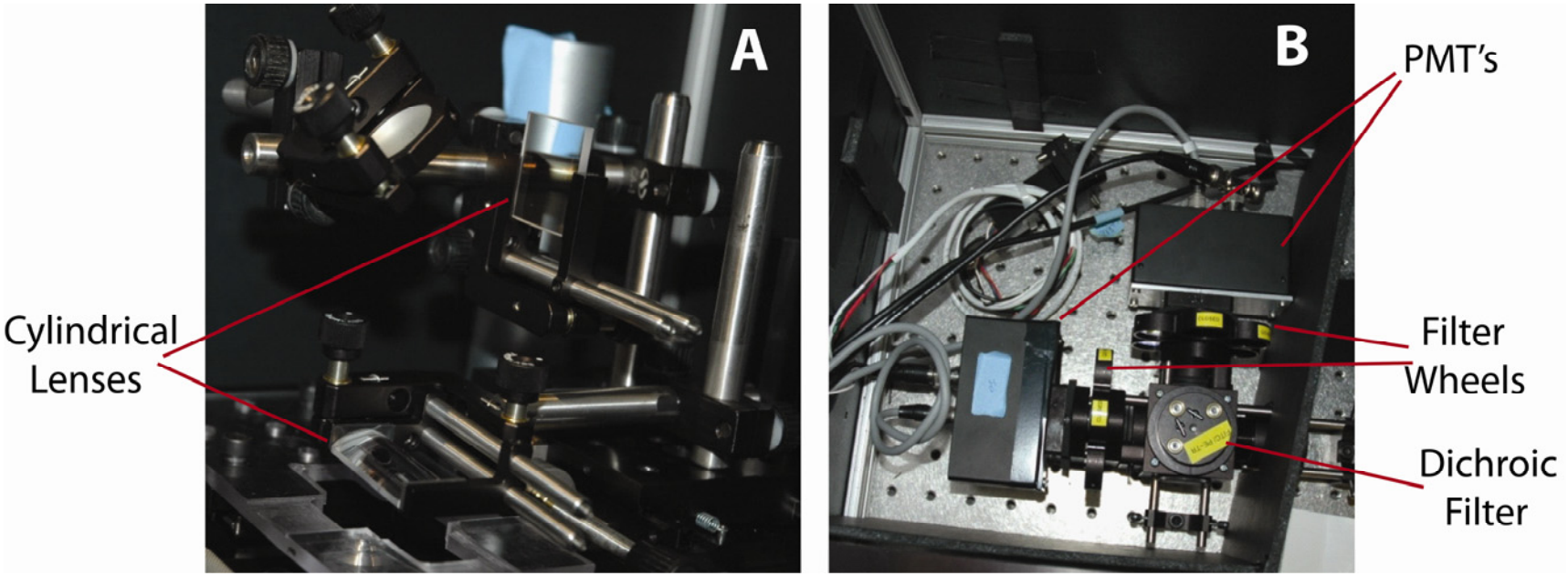

Figure 2.7 (A) Close-up photograph of the laser beam focusing optical lenses. **(B)** Photograph of the fluorescence detection region of the optical assembly including the filter wheels for quickly changing the bandpass filters in front of each PMT.

2.7 References

(1) Watson, J. V. *Cytometry* **1981**, *2*, 14-19.

(2) Jacobson, S. C.; Ramsey, J. M. *Anal Chem* **1997**, *69*, 3212-3217.

(3) McClain, M. A.; Culbertson, C. T.; Jacobson, S. C.; Ramsey, J. M. *Anal Chem* **2001**, *73*, 5334-5338.

(4) Poulsen, C. R.; Culbertson, C. T.; Jacobson, S. C.; Ramsey, J. M. *Analytical Chemistry* **2005**, *77*, 667.

(5) Jacobson, S. C.; Hergenroder, R.; Koutny, L. B.; Warmack, R. J.; Ramsey, J. M. *Analytical Chemistry* **1994**, *66*, 1107-1113.

(6) Razunguzwa, T. T.; Warrier, M.; Timperman, A. T. *Analytical Chemistry* **2006**, *78*, 4326-4333.

CHAPTER 3:

CHARACTERIZATION OF THE MICROFLUIDIC FLOW CYTOMETRY SYSTEM

3.1 Introduction

The instrument described in this dissertation was designed with specific performance objectives. One objective was to ensure proper hydrodynamic focusing of cells on-chip to facilitate accurate flow cytometry measurements. Another goal was to maximize the cell throughput possible using the microfluidic instrument. An additional criterion for this instrument was to have fluorescence detection precision rivaling that of commercial instrumentation. A final goal was to develop and characterize scatter-based detection for label-free identification of cells or particles with accurate size-based discrimination.

This chapter focuses on the initial experiments designed to characterize the hydrodynamic focusing properties, cell throughput, fluorescence detection precision, and scatter detection performance of the microfluidic flow cytometer. Optical imaging, confocal imaging, fluorescent microbead analysis, and fluorescently labeled cells were employed to characterize the performance characteristics of the instrument.

3.2 Experimental

3.2.1 Optical Imaging

Optical images shown were obtained with an inverted microscope (TE300; Nikon, Melville, NY) equipped with a high-pressure mercury arc lamp using 10 - 40x objectives, and a CCD camera (NTE/CCD-512-EBFT; Roper Scientific, Trenton, NJ) using IPlab Spectrum acquisition software (Scanalytics Corp., Vienna, VA). Confocal microscopy images were taken with a Zeiss 510 Meta laser-scanning confocal microscope (Zeiss, Thornwood, NY) using 10x or 60x water immersion objectives.

3.2.2 Cell Handling

Human Jurkat T-cell lines (TIB-152) (American Type Culture Collection, Rockville, MD) were cultured in RPMI 1640 media supplemented with 10% by volume fetal calf serum, penicillin (100 IU/mL), and streptomycin (100 μg/mL) (Invitrogen Corp., Carlsbad, CA). Cell washing and staining were done in phosphate buffered saline (PBS) (pH=7.4) supplemented with fetal calf serum (BD Biosciences, San Jose, CA). The cells ($\approx 10^6$) were washed with 500 μL of the PBS solution and then pelleted by centrifugation at 300x g. The supernatant was discarded and the washing procedure repeated two times before the cells were finally dispersed in 50 μL of the supplemented PBS buffer. Cells were then labeled with an intracellular fluorescent dye by incubating them at room temperature with 2 μL of Calcein-AM (1 μg/mL) (Invitrogen Corp.) for 30 minutes.

3.2.3 Cytometry Comparison Experiments

To evaluate precision, commercially available 6-μm diameter BODIPY doped calibration beads (AlignFlow Plus; Invitrogen) were analyzed on both the microfabricated cytometer and a commercial Cyan ADP flow cytometry system (Beckman-Coulter, Fullerton, CA). Optical filters in the microfluidic instrument were chosen to duplicate those used in the FL1 and FL3 Cyan system fluorescence channels.

3.3 Results

3.3.1 Characterizing Hydrodynamic Focusing Performance

To experimentally assess the hydrodynamic focusing characteristics of the microfluidic flow chamber, a fluorescent dye solution was introduced on-chip at the cell sample reservoir, water was input at the sheath buffer reservoir, and vacuum was applied at the sample waste reservoir. This investigation was an experimental verification of the computational fluid dynamic simulations described in Chapter 2. Figure 3.1a shows the resulting fluorescent image of Rhodamine B dye focused at the intersection of the cell sample channel and focusing channels. Figure 3.1b shows a 60x magnified image of the focused Rhodamine B dye stream as it enters the analysis channel. A line profile taken at the detection region 2 mm below the intersection of the cell and focusing streams shows the dye is hydrodynamically focused to a width of 9 μm. This result corroborates the result of the computational fluid dynamic simulations, and verifies that the flow chamber effectively focuses the cell stream to the approximate diameter of a lymphocyte.

In addition to investigating the flow profile in the xy-plane, confocal imaging was utilized to examine the cell stream profile after hydrodynamic focusing in the z-plane through the depth of the microchannel. A xz-profile was acquired by taking optical measurements translating through the depth of the channel in 2.0 μm steps. The resulting stacked image is shown in Figure 3.2. In this experiment, a solution of Rhodamine B (red) was introduced into the sheath buffer channel, and a solution of FITC dye (green) was introduced at the cell sample input. This result reveals that the width of the focused FITC profile remains constant throughout the depth of the microchannel. This result also confirms that there is no focusing occurring in the z-plane, as expected.

Hydrodynamic focusing of cells was investigated by introducing a solution of Calcein labeled Jurkat cells into the cell sample reservoir and using PBS buffer as the sheath fluid. Figure 3.3 shows a 1-second time-integrated CCD image of the fluorescently-labeled Jurkat cells (10^7/mL) hydrodynamically focused into a single file on-chip. The slightly wider lateral trajectories of the cells compared to the dye molecules at the entrance to the focusing region can be attributed to their larger momentum compared to the dye molecules. Nonetheless, the cells are adequately focused into single file as they enter the center analysis channel downstream from the sheath fluid intersection.

3.3.2 Cytometry Measurement Precision

AlignFlow Plus fluorescent beads having minimal bead-to-bead intensity variation were run on the microfluidic cytometry chip and a Beckman-Coulter Cyan ADP

flow cytometer in order to compare system measurement precision. Comparisons of precision were performed by evaluating the coefficients of variation (CV), defined as the quotient of the standard deviation of the bead intensities and the mean detected bead intensities, obtained from both systems. The fluorescence emission of the beads covers a wide spectrum (515-660 nm) that is detectable by both the green and red fluorescence channels of both systems. The beads were run at a throughput rate of 120 Hz with more than 10,000 beads counted over the course of 90 seconds.

Figure 3.4a displays a segment of the raw PMT data showing the detection of numerous beads in the green fluorescence channel of the microfluidic cytometry system. Figure 3.4b is a histogram showing the intensity distribution (arbitrary units) of the data shown from the analysis of the same beads detected in Figure 3.4a with the green fluorescence channel. Figure 3.5 is a two-color scatter plot for the dual channel detection of the calibration beads, showing narrow intensity distributions in both channels as seen by the tight grouping of the detected events. The resulting histogram has a semi-Gaussian profile with a CV of 5.9% in the green detection channel. Using the Cyan ADP system, a CV of 4.4% was obtained. The manufacturer reports a CV of 4.4% as determined using a FACScan flow cytometry system.

The higher CV value for the microfluidic system compared to both the Cyan and manufacturers' value is most likely due to the planar focusing scheme used for the microchip compared to the focusing used in the commercial instrumentation or other microfluidic designs.[1] For the microchip described here, the beads lateral position—within the plane of the chip—in the detection region should remain constant due to the focused stream; however, the bead position in the z-plane—normal to chip plane—can

vary within the channel depth leading to small variations in the velocity of the bead. These variations result in changes in the measured bead intensity since slower beads remain in the detection region longer than faster traveling beads. This effect can be minimized by reducing the channel depth but at the cost of increasing the possibility of chip failure by fouling or clogging as the channel depth approaches the cell size. As a compromise, a channel depth between 15-20 μm was used for the analysis of cells on the order of 10-μm in diameter. Alternatively, the depth of focus of the collection optics—which is ≈1.2-μm as currently configured—could be increased by reducing the numerical aperture at the cost of reduced light collection.

3.3.3 Assessment of System Throughput

The initial design goal for the throughput of the vacuum driven system was to analyze cells at rates above 1 kHz. While this objective is not close to commercial system throughput, the purpose was to generate sufficient cell counts within a short time period (less than 30 minutes total) to successfully compare results to those obtained using commercial systems. The cellular throughput was determined by analyzing a 100-μL solution of cultured Jurkat cells (10^7/mL) labeled with the intracellular fluorescent dye Calcein. The cell solution was pulled through the chip with a pressure differential of approximately 100 torr. Figure 3.6 shows the detection of 5 individually resolved Jurkat cells in less than 2 ms using a single fluorescence channel. The entire experiment resulted in the detection of over 22,000 cells during a 10 second acquisition. Detected cells had an average linear velocity of approximately 12 cm/s. These results demonstrate

cellular detection at a throughput greater than 2 kHz. Furthermore, fluorescently doped 2-μm diameter polystyrene beads have been detected at rates greater than 5 kHz using the same vacuum driven system, indicating higher cellular throughputs can be achieved using increased cell or particle concentrations and by realizing higher flow rates.

One method to achieve higher flow rates, and therefore higher analysis throughput is by using positive pressure to drive fluid. This can be accomplished using the same microfluidic device described, except threaded nanoport fittings must be secured to the sheath buffer and cell sample inputs. Generated pressure differentials and fluid flow rates can be significantly increased over the vacuum driven system using this approach. Figure 3.7 shows the result obtained from the detection of Calcein labeled SUP-T1 cells pushed through the microfluidic cytometry chip at a concentration of 4 million cells per mL. This result shows the detection of 3 individually resolved cells in less than 200 μs. The flow rates applied to the sheath and cell inputs were 350 μL/min and 100 μL/min, respectively. Cell velocities were measured to be approximately 75 cm/s. This experiment resulted in the detection of over 10^5 cells in a period of 10 seconds, indicating a throughput of approximately 12 kHz.

3.3.4 Scatter Based Detection

In addition to fluorescence based cellular detection, light scattering methods can be used for cellular detection independent of luminescent probes. Scatter signals can help simplify experiments as one less fluorescent probe is necessary for cellular detection, and can be particularly useful for size-based cell type discrimination. Additionally, scatter

based cellular detection is commonly used to trigger data acquisition in the fluorescence channels in order to avoid collecting unnecessary data when no cells are present in the detection region. Forward scatter and extinction have been demonstrated using this system for cellular detection and size-based discrimination. A 1:1 mixture of 5.7-μm and 9.8-μm diameter FITC doped polystyrene beads was analyzed on-chip in order to demonstrate that forward scatter and extinction based detection can be used for cell sizing and label-free cellular enumeration. Figure 3.8 shows the detection of a 9.8-μm bead followed by a 5.7-μm bead, identified as peaks in the bottom fluorescence trace and small forward scatter peaks followed by extinction valleys in the top scatter trace. Since the amplitude of the scatter intensities are related to the square of the detected bead radius, the size of the beads for each detected event was confirmed by ensuring that the ratio of the extinction valley depths corresponded to the expected difference between the 5.7 and 9.8 μm beads. The average ratio of the signal amplitudes was 3.2 ± 0.3, which is statistically the equivalent to an expected ratio of 3.0 ($p > 0.05$, 95% confidence limit).

3.4 Conclusions

The microfluidic cytometry instrument was designed to operate as a simple, miniaturized version of large-scale commercial cytometers. As such, some design criteria were developed to ensure comparable instrumental operation. The fluidic focusing features contained within the glass microchip were designed to focus the cell sample stream to a width of 10-μm, and this result was verified using an inverted fluorescence microscope to characterize the focused profile of a dye solution on-chip.

Confocal microscopy was used to further characterize the hydrodynamic focusing properties of the microfluidic flow chamber by stacking multiple images to reveal the cell stream profile throughout the depth of the microchannel. Further experiments were performed using fluorescently labeled cells to confirm that cells are effectively focused as they enter the analysis channel. These results indicated that the microfluidic device adequately focuses the cell stream to a width of 9-μm and confirmed that the cells are aligned in single-file as they enter the laser interrogation region of the analysis channel.

Measurements of fluorophore doped polystyrene alignment beads were made to test the precision of the microfluidic cytometer. The small variation in detected signal from bead to bead confirms that the time each bead spends in the laser interrogation and detection region is reproducible. The CV values obtained from detecting the beads using the microfluidic system were similar to those obtained using a commercial system, indicating that the measurement precision is close to that obtained using the commercial system. A consequence of the slightly higher CV values obtained using the microfluidic system is lower resolving power. However, this difference should not be significant enough to preclude the utility of the system for many biological diagnostic and monitoring applications.

To ensure that the microfluidic system could operate fast enough to characterize a biological sample within 30 minutes, system throughput was evaluated. Using vacuum to manipulate fluids on-chip, a throughput of 2 kHz was observed, which is sufficient for many applications. With positive pressure the observed system throughput was greater than 12 kHz. This enhanced throughput may prove necessary for applications that require the rapid analysis of large sample volumes to enumerate rare cells. Two pumps

are required for fluid delivery using positive pressure, however, instead of one for vacuum operation.

Light scatter based detection was demonstrated on-chip for many purposes. First, elastic light scatter can be used to detect cells or particles without the use of any extrinsic labels. In addition, the scatter signal can be used to trigger data acquisition to reduce the amount of raw data that requires processing. Finally, light scatter can be used to differentiate cells or particles based on size. A mixture of two different sizes of fluorescently doped beads was analyzed using the microfluidic system to effectively demonstrate the ability to detect cells or particulates independent of fluorescent labels and to differentiate them based on size.

The experiments described in this chapter were devised to characterize the operational performance of the microfluidic cytometry system. The results were used to demonstrate instrument functionality and ensure that design criteria were either met or exceeded. It is important to point out that parameters such as measurement precision and throughput are lower than commercial systems, and scatter based detection capabilities are more limited because side scatter is not detected. This restricts the number of applications for the instrumentation relative to conventional cytometry. However, the performance of the microfluidic system is sufficient for many biological applications, some of which were explored. These will be discussed in the remaining chapters of this dissertation.

3.5 Figures

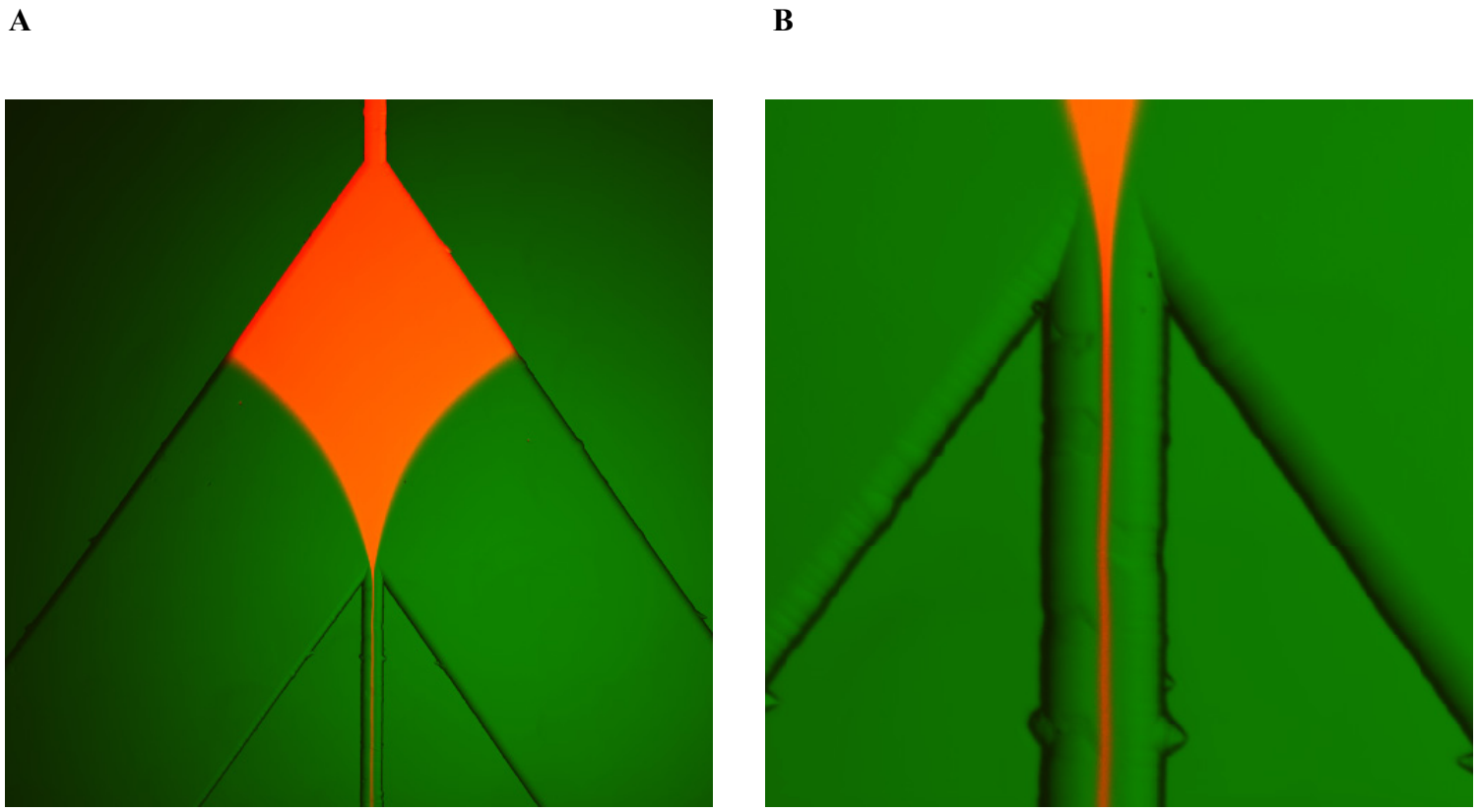

Figure 3.1 Optical images obtained using the Zeiss 510 Meta confocal microscope to characterize the hydrodynamic focusing properties of the microfluidic flow chamber. Vacuum was applied below the sheath buffer and cell sample intersection. **(A)** Magnified image (10x) of Rhodamine B hydrodynamically focused with water. **(B)** Magnified image (60x) of the hydrodynamically focused Rhodamine B dye solution as it enters the analysis channel.

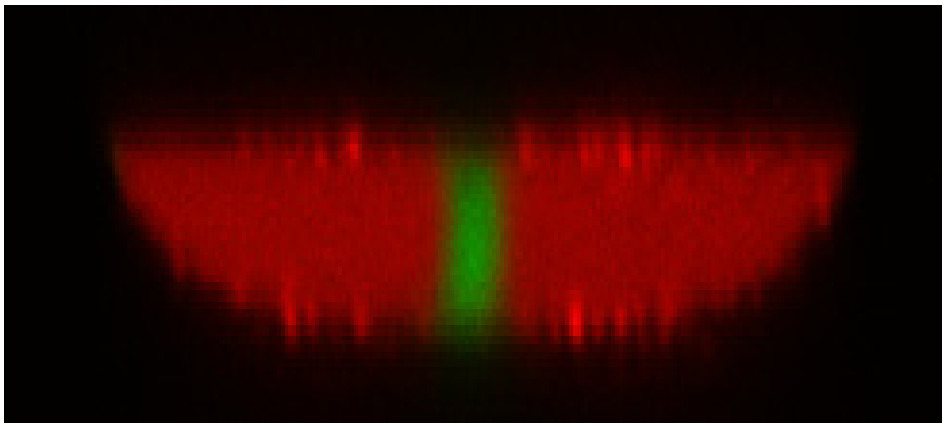

Figure 3.2 Stacked confocal xz-profile using Rhodamine B sheath solution (red) and FITC dye (green) in the sample stream to investigate the fluid profile below the hydrodynamic focusing intersection on the microfluidic flow chamber.

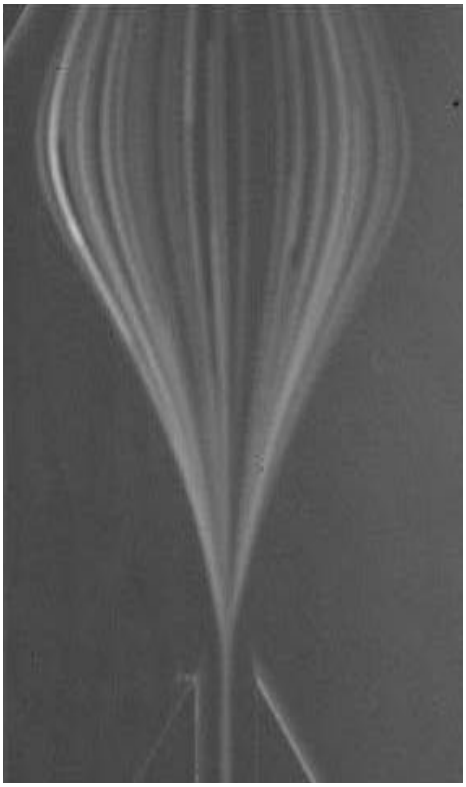

Figure 3.3 Time-integrated (1-sec) CCD image of an operating microfluidic flow cytometry chip taken to investigate hydrodynamic focusing properties. PBS buffer was introduced in the sheath buffer reservoir and a solution of Calcein labeled Jurkat cells at the cell sample input.

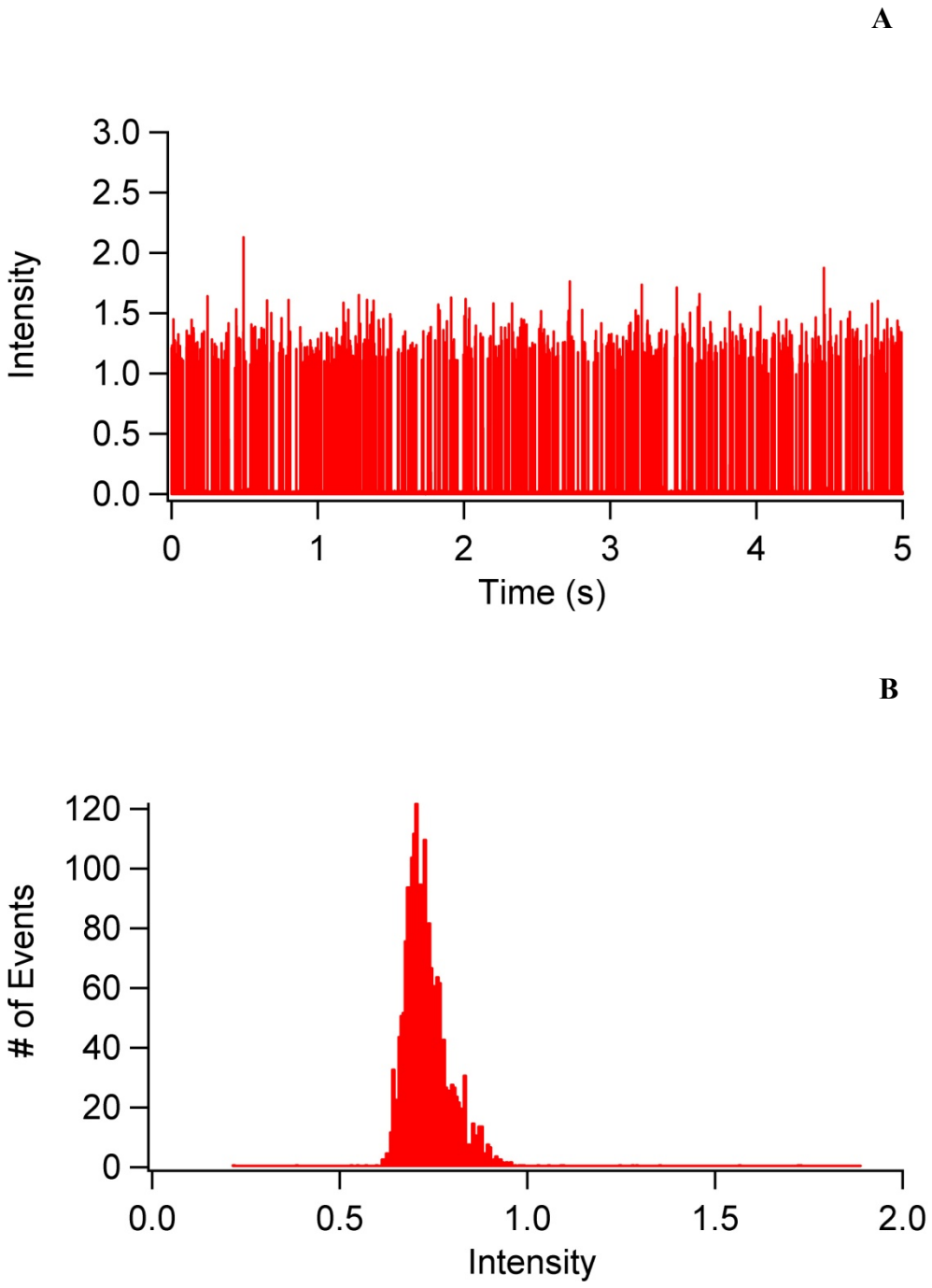

Figure 3.4 **(A)** Raw PMT data for the detection of multiple individually resolved 6-µm AlignFlow Plus fluorescent beads using the red fluorescence channel in the microfluidic cytometry system. **(B)** Peak intensity distribution obtained for the detection of the same beads using the green fluorescence channel.

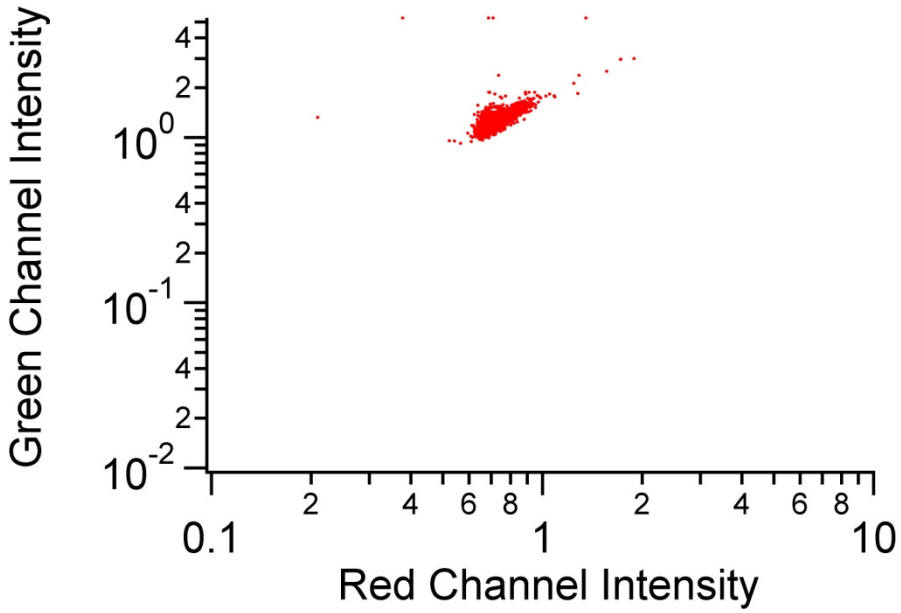

Figure 3.5 Scatter plot showing the result for dual-channel detection of 6-µm AlignFlow Plus calibration beads using the microfluidic system.

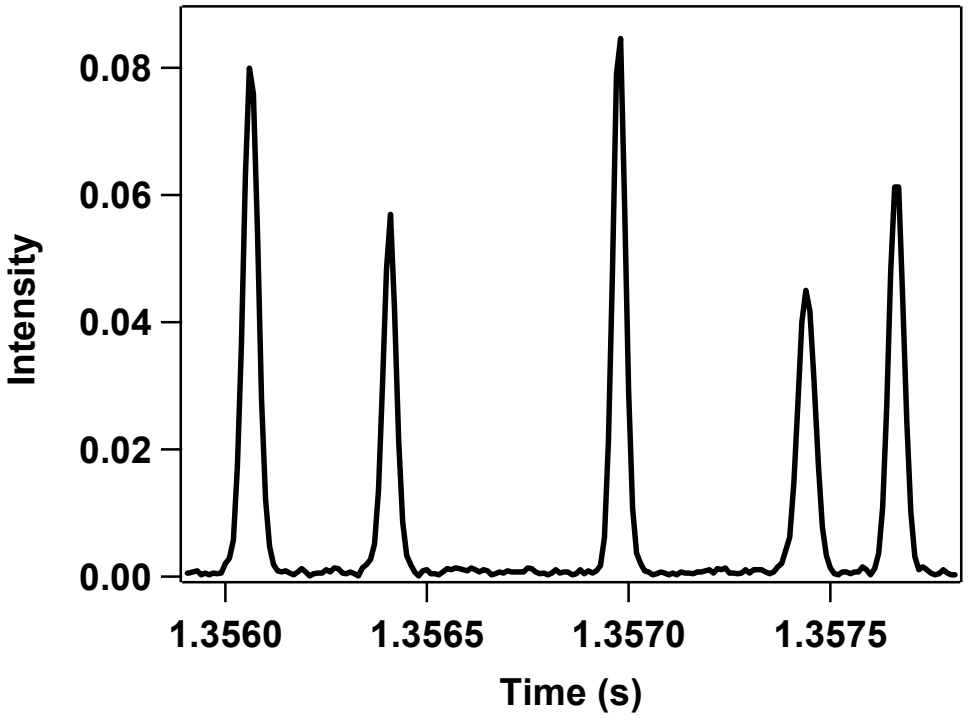

Figure 3.6 Result for the detection of Calcein labeled Jurkat cells using the microfluidic cytometry system and vacuum driven flow to determine throughput. Five cells were detected in less than 2 ms.

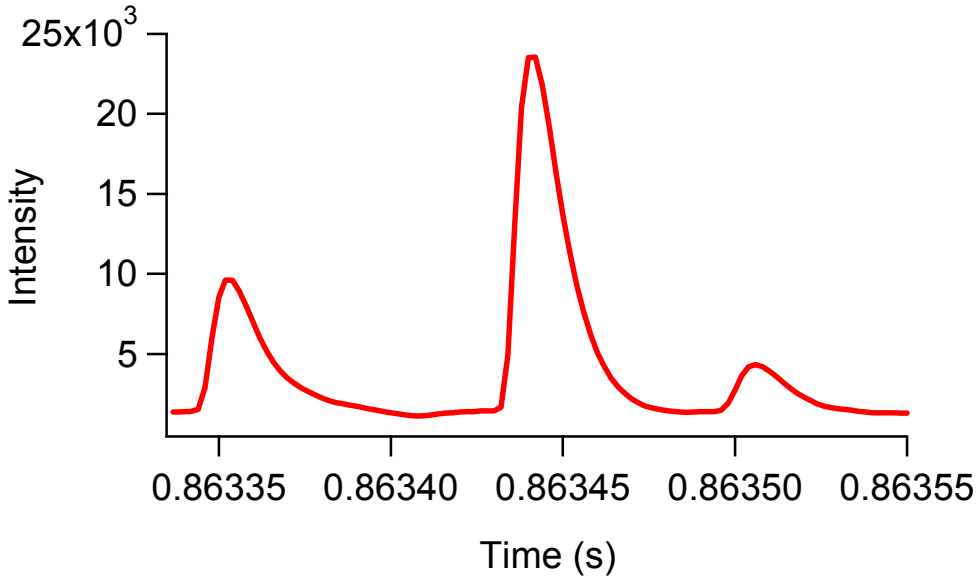

Figure 3.7 Result for the detection of Calcein labeled SUP-T1 cells using positive pressure driven flow on the microfluidic cytometry system. Three cells were detected in less than 200 μs.

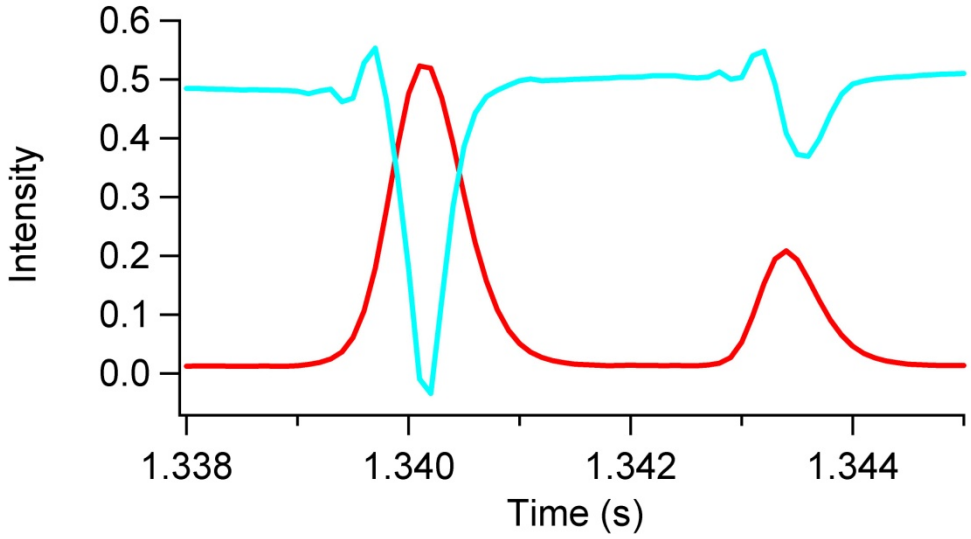

Figure 3.8 Detection of a mixture of 5.7-µm and 9.8-µm diameter FITC doped beads using scatter based detection (blue trace) and fluorescence (red trace).

3.6 References

(1) Mao, X.; Lin, S. C.; Dong, C.; Huang, T. J. *Lab Chip* 2009, *9*, 1583-1589.

CHAPTER 4:

IMMUNOPHENOTYPING ON-CHIP

4.1 Introduction

Blood cell characterization is important in the detection and monitoring of a number of disease states including HIV, leukemia, and lymphomas as concentrations of specific cell subsets can vary considerably from normal levels in infected patients.[1-4] Cellular discrimination based on surface protein expression is also valuable for the detection of rare circulating tumor cells in blood.[5] Therapeutic efficacy and dosage requirements may also be determined by monitoring the modulation in cell counts. On-chip monitoring of these changes in blood cell concentrations may prove valuable for rapid, inexpensive diagnostic and monitoring applications.

The differentiation of cell subsets in complex mixtures is a key aspect of most clinical flow cytometry applications. Populations of cell subsets have specific antigens present on their surfaces, allowing for direct labeling and identification using antibody probes conjugated to fluorescent dyes. Polyclonal antibodies can be utilized to simultaneously detect numerous cell subsets, while monoclonal antibody probes can be used for direct targeting and detection of a single cell subset. Conventional flow cytometry allows for the rapid characterization of cell populations by

immunophenotyping through the use of multiple fluorescently tagged antibodies. Instruments equipped with multiple fluorescence detection channels simultaneously detect multiple fluorescent signals on individual cells. In addition, solutions containing various cell types can be effectively characterized using multiple detection channels for each cell type. This allows for the rapid discrimination of cell subsets in complex cell mixtures such as blood, facilitating the widespread use of flow cytometry in clinical diagnostics.

Experiments testing the immunophenotyping capabilities of the microfluidic flow cytometry system are described in this chapter. Cultured cell mixtures and solutions of peripheral blood mononuclear cells were used to characterize the ability of the microfluidic system to differentiate cell types based on the presence of cell surface antigens using fluorescently labeled antibody probes. Results from the two-color microfluidic system were then compared to results obtained from a commercial cytometer to verify the accuracy of the microfluidic systems' immunophenotyping measurements.

4.2 Experimental

4.2.1 Cell Handling and Labeling

Human leukemic lymphoblasts (CCRF-CEM) and Jurkat cells (TIB-152) (American Type Culture Collection, Rockville, MD) were cultured and washed as previously described in section 3.2.2. Fluorescently labeled antibodies for CD3, CD4, and CD8 (5 μL) (Invitrogen) were added to the cell solutions, which were then incubated for

30 minutes in the dark with continuous mixing. Labeled cells were then washed and centrifuged twice, and redispersed in Cytofix buffer (BD Biosciences). The final cell concentration used for microchip experiments was 10^7/mL. Experiments performed to compare microchip results with a commercial cytometer utilized cell solution concentrations of 2 x 10^6 cells/mL.

4.2.2 Preparation of Peripheral Blood Mononuclear Cells

Whole human blood treated with the anti-coagulant heparin (Research Blood Components, Brighton MA) was purchased and processed to obtain enriched peripheral blood mononuclear cell (PBMC) samples for analysis. A standard density gradient separation was performed using Ficoll-Paque Plus (GE Healthcare, Uppsala, Sweden) to selectively remove unwanted erythrocytes and platelets. This was done by adding 1 mL of whole human blood to a tube containing 1.5 mL Ficoll and 1 mL PBS supplemented with 2% Fetal Bovine Serum, followed by centrifugation at 400g for 30 minutes. The layer of mononuclear cells between the plasma and ficoll media was carefully removed and washed with PBS. Remaining mononuclear cells were counted using a hemacytometer and labeled in the same manner as previously described.

4.2.3 Cytometry Comparison Experiments

To evaluate the immunophenotyping accuracy of the microfabricated cytometer, results were compared to the Cyan ADP flow cytometry system. Solutions of prepared

PBMC samples were analyzed on the Cyan cytometry system to determine CD4:CD8 ratios. Results from these analyses were then compared to results obtained from the analysis of the same samples using the microfluidic system.

4.3 Results

4.3.1 Immunophenotyping Cultured Cells

Model system mixtures of cultured T-lymphocytes and mononuclear cells isolated from whole blood were processed on chip to specifically discriminate T-cell subsets based on CD3, CD4, and CD8 antigen expression. The enumeration of these particular cell subtypes is important for monitoring HIV progression since the relative amount and concentration of $CD4^+$ lymphocytes, and the CD4:CD8 ratio is correlated to disease progression and can affect treatment selection.[6]

Figure 4.1a shows the result for the detection of a 1:1 mixture of cultured Jurkat T-cells ($CD3^+$) and CCRF-CEM human T-cells ($CD3^+$, $CD4^+$). FITC-labeled anti-CD3 and PE-AF610 labeled anti-CD4 antibodies were used to discriminate between the cell lines. Since both T-cell lines are known to express CD3, the FITC fluorescence channel detects every cell in the mixture. The cells expressing CD4 will exhibit a signal in both fluorescence channels and are double positive CCRF-CEM cells, while the cells not expressing CD4 are single positive Jurkat cells. An expanded subset of the data is shown in Figure 4.1b, which shows the detection of two Jurkat cells and two CEM cells as determined by the presence or absence of the CD4 label. A total of four 20 second experimental acquisitions were analyzed. Of the total number of cells counted for the

four experiments, 49.1 ± 3.8% were CD4 positive CCRF-CEM cells, statistically equivalent to the 50% input ratio ($p > 0.05$, 95% confidence limit), demonstrating that this system can accurately determine relative cell ratios from mixtures of T-lymphocytes. A scatter plot showing a subset of this result is shown in Figure 4.2 where the cell types are grouped together and are easily distinguished from each other based on the presence or absence of the CD4 antibody label.

4.3.2 Rare Cell Detection

The detection of rare cells was demonstrated by analyzing the same two labeled cell types as described in the previous section at a ratio of 1000:1 Jurkat to CEM, respectively. Cell concentrations were determined before mixing and labeling using a hemacytometer. The rare cell experiment was performed to ensure the accurate measurement of low concentration cells in the presence of a significantly higher concentration of cells on-chip. Figure 4.3a shows a result for the analysis of the rare cell mixture. Figure 4.3b shows an expanded subset showing the detection of a single rare double-positive CEM cell from the data shown in Figure 4.3a. The results of four experimental acquisitions in which approximately 8000 events were measured in each run reveal CEM cells were detected at an average concentration of 0.12 ± 0.06%, which is statistically equivalent to the expected CEM cell concentration based on the 0.1% sample loading ($p > 0.05$, 95% confidence limit), in less than four minutes per acquisition.

4.3.3 Lymphocyte Characterization From Peripheral Blood Mononuclear Cells

The system was further tested by analyzing CD4:CD8 ratios in a sample of human PBMCs. This analysis is clinically relevant for monitoring HIV progression.[6] PBMC samples contain all leukocytes, so unlike the previous model systems, a positive fluorescence signal will not be present for every cell that passes through the device. Therefore, in addition to the two fluorescence colors for the anti-CD4 and anti-CD8 antibodies, forward scatter signal was also collected. The top trace in Figure 4.4 shows the scatter signal for the detection of the PBMC sample while the bottom traces show the fluorescence signal from the CD4 and CD8 antibody labeled cells. Not all leukocytes are CD4 or CD8 positive, therefore a fluorescence peak is not present for each scatter peak. However, for each florescence peak, a scatter peak is present. The results from the analysis of the same PBMC sample over 5 runs reveal an average CD4:CD8 ratio of 1.3 ± 0.3, over the measurement of more than 2000 fluorescence events. Each of the five runs took 5 minutes and utilized less than 10 μL of cell solution. The results are not statistically different from the ratio obtained on the Cyan system (1.4, $p > 0.05$, 95% confidence limit), suggesting that the microfluidic system can accurately measure clinically relevant cellular ratios in PBMC solutions.

4.4 Conclusions

The experiments described in this chapter were designed to demonstrate the ability of the microfluidic system to differentiate cell subsets in mixed samples. This was investigated by attempting to characterize cell mixtures through immunophenotyping,

which is a key technique employed in most clinical flow cytometry applications. It is therefore critical that any flow cytometry system designed for clinical applications—regardless of the instrument size, complexity, or multiplexing capability—to be sensitive enough to detect specific cell subsets by immunophenotyping.

Mixtures of cultured T-lymphocytes were labeled with fluorescently tagged antibodies specific to the surface proteins CD3 and CD4 for analysis using the microfluidic cytometry system. These mixtures were analyzed to demonstrate the capability of the system to differentiate cell subsets based on the presence or absence of a specific fluorescently tagged antibody. By starting with a known ratio of cells as determined by counting with a hemacytometer, we were able to demonstrate that the microfluidic system is sensitive enough to detect cell subsets based on surface antigen probes. Further, the detected ratio of cell subsets in the contrived mixture was statistically equivalent to the initial cell mixture ratio. The data show that the microfluidic system can accurately characterize the ratios of cell subsets contained within a mixture. Experiments using the same labeled cells at a ratio of 1000:1 were also performed as evidence that the microfluidic system can accurately characterize the relative ratios of cell subsets having a large disparity in concentration. These measurements are important to demonstrate because biological fluids such as blood contain many different cell subtypes present over a wide range of concentrations.

This chapter also discusses efforts to move towards the analysis of more complex biological samples. Solutions of human peripheral blood mononuclear cells were analyzed using the microfluidic system to determine the CD4:CD8 T-lymphocyte ratio. Microchip experiments were performed in parallel with the Cyan flow cytometry system

in order to determine the accuracy of the microfluidic system analysis. Results from this experiment demonstrate that the microfluidic system result is statistically equivalent to the result obtained using the commercial cytometry system. This is an important outcome because this experiment demonstrates the capacity for the microfluidic system to accurately characterize ratios of cell subsets from real biological samples, providing a foundation for the application of this instrument for further analysis of biological samples.

4.5 Figures

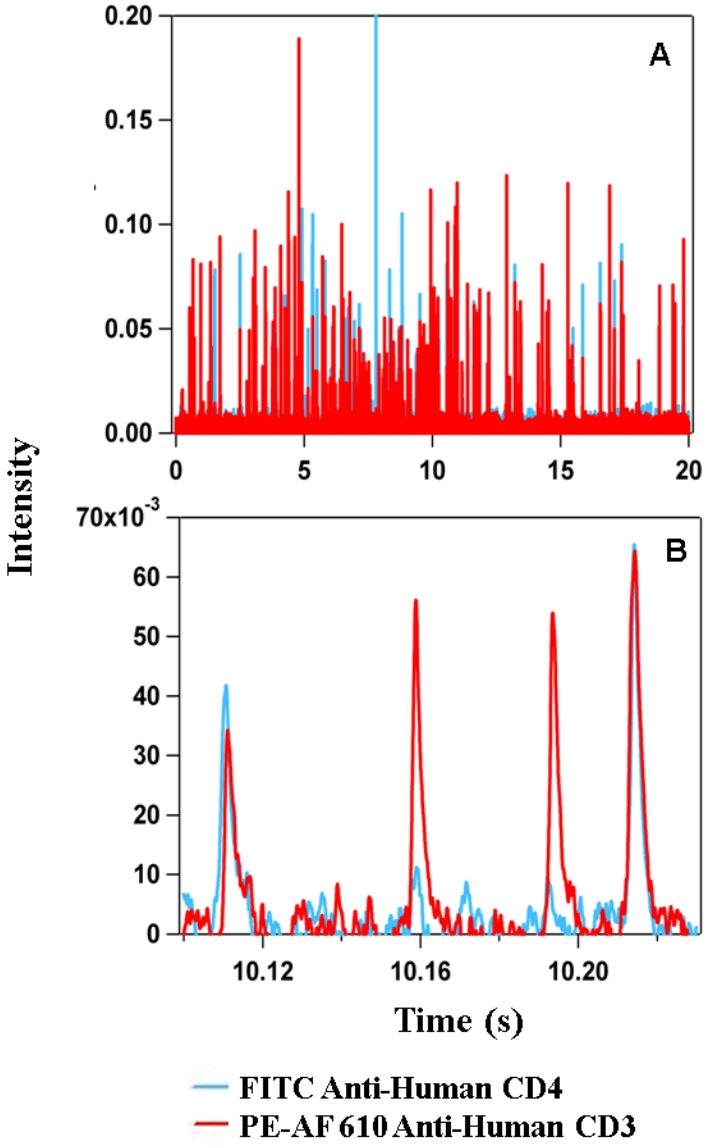

Figure 4.1 **(A)** Result from the analysis of a 1:1 mixture of $CD3^+$ Jurkat cells and $CD3^+$ $CD4^+$ CEM cells where the blue trace shows the fluorescence signals from FITC-anti-CD4 labeled cells, and the red trace shows the fluorescence signal from PE-AF610-anti-CD3 labeled cells. **(B)** Expanded region from the data shown in Figure 4.1a.

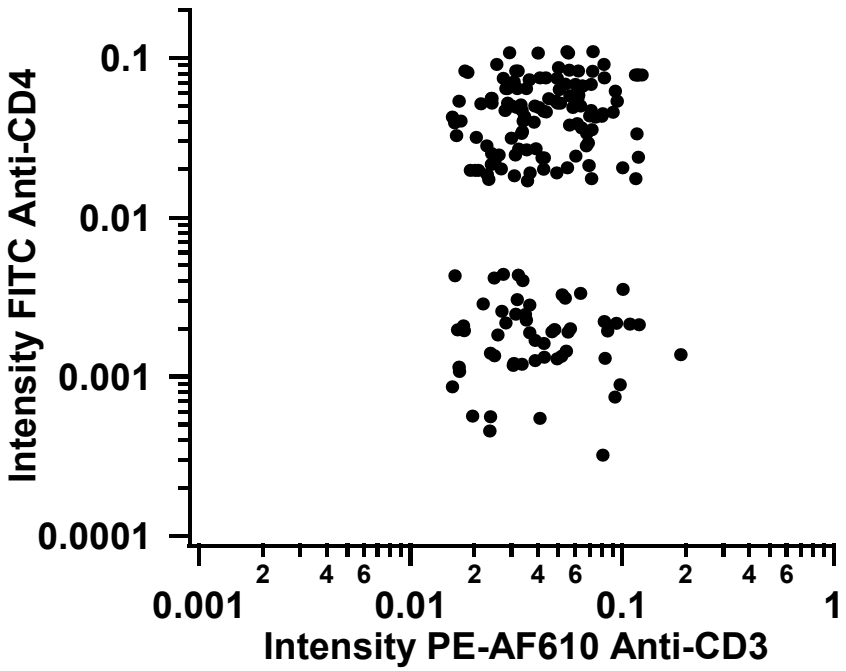

Figure 4.2 Two dimensional scatter plot extracted from the data shown in Figure 4.1 demonstrating the separation between the two cell types based on the intensity of the FITC Anti-CD4 fluorescence signal.

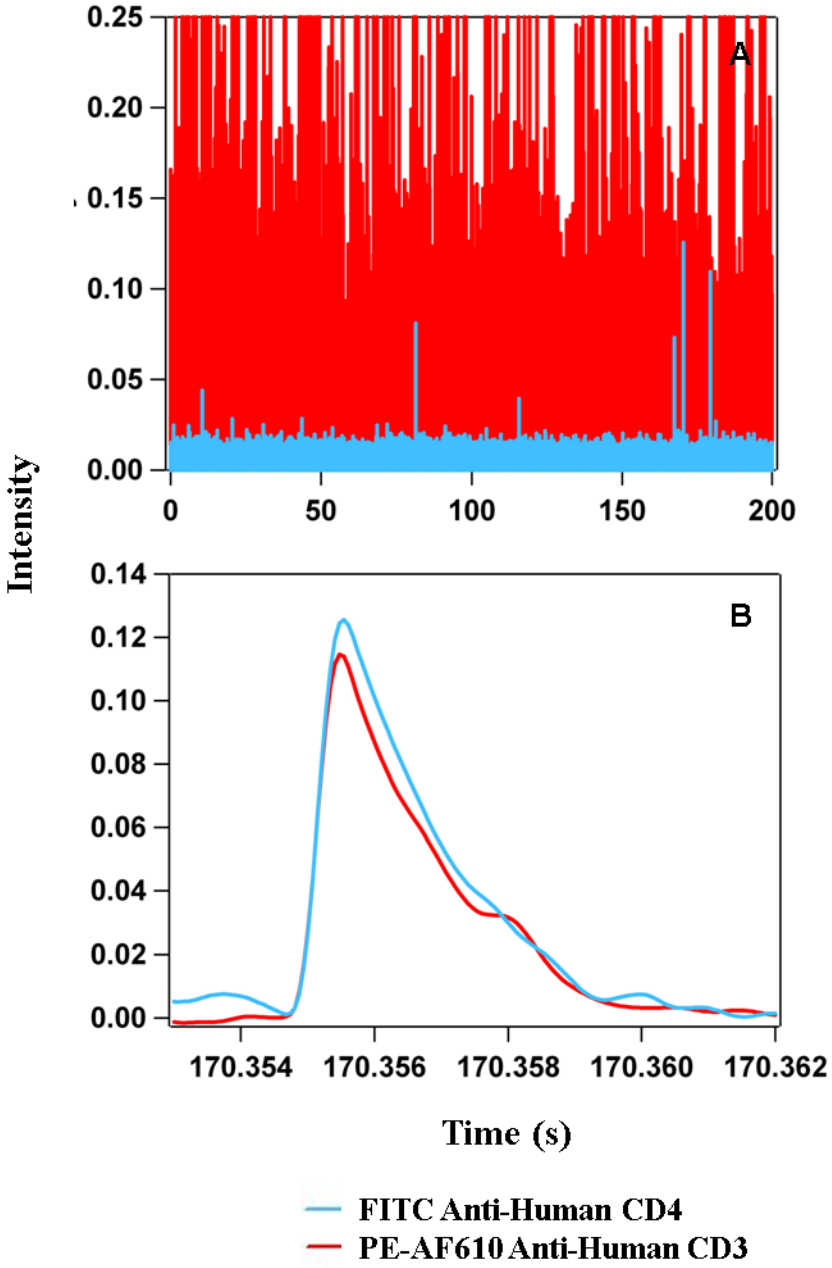

Figure 4.3 **(A)** Result from the analysis of a 1000:1 mixture of $CD3^+$ Jurkat cells and $CD3^+$ $CD4^+$ CEM cells where the blue trace shows the fluorescence signals from FITC-anti-CD4 labeled cells, and the red trace shows the fluorescence signal from PE-AF610-anti-CD3 labeled cells. **(B)** Expanded region from the data shown in Figure 4.3A.

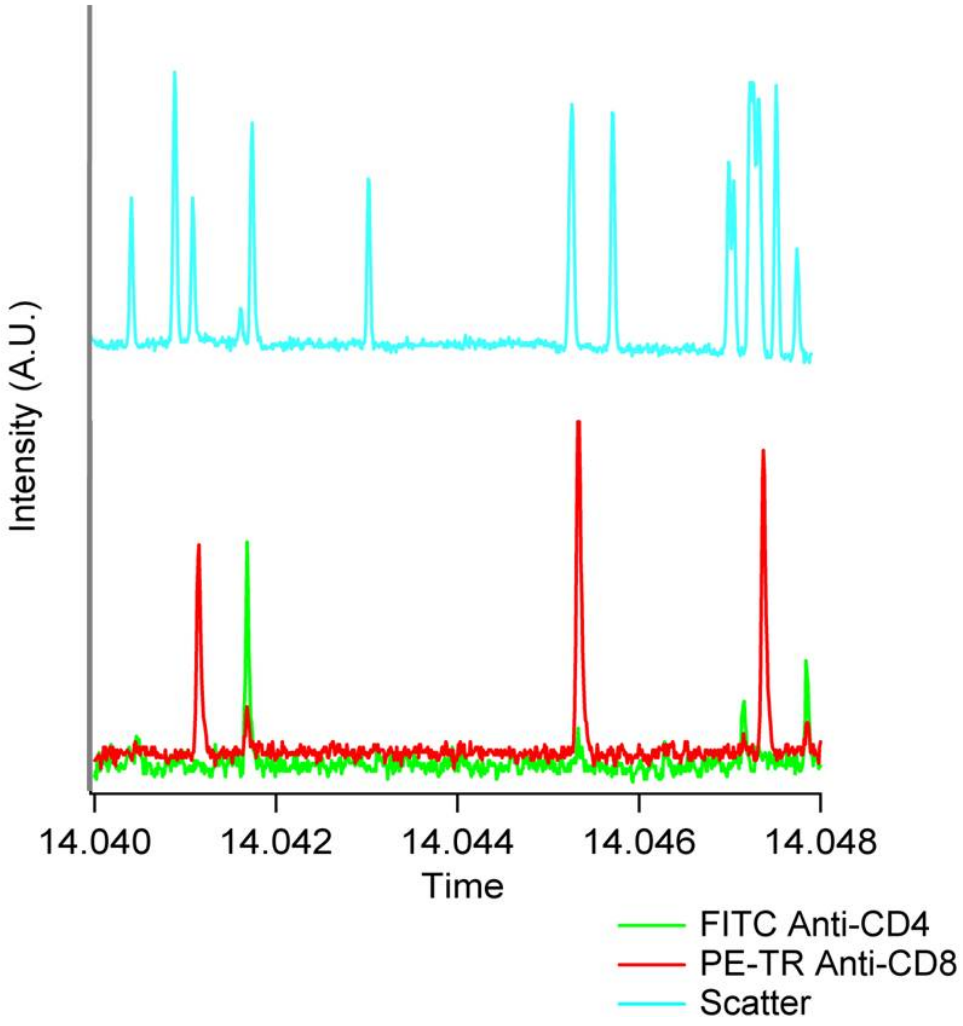

Figure 4.4 Detection of peripheral blood mononuclear cells using elastic light scatter and LIF for the determination of the CD4:CD8 ratio. The top blue trace is the scatter signal, while the green and red traces show the fluorescence signals from FITC-anti-CD4 and PE-Texas red-anti-CD8 labeled cells, respectively.

4.6 References

(1) Douek, D. C.; Picker, L. J.; Koup, R. A. *Annual Review of Immunology* 2003, *21*, 265-304.

(2) Potter, M. N. *Blood Reviews* 1992, *6*, 68-82.

(3) Pui, C. H.; Campana, D. *Leukemia* 2000, *14*, 783-785.

(4) Yin, J. A. L.; Grimwade, D. *Lancet* 2002, *360*, 160-162.

(5) Lancaster, C.; Kokoris, A.; Nabavi, M.; Clemmens, J.; Maloney, P.; Capadanno, J.; Gerdes, J.; Battrell, C. F. *Methods* 2005, *37*, 120-127.

(6) Stein, D. S.; Korvick, J. A.; Vermund, S. H. *Journal of Infectious Diseases* 1992, *165*, 352-363.

CHAPTER 5:

INTEGRATING ERYTHROCYTE LYSIS AND IMMUNOPHENOTYPING ON-CHIP FOR THE ENUMERATION OF LEUKOCYTES FROM WHOLE BLOOD

5.1 Introduction

In order to accurately investigate white blood cell populations by flow cytometry, erythrocytes are normally removed from whole blood.[1-4] This is necessary in order to reduce the potential for interference by red blood cells that are approximately 10^3 times more abundant in blood than leukocytes.[3,4] The process of erythrocyte removal consists of either differential centrifugation[2] or bulk red blood cell lysis followed by centrifugation to remove the lysate debris from the intact leukocytes before flow cytometry analysis.[3] These processes are performed manually, and therefore considerable variation in lysis efficiency is possible between sample batches. As such, an automated platform for erythrocyte lysis from whole blood could rapidly provide consistent enriched leukocyte samples for immediate flow cytometry analysis.

Significant efforts to develop new, inexpensive instrumentation for diagnostics and disease monitoring have focused on microfluidic based point of care clinical assays.[5-12] The foundation for these efforts is the low cost, portability, and small sample volume requirements associated with microfluidic devices.[9,10] Microfluidic assays have been

developed for cell sorting,[3,13-16] identifying rare circulating tumor cells,[17] and detecting specific plasma analytes.[18,19] In addition, flow cytometry has been previously described on microfluidic devices for the detection of leukocytes and bacteria.[20] While these examples provide a strong foundation for the use of microfluidics in flow cytometry applications, there has been little focus on the integration of flow cytometry with sample processing necessary for biological sample analysis. Given the precise fluidic control capabilities of these devices, the development of a rapid, sample-in answer-out instrument could significantly increase the accuracy, efficiency, and cost effectiveness of clinical diagnostics.

In this chapter, the development and initial operational characterization of a microfluidic device combining selective erythrocyte lysis with flow cytometry are described. A diluted blood sample labeled with fluorescently tagged antibodies is infused onto a glass microchip where it interacts with a chemical lysis solution to selectively remove erythrocytes from the sample. The lysis debris is shunted into a waste channel, while the remaining intact leukocytes continue through the device for laser induced fluorescence and elastic scatter based flow cytometric detection. The enumeration of CD4 and CD8 T-lymphocytes—which is applicable to monitoring HIV progression[21] and other immune disorders—has been chosen as a proof of concept to demonstrate the advantageous integration of sample processing with cytometry for automated, efficient leukocyte characterization from blood on-chip.

5.2 Experimental

5.2.1 Microchip Fabrication

Microfluidic devices were fabricated as described in Chapter 2. A piece of polydimethylsiloxane (PDMS) (Sylgard 184; Dow Corning, Midland, MI) bonded to the top of the device after plasma cleaning was used to make direct tubing connections from syringe pumps as well as fluid reservoirs for blood and buffer. An image of the glass microchip designed to combine erythrocyte lysis and cytometry is shown in Figure 5.1a. The sheath buffer channels are 400-μm wide with all remaining channels 80-μm wide. All channels in the device are etched to a depth of 20-μm.

5.2.2 Detection Configuration

The detection configuration used for the experiments described in this chapter is the same as described in Chapter 3. Optical filters were exchanged in order to accommodate detection of Quantum Dot labeled antibodies. Optical images were obtained with an inverted microscope (TE300; Nikon, Melville, NY) equipped with a high-pressure mercury arc lamp using a 20x objective, and a CCD camera (NTE/CCD-512-EBFT; Roper Scientific, Trenton, NJ) using IPlab Spectrum acquisition software (Scanalytics Corp., Vienna, VA). Photographs of the microfluidic device were taken using a Nikon D70 digital camera.

5.2.3 Blood and Cultured Cell Handling

The human T-cell line CRL-1942 (American Type Culture Collection, Rockville, MD) was cultured in RPMI 1640 media supplemented with 10% fetal calf serum, penicillin (100 µg/mL), and streptomycin (100 µg/mL) (Invitrogen Corp., Carlsbad, CA). Cells were washed with PBS two times by centrifugation at 1500 rpm, and dispersed in PBS buffer (pH=7.4) supplemented with fetal calf serum (BD Biosciences, San Jose, CA). Whole human blood was extracted by fingerstick and immediately transferred to a tube containing EDTA (BD Medical, New Brunswick, NJ) to prevent blood coagulation. The blood was then diluted (1:10) in PBS buffer. Quantum Dot 605 Anti-CD8 and Quantum Dot 655 Anti-CD4 antibodies (Invitrogen) (5 µL each) were then added to the diluted blood (to obtain a final sample volume of 200 µL) and mixed for 30 minutes in the dark with continuous mixing.

5.2.4 Cytometry Comparison Experiments

To evaluate the accuracy of microfluidic based immunophenotyping, results were compared to the Cyan ADP flow cytometry system (Beckman-Coulter, Fullerton, CA). Human blood—collected simultaneously with the blood analyzed using the microfluidic system—was labeled the same as described in the previous section. Zapoglobin (Beckman Coulter, Brea, CA) lysis solution was then added to the labeled blood solutions and incubated for 5 minutes. Solutions were then washed by centrifugation two times and dispersed in PBS buffer (500 µL) in polypropylene tubes for flow cytometric analysis.

5.3 Results

5.3.1 Microchip Operation

A 100-µL aliquot of the antibody labeled blood sample is introduced at the sample reservoir on the chip. The blood sample is driven through the chip by applying a sub-ambient pressure using a syringe pump attached to the Waste 2 reservoir (Figure 5.1a). As the blood travels through the device, it approaches an intersecting orthogonal channel—labeled Lyse in Figure 5.1a—containing the commercially available lysis solution Zapoglobin.

Figure 5.1b shows the intersecting fluid flow containing the Zapoglobin from the lyse channel and the blood sample from the main channel, with arrows indicating flow direction. The Zapoglobin is continuously infused onto the device using a syringe pump at a flow rate of 1 µL/min. The blood sample stream is hydrodynamically focused against the channel wall by the infused lysis solution (Fig. 1B). This reduces the distance required for the Zapoglobin to diffuse into the blood sample stream, leading to increased erythrocyte lysis efficiency. After an interaction time of approximately 2 seconds, the cell stream arrives at a second orthogonal channel (labeled Waste 1 in Figure 5.1a) as depicted in Figure 5.1c. Fluid is withdrawn at this intersection (arrows in Figure 5.1c indicate flow direction) at a flow rate of 1 µL/min, equivalent to the flow rate of the infused lysis solution, using another syringe pump to remove unwanted lysis debris. Intact cells have a much lower diffusion coefficient than cell lysate debris and remain primarily within the cell sample stream. Visual monitoring confirmed minimal intact cell losses through this side channel.

The remaining cells travel through one final intersection that is used for hydrodynamic focusing. Buffer solution focuses the cell stream from both sides to ensure the cells are in single file at the detection point. The cells pass through a focused laser beam used for light scatter and laser induced fluorescence based detection. Figure 5.1d shows the fully assembled microchip with a piece of PDMS bonded to the top of the glass. Cutouts for blood sample and sheath focusing buffer fluid reservoirs and via holes for tubing connections are integrated into the PDMS slab. Another rectangular cutout in the PDMS slab provides a clear path for the incident laser beam to pass through the glass microchip, eliminating unnecessary optical effects caused by passing the beam through another material.

5.3.2 Lysis Efficiency

To assess the efficiency of selective erythrocyte lysis on-chip, the forward scatter signal obtained when a diluted blood sample was infused with lysis solution was compared to the result obtained using an isotonic (non-lysing) buffer solution. Figure 5.2a shows a representative segment of the forward scatter signal obtained when the blood sample was infused with buffer solution. In this result, thousands of cells pass by the detection point every second as both erythrocytes and leukocytes are being detected. Figure 5.2b shows the forward scatter signal obtained when the blood sample is infused with lysis solution. Significantly fewer forward scatter peaks can be seen as compared to runs where non-lysing buffer is infused. A total of five 60 second acquisitions were obtained for both the lysis and buffer tests. Compared with the non-lysing buffer

experiment, 86 ± 7 % fewer cells were detected when the lysis solution was infused with the blood sample. Considering the large initial ratio of erythrocytes to leukocytes in the diluted blood sample, the magnitude of cell depletion shown here indicates that a majority of erythrocytes are lysed. The depletion percentage could be increased by infusing a more potent lysis solution on-chip; however, a balance must be achieved between removing a significant fraction of erythrocytes to reduce the possibility of interference, and ensuring the viability of leukocytes for downstream analysis.

5.3.3 Lysis Selectivity

To demonstrate that on-chip lysis selectivity is maintained, a solution of cultured T-lymphocytes was analyzed to ensure that no significant leukocyte depletion occurrs. The same protocol as described in the lysis efficiency experiments was used. A representative signal from the result obtained by infusing non-lysing buffer with a solution of cultured T-lymphocytes is shown in Figure 5.3a. The concentration of cells detected on-chip is unchanged from the initial cell solution concentration. A subset of the result from analyzing the T-lymphocytes infused with lysis solution is shown in Figure 5.3b. Compared to the non-lysing buffer, infusion of lysis solution resulted in T-lymphocyte losses of 6 ± 2%. This result indicates the preservation of lysis selectivity on-chip and confirms that the protocol and solution concentrations chosen lyse erythrocytes with minimal leukocyte losses.

5.3.4 Immunophenotyping Erythrocyte Depleted Blood Samples

Human blood extracted by a finger stick was used for immunophenotypic detection of lymphocytes on-chip. CD4:CD8 ratios were measured from these blood samples and compared to results obtained using the commercially available Cyan flow cytometry system. Diluted whole human blood with quantum dot labeled antibodies specific for $CD4^+$ and $CD8^+$ T-lymphocytes was added to the sample reservoir, and subjected to on-chip lysis to selectively deplete the concentration of unwanted erythrocytes. Although complete erythrocyte depletion is not expected, a substantial reduction in erythrocyte numbers is adequate to facilitate the detection of target leukocytes without significant interference. Fluorescence from the two types of quantum dots was measured as the erythrocyte depleted solution passed by the laser interrogation point after hydrodynamic focusing.

Shown in Figure 5.4a is a subset from the raw PMT data for the two fluorescence channels. The QD605 Anti-CD8 fluorescence signal is shown in black and the QD655 Anti-CD4 fluorescence signal is shown in gray (offset for easier visualization). This data was processed by extracting peak intensities for each detected event and plotted in a two-dimensional scatter plot shown in Figure 5.4b. A clear distinction between the two cell types is shown, demonstrating that the microfluidic device is capable of discriminating $CD4^+$ and $CD8^+$ T-lymphocytes in less than 30 minutes (including antibody labeling), which is clinically relevant for monitoring HIV and other immune disorders. A minimum of 5 samples from the same donor sample were analyzed both on-chip and using the Cyan flow cytometer. The CD4:CD8 ratio measured on the microfluidic device was 2.0 ± 0.4. In comparison, the CD4:CD8 ratio measured from the same blood donor using the Cyan

flow cytometer was 2.2 ± 0.2, demonstrating that the automated microfluidic lysis and cytometry instrument can accurately measure cell ratios comparable to those obtained using standard flow cytometry instrumentation.

5.4 Conclusions

The characterization of an automated microfluidic system incorporating selective erythrocyte lysis with flow cytometry for biomedical monitoring and diagnostic applications was described in this chapter. Incorporating erythrocyte lysis on-chip reduces the number of manual sample processing steps required for sample analysis, providing an automated platform for erythrocyte lysis from clinical samples. The device described is a modification of the device first described in Chapter 2, having the erythrocyte lysis component added to the front end of the chip. This advancement provides a step towards the development of an automated "sample-in, answer-out" platform for blood leukocyte analysis.

Lysis efficiency experiments were performed to ensure that a significant number of erythrocytes were removed from the blood sample, leaving a solution of enriched leukocytes for flow cytometry analysis. Forward scatter signal was monitored as a blood sample was processed through the microfluidic device when Zapoglobin or non-lysing buffer was introduced into the Lysis input. Results show that when Zapoglobin is introduced, more than 85% of cells were lysed compared to the concentration of cells observed with the non-lysing buffer. However, not all erythrocytes were removed from the sample. This is acceptable because the purpose of erythrocyte removal is to reduce

the potential for interference from the red blood cells during leukocyte detection. As the erythrocyte to leukocyte ratio is reduced by selective cell lysis, the likelihood of interference is lessened.

Further testing of the integrated device was done to ensure that the selectivity of the lysis solution was maintained during the on-chip lysis and cytometry assay. Cultured T-lymphocytes were drawn through the device when Zapoglobin or non-lysing buffer was introduced into the Lysis input. The forward scatter signal was compared for the two experiments and revealed minimal losses of the T-cells on-chip. It was determined that approximately 6% of the white blood cells are lost due to the interaction with the lysis solution. This demonstrates that the lysis solution selectively depletes erythrocytes without significantly altering the concentration of leukocytes of interest contained in the blood sample on-chip.

Immunophenotyping results for T-lymphocyte ratio measurements from a human blood sample after automated erythrocyte lysis on-chip show clear agreement with results obtained using standard manual erythorocyte lysis procedures followed by commercial flow cytometry analysis. This result reveals the potential application of the integrated device for cell immunophenotyping of clinical samples for applications monitoring HIV progression, leukocyte malignancies, and other disorders. Further, this result establishes a foundation for the use of this instrument for automated leukocyte characterization from whole blood.

5.5 Figures

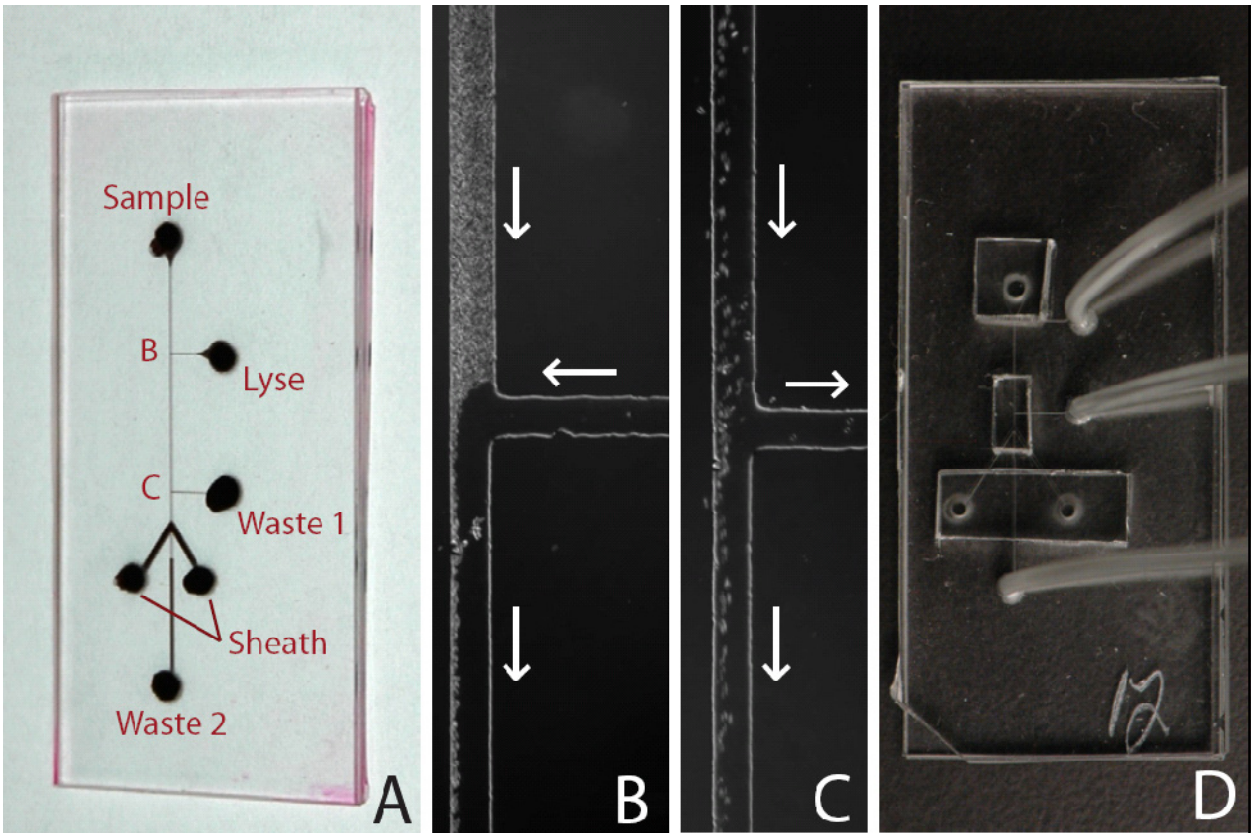

Figure 5.1 **(A)** Glass microfluidic chip used for integrated erythrocyte lysis and flow cytometry. **(B)** Image of blood and lysis solution intersection. **(C)** Image of lysis debris removal via side channel (Waste 1) and intact cells continuing downstream. **(D)** Photograph of functional microfluidic device with a PDMS slab bonded on top of the glass to make tubing connections and fluid reservoirs for blood and sheath focusing buffer.

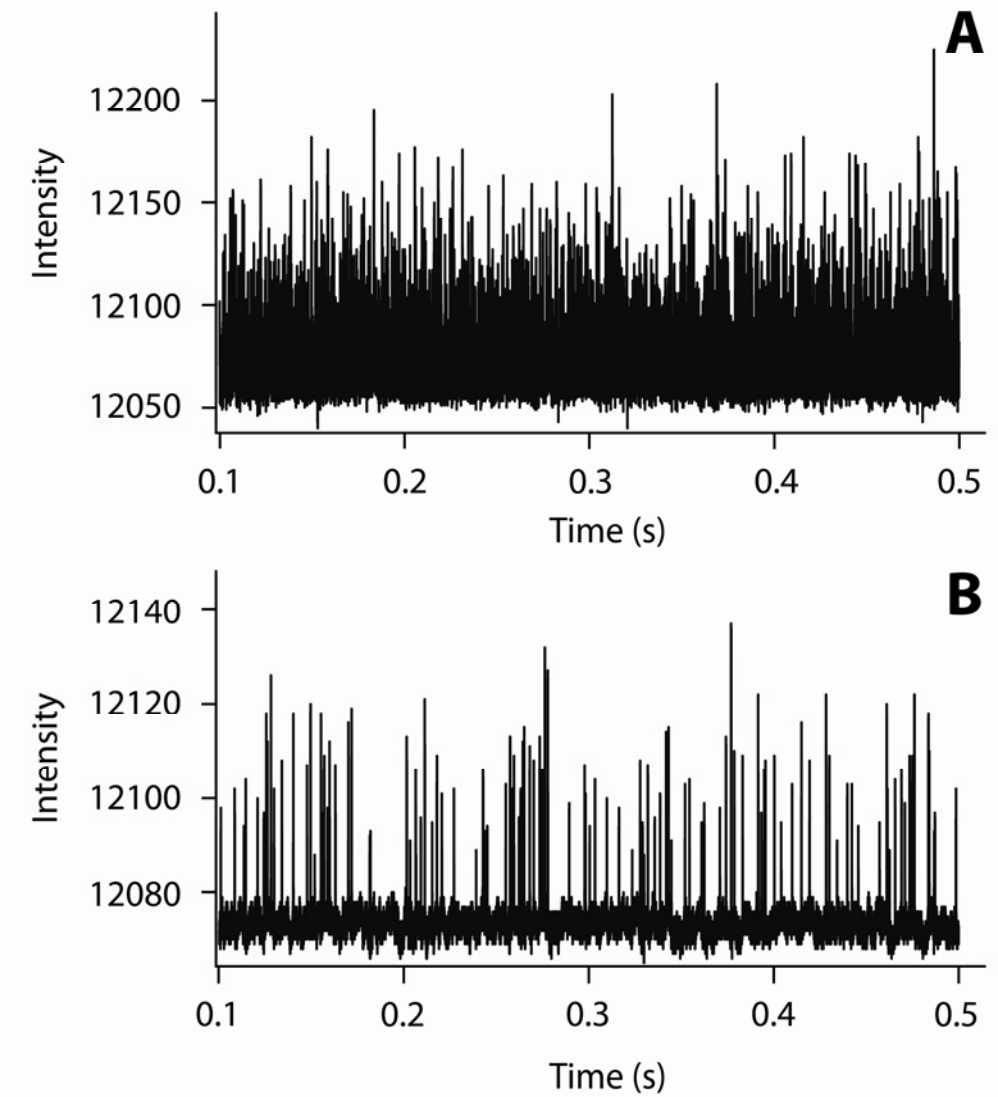

Figure 5.2 Representative signal from lysis efficiency experiments measuring forward scatter detection of diluted whole human blood **(A)** after on-chip infusion with non-lysing PBS buffer and **(B)** after on-chip infusion with Zapoglobin lysis buffer.

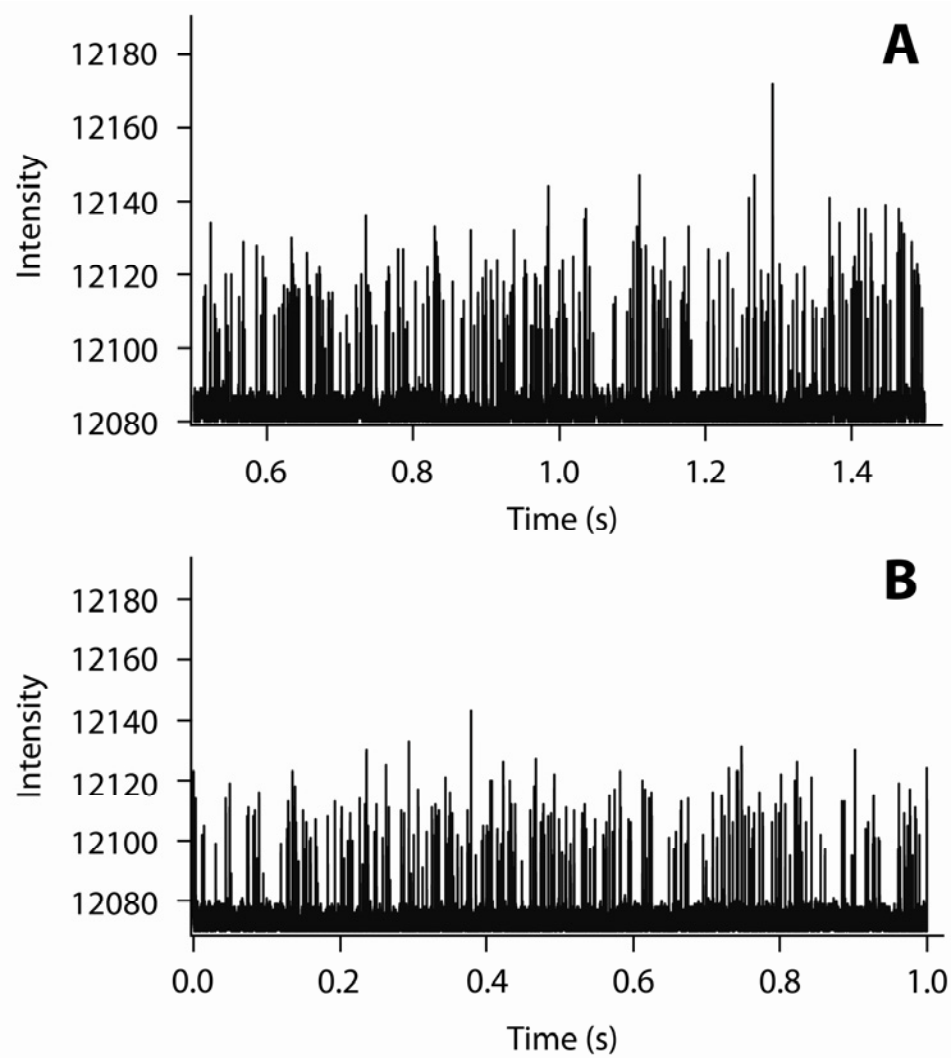

Figure 5.3 Representative signal from experiments employing CRL-1942 T-lymphocytes detected on-chip for lysis selectivity studies after **(A)** infusion with PBS (non-lysing) buffer and **(B)** infusion with Zapoglobin lysis buffer.

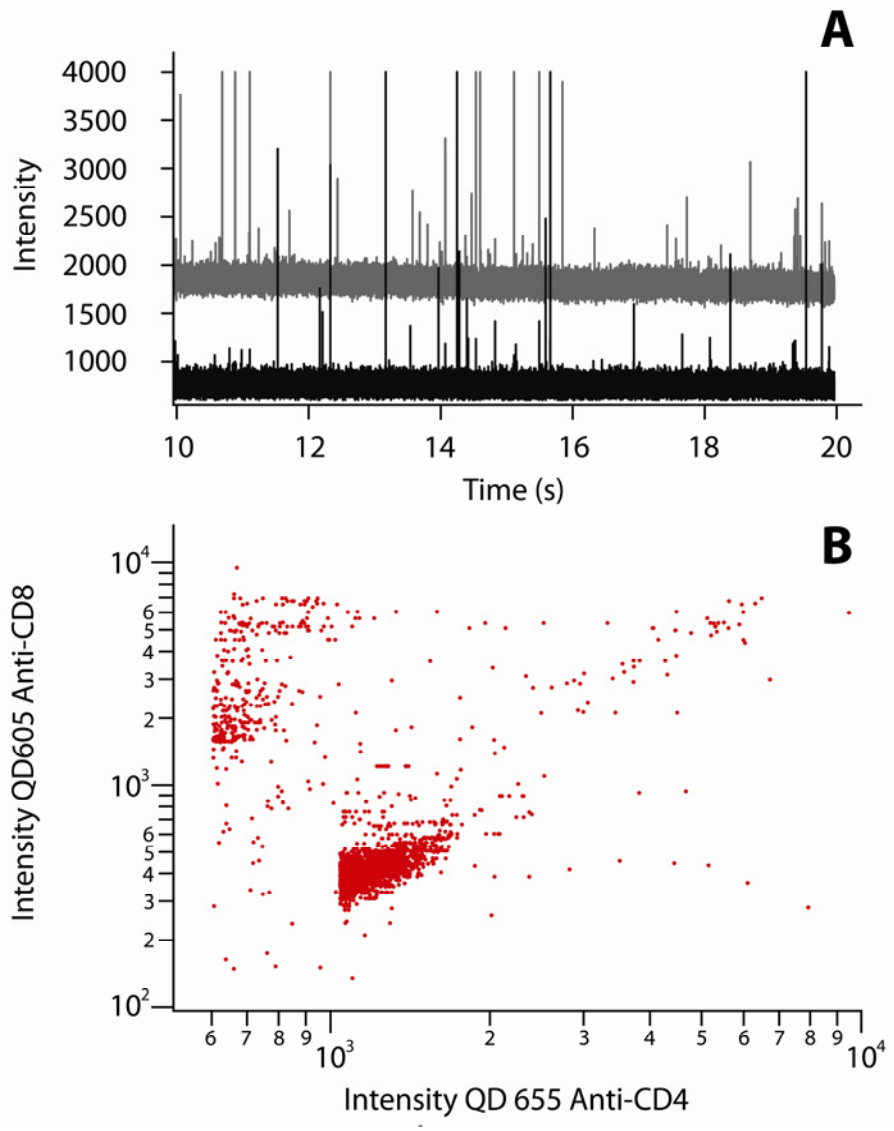

Figure 5.4 **(A)** Subset of raw PMT data showing CD8 fluorescence signal in black and CD4 fluorescence signal (offset by 1000) in gray. **(B)** Scatter plot for on-chip detection of $CD4^+$ and $CD8^+$ T-lymphocytes from erythrocyte depleted whole human blood.

5.6 References

(1) Sethu, P.; Anahtar, M.; Moldawer, L. L.; Tompkins, R. G.; Toner, M. *Anal Chem* **2004**, *76*, 6247-6253.

(2) Sethu, P.; Moldawer, L. L.; Mindrinos, M. N.; Scumpia, P. O.; Tannahill, C. L.; Wilhelmy, J.; Efron, P. A.; Brownstein, B. H.; Tompkins, R. G.; Toner, M. *Anal Chem* **2006**, *78*, 5453-5461.

(3) Soohoo, J. R.; Walker, G. M. *Biomed Microdevices* **2009**, *11*, 323-329.

(4) VanDelinder, V.; Groisman, A. *Anal Chem* **2007**, *79*, 2023-2030.

(5) Blankenstein, G.; Larsen, U. D. *Biosensors & Bioelectronics* **1998**, *13*, 427-438.

(6) Chan, S. D. H.; Luedke, G.; Valer, M.; Buhlmann, C.; Preckel, T. *Cytometry Part A* **2003**, *55A*, 119-125.

(7) Chien, C. M.; Cheng, J. L.; Chang, W. T.; Tien, M. H.; Wu, W. Y.; Chang, Y. H.; Chang, H. Y.; Chen, S. T. *J Chromatogr B Analyt Technol Biomed Life Sci* **2003**, *795*, 1-8.

(8) Lancaster, C.; Kokoris, A.; Nabavi, M.; Clemmens, J.; Maloney, P.; Capadanno, J.; Gerdes, J.; Battrell, C. F. *Methods* **2005**, *37*, 120-127.

(9) Lee, G.-B.; Lin, C.-H.; Chang, S.-C. *J Micromech. Microeng.* **2005**, *15*, 447-454.

(10) McClain, M. A.; Culbertson, C. T.; Jacobson, S. C.; Ramsey, J. M. *Anal Chem* **2001**, *73*, 5334-5338.

(11) Poulsen, C. R.; Culbertson, C. T.; Jacobson, S. C.; Ramsey, J. M. *Analytical Chemistry* **2005**, *77*, 667.

(12) Sakamoto, C.; Yamaguchi, N.; Nasu, M. *Appl Environ Microbiol* **2005**, *71*, 1117-1121.

(13) Emmelkamp, J.; Wolbers, F.; Andersson, H.; Dacosta, R. S.; Wilson, B. C.; Vermes, I.; van den Berg, A. *Electrophoresis* **2004**, *25*, 3740-3745.

(14) Fu, A. Y.; Spence, C.; Scherer, A.; Arnold, F. H.; Quake, S. R. *Nat Biotechnol* **1999**, *17*, 1109-1111.

(15) Dittrich, P. S.; Schwille, P. *Anal Chem* **2003**, *75*, 5767-5774.

(16) Wolff, A.; Perch-Nielsen, I. R.; Larsen, U. D.; Friis, P.; Goranovic, G.; Poulsen, C. R.; Kutter, J. P.; Telleman, P. *Lab Chip* **2003**, *3*, 22-27.

(17) Nagrath, S.; Sequist, L. V.; Maheswaran, S.; Bell, D. W.; Irimia, D.; Ulkus, L.; Smith, M. R.; Kwak, E. L.; Digumarthy, S.; Muzikansky, A.; Ryan, P.; Balis, U. J.; Tompkins, R. G.; Haber, D. A.; Toner, M. *Nature* **2007**, *450*, 1235-1239.

(18) Fan, R.; Vermesh, O.; Srivastava, A.; Yen, B. K.; Qin, L.; Ahmad, H.; Kwong, G. A.; Liu, C. C.; Gould, J.; Hood, L.; Heath, J. R. *Nat Biotechnol* **2008**, *26*, 1373-1378.

(19) Qin, L.; Vermesh, O.; Shi, Q.; Heath, J. R. *Lab Chip* **2009**, *9*, 2016-2020.

(20) Golden, J. P.; Kim, J. S.; Erickson, J. S.; Hilliard, L. R.; Howell, P. B.; Anderson, G. P.; Nasir, M.; Ligler, F. S. *Lab Chip* **2009**, *9*, 1942-1950.

(21) Stein, D. S.; Korvick, J. A.; Vermund, S. H. *Journal of Infectious Diseases* **1992**, *165*, 352-363.

CHAPTER 6:

MONITORING LEUKOCYTE DEPLETION ON-CHIP – MOUSE BLOOD DOSIMETRY

6.1 Introduction

Leukocytes are depleted from blood when exposed to ionizing radiation or chemotherapeutic drugs. This effect is known as leucopenia, and is a result of irreversible cell damage caused by the induced radiation or drug interaction. Exposed blood mononuclear cells are depleted by apoptosis or necrosis, and severely damaged or dead cells are cleared from the blood by phagocytosis.[1] This causes a reduced number of circulating blood mononuclear cells in the affected host, which can lead to increased susceptibility to opportunistic infections, and can be fatal in severe cases.

Monitoring the extent of damaging effects caused by ionizing radiation or drug interactions is known as dosimetry, and significant efforts have been made to develop accurate, reliable dosimetry assays for a large range of exposures. Dosimetry assays are normally performed by monitoring the concentration of apoptotic cells in blood.[1-8] Examples of tests developed to detect apoptosis include fluorescence analysis of DNA unwinding (FADU) [2] and the terminal deoxynucleotidyl transferase (TDT) assay.[2,9] Additionally, numerous studies have been performed to establish the most suitable cell

types to monitor for these measurements. Findings from these studies have shown that leukocytes such as $CD4^+$ and $CD8^+$ T-lymphocytes and $CD27^+$ B-lymphocytes are of particular importance due to the increased sensitivity of these cell types to ionizing radiation or chemotherapeutic drug interaction.[7,8,10,11]

Other assays performed for dosimetry applications monitor DNA damage in the form of chromosomal aberrations.[2,12,13] The frequency of observed aberrations is used to determine dose. Some other assays developed for dosimetry are based on monitoring micronucleus formation[14-18] or detecting chromosomal translocations using fluorescence in situ hybridization (FISH).[19,20] Though all these methods have proven to be accurate and effective for dosimetry applications, they are time consuming and require skilled technicians to execute. As such, the development of a simple, inexpensive, and rapid dosimetry assay would be valuable.

An important application for dosimeters is for monitoring the efficacy of drug and radiation therapies and determining proper chemotherapeutic and radiation dosing in cancer patients. Studies have also suggested dosimetry measurements may be particularly useful for the prediction of clinical response to cancer therapies.[7] Dosimetry also has important applications in the areas of rapid evaluation of radiation exposure from industrial accidents or in homeland security applications.

The experiments described in this chapter use the microfluidic flow cytometry system to measure the depletion effects of different blood leukocyte subsets due to ionizing radiation or chemotherapeutic drug injection. The microfluidic system may prove particularly advantageous for dosimetry applications since it can rapidly phenotype

leukocytes from the volume equivalent to a finger-stick of blood. A similar approach was previously described by Chambers et al, where they monitored the dose dependent depletion of human peripheral blood mononuclear (PBM) cells by conventional flow cytometry.[10] This application demonstrated cell depletion measurements from blood, but required large blood volumes for analysis using conventional flow cytometry. A previously described protocol for phenotypic analysis of mouse peripheral blood leukocytes was employed for the assay described here, reducing processing requirements to immunophenotypically characterize cells from blood by applying a "no-lyse, no-wash" sample preparation protocol.[21]

Mouse models were used for experimental testing of the microfluidic dosimetry system. Animals were tested before and at regular intervals after exposure to total body irradiation (TBI) or chemotherapeutic drugs to demonstrate the use of the microfluidic system to monitor changes in specific blood leukocyte levels due to induced leucopenia. Cell depletion results were compared to results obtained using conventional flow cytometry, and specific assays were demonstrated using the microfluidic device as a proof of concept to reveal distinct advantages to performing these assays on-chip.

6.2 Experimental

6.2.1 Detection Configuration

A simplified detection configuration used for the experiments described in this chapter is shown in Figure 6.1. Experiments described utilize a single fluorescence channel for immunophenotyping applications without elastic scatter based detection. The

optics are the same as described in Chapter 3 with the exception of the fewer detection channels.

6.2.2 Animal Experiments

All animal experiments were performed in accordance with the UNC Institutional Animal Care and Use Committee requirements. Peripheral blood was collected by tail vein nick from adult C57Bl/6 mice (Jackson Labs, Bar Harbor, MA). Doxorubicin HCl (Bedford Laboratories) was administered by intraperitoneal injection in a 2 mg/mL solution. Animals were irradiated using a ^{137}Cs AECL GammaCell 40 Irradiator (Atomic Energy of Canada), or using a XRAD320 (Precision XRay Inc.) biological irradiator with exposures performed at 320 kV, 12.5 mA. Animals were placed 70 cm from the Cs or x-ray source where they received an average dose rate of 0.53 Gy/min.

6.2.3 Blood Sample Preparation

Blood samples obtained from tail nicks were collected into EDTA lined tubes (Vacutainer; BD Medical) and diluted by a factor of 10 with a solution of PBS stain buffer (BD Biosciences) to a final volume of 200-µL. Fluorescently labeled antibodies (5-µL) for CD3 or CD11b were incubated and mixed with the blood samples for 30 minutes. Labeled blood solutions were then directly analyzed without any erythrocyte lysis or washing steps.[21]

6.2.4 Cytometry Comparison Experiments

To evaluate the accuracy of microfluidic dosimetry measurements, results were compared to the Cyan ADP flow cytometry system (Beckman-Coulter). Mouse blood (100-μL)—collected simultaneously with the blood analyzed using the microfluidic system—was prepared in the same manner as the samples tested with the microfluidic system. Measured cell concentrations were obtained from the Cyan using CountBright Absolute Counting Beads (Invitrogen).

6.3 Results

6.3.1 Comparison to Conventional Flow Cytometry

To assess whether the microfluidic flow cytometry system could accurately monitor leukocyte depletion for dosimetry applications, experiments were run in parallel with the Cyan flow cytometry system. The experimental protocol involved measuring the $CD3^+$ T-lymphocyte counts from the blood of 5 healthy animals using both systems. All animals were then simultaneously exposed to 7.5 Gy of Cesium radiation, and allowed to rest for 3 days. Blood samples from each animal were then obtained 72 hours after irradiation and again analyzed using both systems.

The result for this comparison study is shown in Figure 6.2. The percent depletion measured for each individual animal using the microfluidic system is similar to the values obtained by conventional cytometry. The average percent depletion from the microfluidic system for the 5 animals is 87.7%. In comparison, the average percent

depletion measured using the Cyan system is 87.1%. A two-tailed T-test reveals that these results are statistically equivalent ($p > 0.05$, 95% confidence limit). It is important to note that the volumetric requirements for the commercial system are significantly higher than that of the microfluidic system. Equivalent results were obtained in this study with less than 20-µL of blood for microfluidic analysis as compared to 100-µL required for the commercial system.

6.3.2 Radiation Dosimetry

The microfluidic cytometer was used to monitor leukocyte depletion due to radiation exposure over the course of 5 weeks. These experiments demonstrate the advantages associated with performing dosimetry measurements using the microfluidic system (low blood volume requirement, rapid analysis time, and low-cost) for applications in dose assessment for cancer treatment and patient evaluation in radiation exposure incidents. Evaluation of lymphocytes after irradiation has been shown previously,[4-8,11,12,19] and results from these studies have demonstrated a positive correlation between the extent of lymphocyte damage and dose.

The microfluidic cytometry system was used to monitor changes in the concentration of $CD3^+$ T-lymphocytes from 16 mice. The animals were separated into 4 groups, and 3 of those groups were exposed to increasing amounts of x-ray irradiation. One group of animals was not irradiated, and served as a control. The irradiated groups received x-ray doses ranging from 2.5 Gy up to a lethal 10 Gy. Animals were then bled

every 7 days for 5 weeks to monitor radiation induced lymphocyte depletion at different doses using the microfluidic system.

Figure 6.3 shows the result for the 5 week, 16 animal radiation dosimetry experiments. Each trace represents the average $CD3^+$ T-lymphocyte depletion percent measured for each group. A minimum of 2000 events was measured from each sample, with data acquisition taking less than 10 minutes per sample. The blue trace represents the average change in $CD3^+$ percent for the non-irradiated control group. This group did not show any significant depletion, as expected. Further, a small increase was observed over the duration of the experiment, which is within the observed standard measurement error. This small increase may be simply due to measurement variability, but it has also been considered that the increase may be due to either the method of tail bleeding or a stress response from the animals due to increased handling and bleeding. The green and red traces represent the average depletion percentages observed for the groups receiving 2.5 and 5 Gy doses, respectively. For both traces, a nadir is reached approximately 7 days post-irradiation, followed by a gradual recovery of cell counts. The 5 Gy dose caused a larger depletion response than the 2.5 Gy dose, and recovery of cell counts from the 5 Gy dose group is much slower than the lower irradiated dose. The black trace represents the group of animals irradiated with the highest x-ray dose (10 Gy). This dose was projected to be lethal, and after 7 days, all animals in the group were euthanized due to their exceedingly poor health. Measurements were made from the blood of the animals prior to being euthanized, and the results reveal that the $CD3^+$ T-lymphocyte counts in these animals had been reduced to near zero. This result is consistent with previous studies describing increased cell necrosis at high radiation levels.[5,10]

6.3.3 Serial Murine Dosimetry Measurements

In addition to demonstrating the use of the microfluidic cytometer for human dosimetry applications, the system was tested to establish the potential application for serial murine dosimetry measurements. One important application for mouse dosimetry measurements is testing the efficacy of protective drugs that may be developed to reduce unwanted leucopenic effects after radiation or chemotherapy treatment. These experiments can also give valuable information regarding initial depletion kinetics due to induced radiation or chemotherapeutic injection.

The microfluidic system is uniquely capable of performing these measurements due to the low blood volume required for analysis. An average sized mouse (20 grams) contains only about 2 mL of blood. Conventional flow cytometry normally requires several hundred microliters of blood for analysis, which can only be obtained through a lethal cardiac puncture. In contrast, we have demonstrated the ability to accurately monitor cell depletion from blood volumes under 20-μL. If serial bleeds are to be performed, there are limitations to the amount of blood that may be removed and the frequency of bleeding to maintain animal health. Performing serial bleeds instead of lethal cardiac punctures can provide more accurate results since using different animals at each time point can contribute added experimental variability. Further, serial bleeds significantly reduce the number of animals required for these assays. It would therefore be beneficial to have a platform capable of providing accurate dosimetry measurements from small volumes of mouse blood to facilitate serial measurements from each animal over short time periods.

The microfluidic dosimetry measurements were performed as described earlier, except serial bleeds were done over the course of 12 hours. Figure 6.4 shows the result from the analysis of average $CD3^+$ cell depletion from 3 control animals receiving no radiation dose, and 3 animals receiving a lethal 10 Gy dose of TBI. Serial bleeds were performed on each animal (including controls) before irradiation, and 1, 4, 8 and 12 hours post-irradiation. The result shows a clear distinction between the irradiated and non-irradiated control group, demonstrating the significant leucopenic effects of ionizing radiation immediately after TBI. The control group showed no cell depletion, but did have an increase in measured $CD3^+$ cell counts similar to the control group result observed in Figure 6.3.

6.3.4 Doxorubicin Dosimetry

Cell depletion was also monitored using the microfluidic device for applications relating to chemotherapy induced leucopenia from peripheral blood. The absence of selectivity exhibited by many chemotherapeutic drugs causes a significant depletion of PBM cells, in addition to the intended target tumor cells.[22] Studies have shown that the chemotherapeutic drug Doxorubicin causes apoptosis in PBM cells within 24 hours of injection.[23] It is therefore vital for clinicians to carefully monitor the damaging effects these non-discriminating pharmaceuticals have on cancer patients to ensure proper dosage. This is especially critical for patients receiving multiple rounds of chemotherapy since their leukocyte levels may already be depleted from previous treatment.

Experiments developed to test the microfluidic device for measuring depletion due to drug injection monitored the number $CD11b^+$ cells in mouse peripheral blood. The CD11b antigen is expressed on monocytes, neutrophils and granulocytes, and it has been previously demonstrated that the chemotherapeutic drug Doxorubicin induces apoptosis in PBM cells expressing this antigen.[23] We have chosen to monitor the deleterious effects of Doxorubicin on PBM cells expressing the CD11b antigen to demonstrate the use of the microfluidic system for rapid clinical blood testing to monitor therapeutic efficacy and for proper dose determination.

Figure 6.5 shows the result for the experiment monitoring $CD11b^+$ leukocyte depletion from mouse peripheral blood. This experiment tested the blood from a total of 16 animals, split into 4 groups. Blood samples were extracted from each animal and analyzed prior to, and every 7 days after Doxorubicin injection for 3 weeks. A minimum of 2000 events was measured from each sample, with acquisition times under 10 minutes per sample. Three groups of animals were given successively larger doses of Doxorubicin, while one control group of animals had no drug administered. The average cell depletion result for the control group is shown in the black trace, while the average depletion result for the groups administered Doxorubicin are shown in green, red, and blue, representing doses of 5, 10, and 18 mg/ kg. While there was no significant change in the average depletion measured for the control group over the 3 week experiment, all 3 groups administered Doxorubicin showed measurable depletion depending on dose. The depletion for each of those groups reached a nadir around the 7 day measurement, followed by a recovery in the $CD11b^+$ cell counts. There is a significant difference in the overall maximum depletion observed based on initial Doxorubicin dose. Further, the

$CD11b^+$ cell counts in animals receiving the larger doses take longer to recover. Cell counts in the 5 and 10 mg/ kg group reach pre-dose levels after 21 days, while the cell counts remain significantly depleted at 21 days for the 18 mg/ kg dose group.

Results from this assay could be particularly useful in the selection of subsequent chemotherapy doses. For example, if a second dose were to be administered to each group after 21 days, the 18 mg/ kg group would likely be most susceptible to opportunistic infection or death caused by additional leucopenia since peripheral blood $CD11b^+$ levels would already be reduced by half. Performing these tests in clinics could substantially reduce the time patients wait for blood work—required for proper dosage determination—which can currently take hours.

6.4 Conclusions

The experiments detailed in this chapter were intended to demonstrate the use of the microfluidic cytometry system for blood based dosimetry applications. The microfluidic system can perform dosimetry assays using less than 20-µL of whole blood, which is considerably less than required for conventional cytometry assays. This is particularly advantageous when performing dosimetry measurements on mouse models because of their limited available volume of blood. A "no-lyse, no-wash" protocol was employed for blood sample preparation to minimize sample processing steps and time required between blood extraction and analysis. Results obtained using the microfluidic system for the depletion of $CD3^+$ T-lymphocytes were compared to the Cyan system to demonstrate the accuracy of dosimetry measurements performed on-chip. The results

clearly demonstrate that the results obtained from the low-volume assay performed using the microfluidic system are comparable to conventional cytometry results, establishing the foundation for use of the microchip system for additional applications in blood dosimetry.

The microfluidic cytometry system was tested for the ability to monitor the extent of leucopenia after radiation exposure. Results from this experiment clearly show that the microfluidic system can be used to discriminate between different groups of animals given successively larger doses of radiation based on cell depletion measurements. This result is particularly useful for applications in clinics where blood testing is required for each radiation therapy patient before more radiation can be administered. Since leucopenic effects must be carefully monitored to determine proper radiation dosage, a rapid inexpensive platform for performing these assays could significantly reduce the time patients need to wait for results.

Experiments similar to those described for monitoring radiation induced leucopenia were investigated to monitor cell depletion due to chemotherapeutic drug injection. The results from these experiments demonstrate the capacity for the microfluidic system to determine the extent of cell depletion based on administered Doxorubicin dose. This result supports our assessment that the microfluidic system could be used by clinicians to facilitate the rapid determination of proper doses for patients undergoing multiple rounds of treatment.

Another area investigated using the microfluidic system is the analysis of mouse blood from serial bleeds. To extract a sufficient volume of mouse blood for conventional

cytometry analysis lethal bleeds are normally performed. A platform that requires low sample volumes would enable serial bleed analyses that may provide more accurate results since the same animals are being monitored, eliminating the variability of using different animals for each measurement.

The experimental result demonstrates the microfluidic systems' capacity to perform multiple dosimetry measurements from low-volume tail bleeds over a 12 hour period, and clearly shows the rapid depletion effect caused by high doses of TBI. These experiments may prove useful for the investigation of depletion kinetics for specific cell types, potentially providing important information regarding the sensitivity of specific cell subsets to chemotherapeutic agents or ionizing radiation. The analysis of cell depletion from serial animal bleeds can also be used for applications relating to the development and testing of new drugs meant to inhibit unwanted leucopenic effects induced by radiation or chemotherapy treatments. This method can rapidly carry out these applications while significantly reducing animal use requirements.

The microfluidic cytometry system was tested for use in dosimetry applications for the determination of proper therapeutic dosage. Mouse models were used to demonstrate the potential advantages of performing these assays on-chip, and in the process, specific advantages relating to performing dosimetry assays from serial low-volume tail bleeds were revealed. These proof of concept experiments all monitored deleterious effects on blood cells due to induced radiation or administered drug, but other applications for this platform exist. One major application that could be easily performed with the same system would be monitoring increases in blood cell concentrations due to

infection or leukemia, for example. The same advantages detailed above would be relevant for performing such measurements on-chip.

6.5 Figures

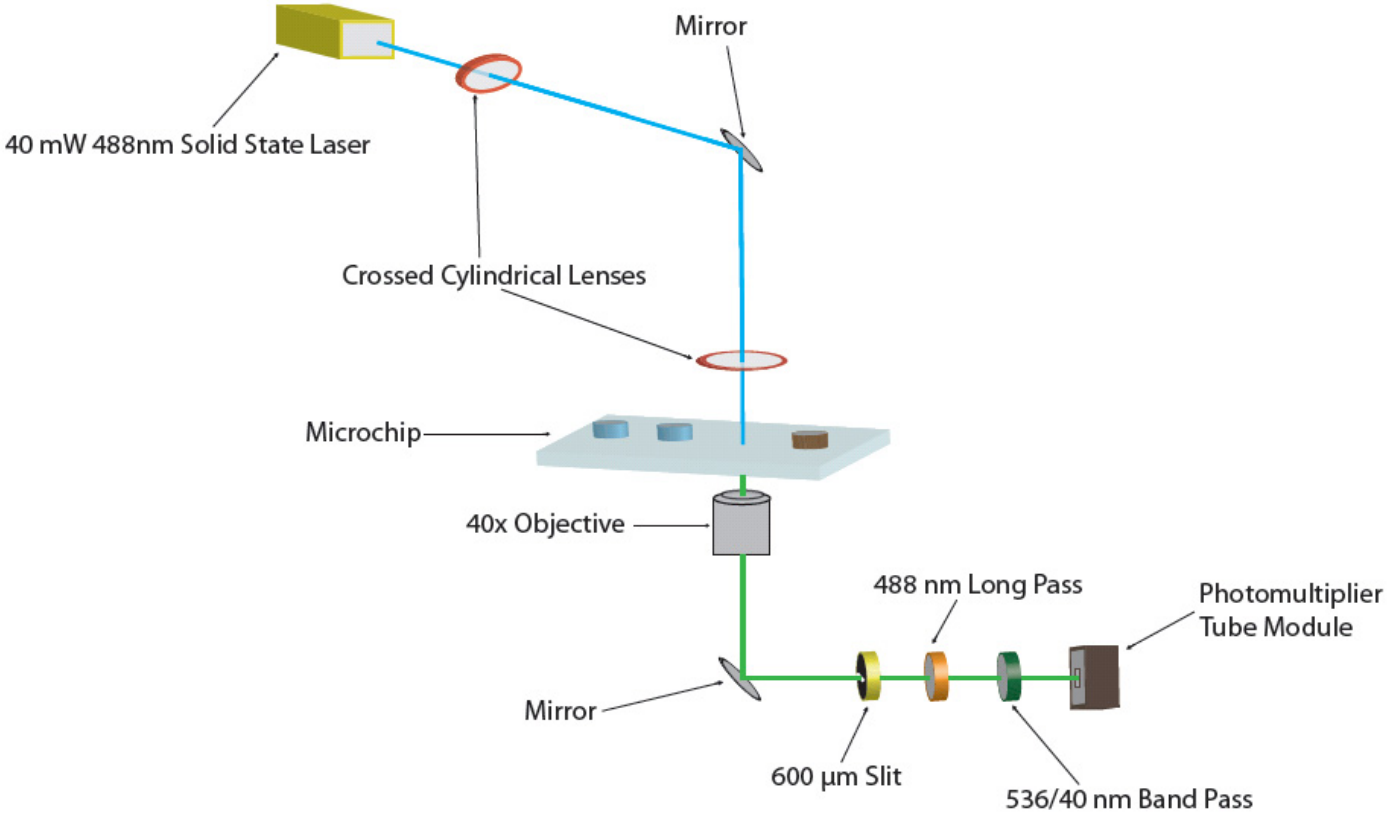

Figure 6.1 Schematic of the optical detection configuration for dosimetry experiments using the microfluidic cytometry instrument for the detection of a single fluorescence channel.

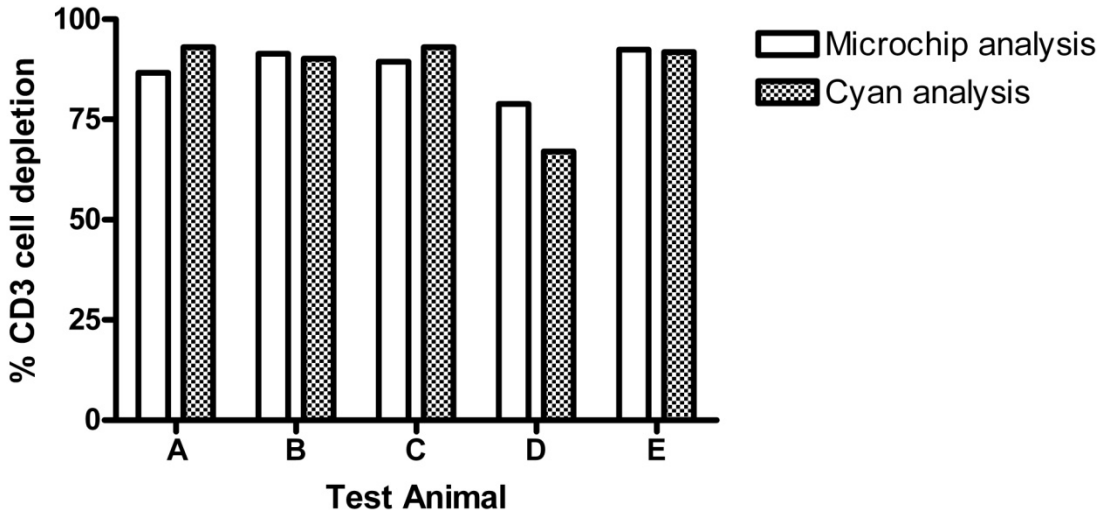

Figure 6.2 Comparison of Cs-radiation (7.5-Gy, total body irradiation) induced $CD3^+$ T-cell depletion results obtained using the microfluidic system and the Cyan cytometry system.

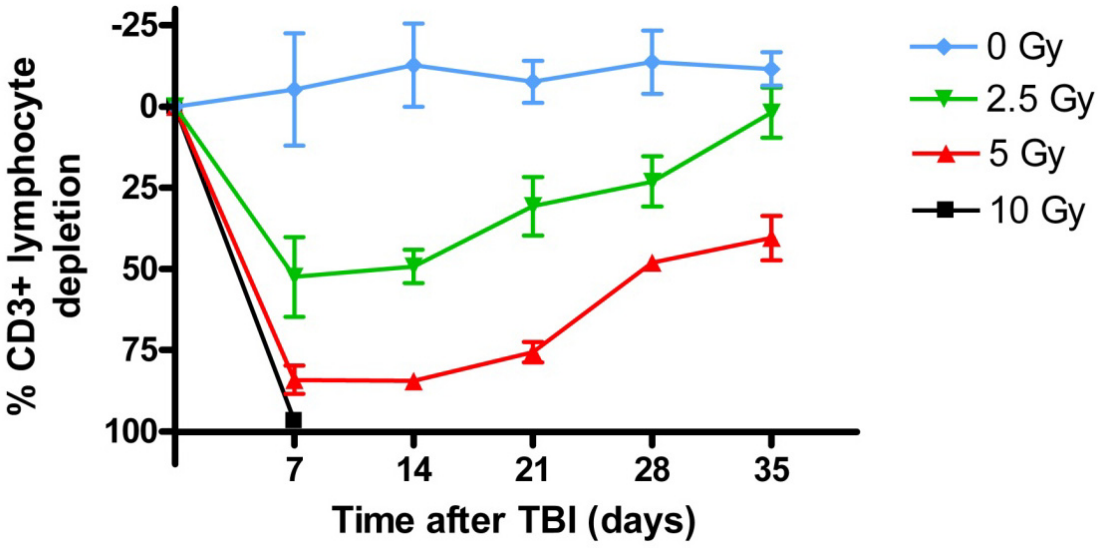

Figure 6.3 Monitoring the percent of $CD3^+$ lymphocyte depletion from the blood of 4 groups of mice receiving different doses of x-ray total body irradiation (n=4).

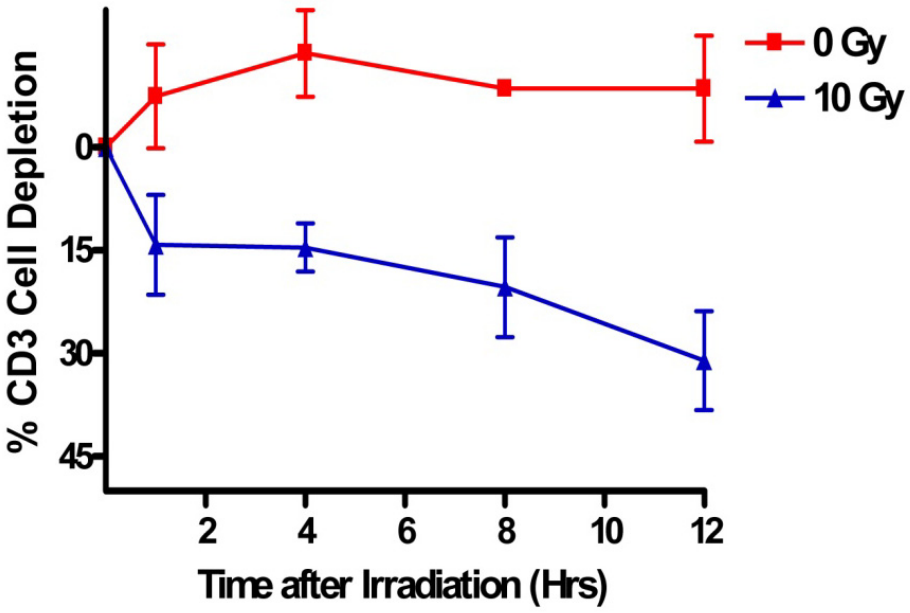

Figure 6.4 Monitoring the percent of $CD3^+$ lymphocyte depletion from serial bleeds of 2 groups of mice receiving different doses of x-ray total body radiation over the course of 12 hours (n=3).

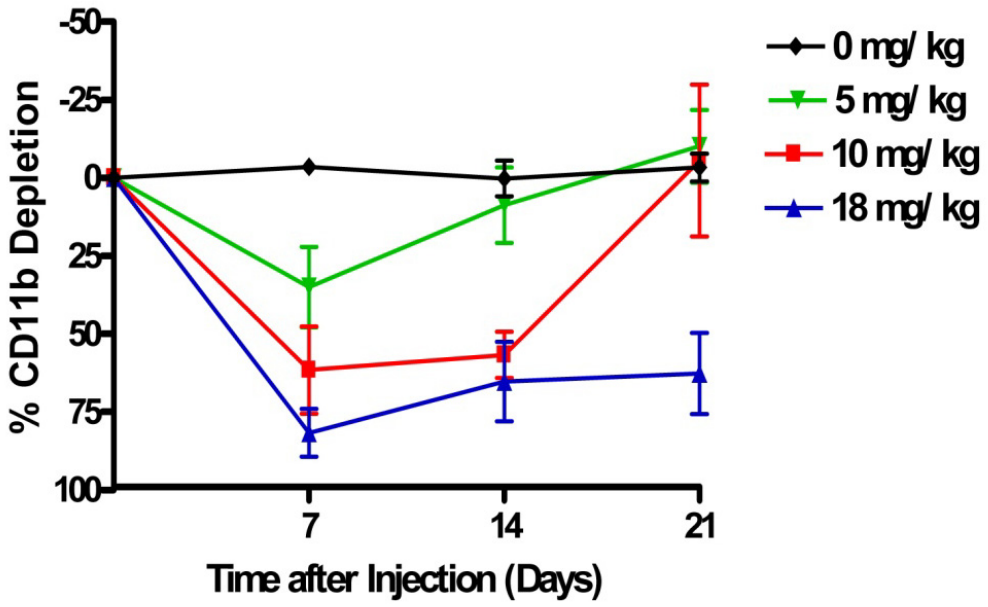

Figure 6.5 Monitoring the percent of $CD11b^{+}$ cell depletion from the blood of 4 groups of mice receiving different doses of Doxorubicin (n=4).

6.6 References

(1) Benderitter, M.; Durand, V.; Caux, C.; Voisin, R. *Radiation Research* **2002**, *158*, 464-474.

(2) Boreham, D. R.; Gale, K. L.; Maves, S. R.; Walker, J. A.; Morrison, D. P. *Health Physics* **1996**, *71*, 685-691.

(3) Gault, N.; Lefaix, J. L. *Radiation Research* **2003**, *160*, 238-250.

(4) Newton, K.; Strasser, A. *Journal of Experimental Medicine* **2000**, *191*, 195-200.

(5) Lemon, J. A.; Rollo, C. D.; McFarlane, N. M.; Boreham, D. R. *Mutagenesis* **2008**, *23*, 465-472.

(6) Menz, R.; Andres, R.; Larsson, B.; Ozsahin, M.; Trott, K.; Crompton, N. E. A. *Radiation and Environmental Biophysics* **1997**, *36*, 175-181.

(7) Ozsahin, M.; Ozsahin, H.; Shi, Y. Q.; Larsson, B.; Wurgler, F. E.; Crompton, N. E. A. *International Journal of Radiation Oncology Biology Physics* **1997**, *38*, 429-440.

(8) Wilkins, R. C.; Kutzner, B. C.; Truong, M.; McLean, J. R. N. *International Journal of Radiation Biology* **2002**, *78*, 681-688.

(9) Gorczyca, W.; Gong, J. P.; Darzynkiewicz, Z. *Cancer Research* **1993**, *53*, 1945-1951.

(10) Chambers, K. A.; Harrington, N. P.; Ross, W. M.; Filion, L. G. *Cytometry* **1998**, *31*, 45-52.

(11) Rehakova, Z.; Sinkora, J.; Vlkova, M.; Vokurkova, D.; Osterreicher, J.; Vavrova, J.; Driak, D. *Physiological Research* **2008**, *57*, 589-600.

(12) Muller, W. U.; Streffer, C. *International Journal of Radiation Biology* **1991**, *59*, 863-873.

(13) Lloyd, D. C.; Purrott, R. J.; Dolphin, G. W. *Nature* **1973**, *241*, 69-70.

(14) Lee, T. K.; O'Brien, K. F.; Naves, J. L.; Christie, K. I.; Arastu, H. H.; Eaves, G. S.; Wiley, A. L.; Karlsson, U. L.; Salehpour, M. R. *Mutation Research-Genetic Toxicology and Environmental Mutagenesis* **2000**, *469*, 63-70.

(15) Thierens, H.; Vral, A.; Deridder, L. *Health Physics* **1991**, *61*, 623-630.

(16) Fenech, M.; Morley, A. A. *Mutation Research* **1985**, *147*, 29-36.

(17) Gantenberg, H. W.; Wuttke, K.; Streffer, C.; Muller, W. U. *Radiation Research* **1991**, *128*, 276-281.

(18) Ramalho, A.; Sunjevaric, I.; Natarajan, A. T. *Mutation Research* **1988**, *207*, 141-146.

(19) Lucas, J. N.; Hill, F.; Burk, C.; Fester, T.; Straume, T. *Health Physics* **1995**, *68*, 761-765.

(20) Szeles, A.; Joussineau, S.; Lewensohn, R.; Lagercrantz, S.; Larsson, C. *International Journal of Radiation Biology* **2006**, *82*, 87-96.

(21) Weaver, J. L.; Broud, D. D.; McKinnon, K.; Germolec, D. R. *Toxicology Mechanisms and Methods* **2002**, *12*, 95-118.

(22) Hickman, J. A. *Cancer and Metastasis Reviews* **1992**, *11*, 121-139.

(23) Ciobotaro, P.; Drucker, L.; Neumann, A.; Shapiro, H.; Shapira, J.; Radnay, J.; Lishner, M. *Anti-Cancer Drugs* **2003**, *14*, 383-389.

CHAPTER 7:

INVESTIGATION OF OTHER MICRO-FLOW CYTOMETRY APPLICATIONS AND FUTURE DIRECTIONS

7.1 Introduction

Many applications exist for a portable, inexpensive flow cytometry system such as the one described in this dissertation. Another application that we have investigated is the enumeration of rare circulating tumor cells that can be detected in blood for clinical cancer diagnostic purposes.[1,2] We have also demonstrated the detection of intracellular components using the microfluidic system. The ability to detect these entities, including nucleic acid content [3-6] and phosphorylated proteins[7-11], on-chip greatly increases the number of possible applications for the device. Other applications and possible future directions, including advancements in instrumental design and hardware, for this project are discussed in this chapter. The continued integration of other sample processing and analysis steps is also discussed as potential future modifications to the system.

7.2 Experimental

7.2.1 Cell Culture and Staining Protocols

The human T-cell line CRL-1942 (American Type Culture Collection, Rockville, MD) was cultured in RPMI 1640 media supplemented with 10% fetal calf serum, penicillin (100 μg/mL), and streptomycin (100 μg/mL) (Invitrogen Corp., Carlsbad, CA). Cells were washed and centrifuged at 1500 rpm, twice, and redispersed in PBS buffer (pH=7.4) supplemented with fetal calf serum (BD Biosciences, San Jose, CA). Cells were prepared for staining by washing $\approx 10^6$ cells by centrifugation at 300x g three times and redispersing cells in 50 μL of PBS buffer. Cells were then labeled with an intracellular fluorescent dye by incubating them with 2 μL Calcein-AM (1 μg/ mL) (Invitrogen Corp., Carlsbad, CA) for 30 minutes.

7.2.2 Animal Protocols

All animal experiments were performed in accordance with the UNC Institutional Animal Care and Use Committee regulations. Peripheral blood was collected by tail vein nick from adult C57Bl/6 mice (Jackson Labs). Animals were irradiated using a ^{137}Cs AECL GammaCell 40 Irradiator (Atomic Energy of Canada) with exposures performed at 320 kV, 12.5 mA. Animals were placed 70 cm from the Cs source where they received an average dose rate of 0.53 Gy/min.

7.2.3 Blood Sample Preparation

Blood samples obtained from tail nicks were collected into EDTA lined tubes (Vacutainer; BD Medical) and diluted by a factor of 5 with a solution of PBS stain buffer (BD Biosciences) to a volume of 100-µL. Antibodies for CD3 (PE-Texas Red conjugated, 5-µL) (Invitrogen) were incubated with the blood samples for 20 minutes with continuous mixing. Blood solutions were then diluted 2x with Cytofix buffer (BD Biosciences) to fix and permeabilize the target cells. Caspase-3 antibody conjugated to FITC (BD Biosciences) (5-µL) was then added and the solution was incubated and continuously mixed for 20 minutes. Labeled blood solutions were then directly analyzed without erythrocyte lysis or washing steps.[12]

7.3 Results

7.3.1 Rare Cell Detection

Previous work described in Chapter 4 was performed to establish the ability to accurately detect a particular cell line in a mixture at a concentration of one part per thousand Many applications can be addressed given this level of sensitivity but the enumeration of rare circulating tumor cells requires the ability to detect cells at much lower concentrations. Circulating tumor cells may be found at concentrations ranging from tens to hundreds per mL of whole blood.[1,2] As such, detecting a substantial number of these cells requires the analysis of large sample volumes. Using positive pressure to drive fluid flow as described in Chapter 3, large sample volumes may be accommodated with the microfabricated device.

Positive pressure driven microfluidic cytometry was performed on manufactured solutions of cultured T-lymphocytes dispersed at known concentrations into PBS buffer. The cell and buffer solutions were loaded into syringes and driven through the microfluidic system at a sample flow rate of 100 μL/ min and a sheath flow rate of 250 μL/ min. Three solutions of different cell concentrations were processed through the device, and 5 ten minute acquisitions were performed for each solution. Figure 7.1 shows the result for these experiments where the average normalized detected concentration is plotted for each of the three different cell solutions tested. These results show that the microfluidic system is capable of accurately detecting cells in solutions at each of the concentrations tested, including the lowest tested concentration of 50 cells per mL, with a standard error of ± 9%.

Experiments described based on the detection of T-lymphocytes in buffer solutions are only the first step in demonstrating the applicability of this instrument for determining levels of rare circulating tumor cells in blood. Further experiments may also be performed to demonstrate the application to rare cell detection by spiking known concentrations of fluorescently labeled cells into a whole blood solution. This experiment will verify whether or not the rare target cells can be detected in a complex mixture of many other cell types at significantly higher concentrations. Clinical blood samples from cancer patients may be also tested to confirm that this system can be used for rare cell applications.

7.3.2 Intracellular Protein Detection

The detection of intracellular components requires the ability to permeabilize the cell membrane in order to introduce fluorescently labeled antibodies inside the cell. Commercially available products are made to fix and permeabilize cells for this purpose, and many assays have been developed to detect intracellular components using conventional flow cytometry.[3-11] To demonstrate the use of the microfluidic system for the detection of intracellular components, the cysteine protease caspase-3 was monitored in T-lymphocytes from mouse blood after animals were exposed to TBI. Caspases are key effectors in apoptosis, and T-cells in animals exposed to TBI should show increasing levels of many caspases, including caspase-3 expression over time as the number of apoptotic cells increases.[13,14]

Two animals exposed to 10 Gy of TBI were bled before and at multiple times after irradiation to simultaneously monitor changes in $CD3^+$ T-cell concentrations and percent caspase-3 expression in detected lymphocytes. The result for this experiment is shown in Figure 7.2. Bleeds were performed 3 hrs, 24 hrs, 48 hrs, 120 hrs, and 288 hrs post TBI. As shown in earlier experiments in Chapter 6, the $CD3^+$ cell concentrations are depleted after TBI. Due to diminishing health, animal M319 was euthanized 9 days post-TBI, and animal M317 was euthanized after a tail bleed 288 hrs post-TBI. Starting at the 24 hrs post-TBI time point, the percent of $CD3^+$ T-lymphocytes with measureable caspase-3 expression was monitored using the microfluidic system. The percent of measurable caspase-3 expression in detected $CD3^+$ cells increased post-TBI as expected, and the percent of remaining $CD3^+$ cells expressing caspase-3 was close to 100% for animal M317 at 288 hours post-TBI. This result demonstrates the capability of the

microfluidic cytometry system to monitor changes in intracellular protease caspase-3 and potentially many other intracellular components, as results obtained were as expected based on previous conventional flow cytometry results.[13,14]

7.4 Future Directions

There are a variety of potential future directions for the microfluidic cytometry system, including advanced instrument development, further integration of sample preparation or analysis processes, and continued demonstration of clinical applications that would benefit from the advantages afforded by the microchip system. All of these areas are equally important, and future work may require advancements within each of these areas to demonstrate added functionality to the scientific community. Specific advancements relating to the applicability of the system for field work and point-of-care applications would be most valuable considering the shortage of available inexpensive diagnostic and monitoring devices in resource poor settings throughout the world.

To modify or improve upon the microfluidic cytometry system hardware, a few approaches may be taken, including advanced multiplexing capabilities, simplification for 3rd world applications, or parallel processing. Advancing the multiplexing capacity of the microfluidic cytometer would require the addition of PMT's and optical filters to obtain more fluorescence detection channels. Additional lasers could also be incorporated to increase the number of detectable fluorescent molecules available for sample characterization. The addition of more detection channels would significantly increase the number of potential clinical and research applications by providing more

information about cell samples, but this comes at an increased cost and larger footprint. It must also be noted that with the continued addition of fluorescence detection channels, the potential for spectral crossover increases. This will require advancement in software to compensate for the fluorescence spillover. In addition, efforts could be made to modify the current optical configuration to accommodate side-scatter measurements.

Another potential area for advancement would be to focus on instrument simplification and the use of inexpensive components to make the system more attractive for applications in resource limited settings. One example of a modification that could be made is the use of high power LED light sources instead of lasers. Using smaller optical components and a smaller vacuum source could also significantly reduce the size of the instrument. Additionally, efforts could be made to incorporate components with low power requirements to accommodate the operation of the instrument using batteries, thus facilitating use for applications in resource poor settings.

For situations where the sample throughput of the microfluidic system is too low for practical application, parallel processing may be employed. A specific application where this may be necessary is for the detection of circulating tumor cells present at very low concentrations in blood. The current system has been used to analyze blood samples at a maximum throughput of 100-μL per minute. When looking for cells present at concentrations at or lower than 10 per mL, the microchip as currently configured would take many hours to analyze the volume required to count enough positive events to have statistical significance. Modifying the microfluidic device design and detection configuration to accommodate multiple simultaneous parallel cytometry measurements

could greatly increase the maximum achievable sample throughput, resulting in faster analysis times for large sample volumes.[15]

In addition to improvements based on hardware, further integration of sample processing or cell analysis steps could significantly improve the ease of use and number of potential applications for the microfluidic system. The integration of sample processing steps as discussed in Chapter 5 could significantly reduce the number of manual sample processing steps required for cell analysis from complex mixtures, potentially reducing overall assay times and providing more reproducible sample processing conditions compared to manual sample preparations. Another sample processing step that could be integrated on-chip is fluorescent labeling.[16,17] The interaction time of cell and antibody solutions can be precisely controlled on-chip, and washing steps could be included if determined necessary.

The cytometry signals obtained from the current system configuration could be used for selective cell isolation, and this has been described on-chip previously.[18-21] Cell sorting on-chip can be particularly useful when further testing on specific cell subsets isolated from a complex cell solution is necessary. An on-chip assay has also been described for the analysis of cell lysate contents.[22] Cytometry information could be used to selectively lyse target cells, followed by electrophoretic separation of lysate contents to identify specific analytes. All of these examples could greatly increase the functionality of the microfluidic system while reducing the overall analysis efforts required as compared to conventional assays.

The microfluidic system as currently configured, or with added improvements as described earlier could be tested to reveal numerous other potential clinical and research applications. Areas of particular importance are applications in tuberculosis and malaria detection and monitoring. These diseases affect millions of people worldwide—mostly in resource limited settings—and the application of the microfluidic system (with specific advancements in engineering and portability) could provide an inexpensive platform for testing in these areas.[23]

All of the suggestions for improvements and advancements are proposed in consideration for the development a multifunctional platform for numerous clinical and research applications. Successful commercialization of a device targeting a specific application will require optimization of operational parameters and instrumental features. I have presented here a short list of improvements that may serve as a starting point allowing for continued progress toward the development of a commercially viable microfluidic instrument.

7.5 Conclusions

This dissertation described the development, initial characterization, and performance of a microfluidic-based flow cytometry system for biomedical monitoring and diagnostic applications. Employing inexpensive microfluidic chips is advantageous for the analysis of potentially infectious samples as the entire device is disposable, thereby reducing the potential of cross-contamination and eliminating the need for instrument sterilization procedures. In addition, a single syringe pump or other simple

vacuum source can by employed for successful operation of the device. Hydrodynamic focusing properties of the microfluidic flow chamber were characterized to ensure proper cell focusing, and optical measurement precision was assessed and compared to conventional flow cytometry results.

T-cell enumeration has been demonstrated to confirm the potential use of this system for immunophenotypic analysis from blood or bone marrow aspirates. Further development let to the integration of erythrocyte lysis on-chip to reduce manual sample processing steps required for blood analysis. To demonstrate the capacity of this integrated device to analyze T-cells from whole blood, results from the integrated erythrocyte lysis and cytometry device were again compared to results obtained using a standard lysis protocol followed by analysis by conventional flow cytometry. Another application investigated for this microfluidic system was blood dosimetry. Mouse models exposed to radiation or a chemotherapeutic drug were used as models to demonstrate the potential use of this system to monitor cell depletion effects. These measurements may prove particularly useful in the areas of dose assessment by clinicians and for rapid assessment of radiation exposure. Continued demonstrations of potential applications included the detection of low concentration cells for detecting rare circulating tumor cells, and for the detection of intracellular proteins.

All of the work described in this dissertation is meant to provide evidence that a functional flow cytometer can be fabricated using microfluidic chips, and to establish a foundation for the use of this instrument for numerous clinical and research applications. Significant efforts may prove necessary to advance this prototype into a commercially viable instrument, however, the fundamental components assembled, characterized, and

applied to proof-of-concept applications described here provide a basis from which the process can be initiated. To date, this instrument has been demonstrated to function—as currently configured—as well as conventional cytometry instrumentation for initial proof-of-concept experiments in a smaller, less-expensive form, and has been successfully tested for use as a multifunctional platform for the analysis of numerous medical disorders based on established flow cytometry-based assays.

7.6 Figures

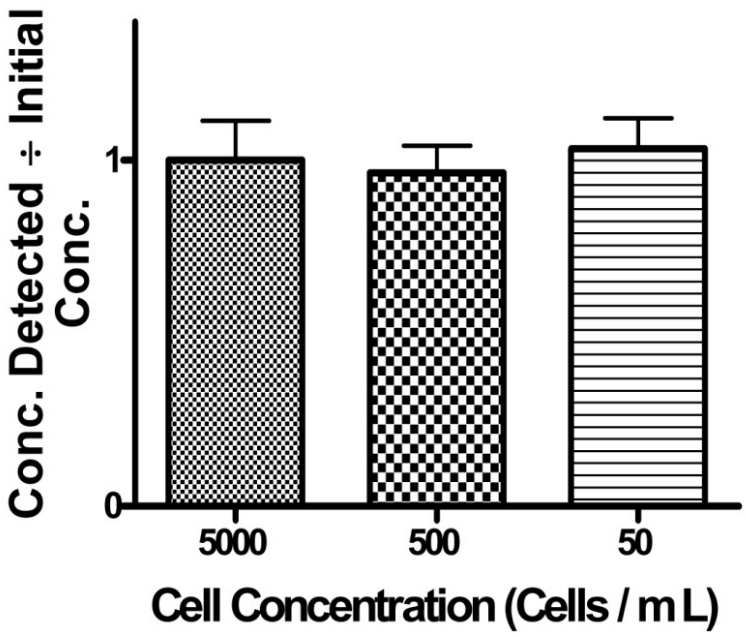

Figure 7.1 Detection of low concentration solutions of cells in buffer to simulate the application of the microfluidic cytometry system for counting rare circulating tumor cells.

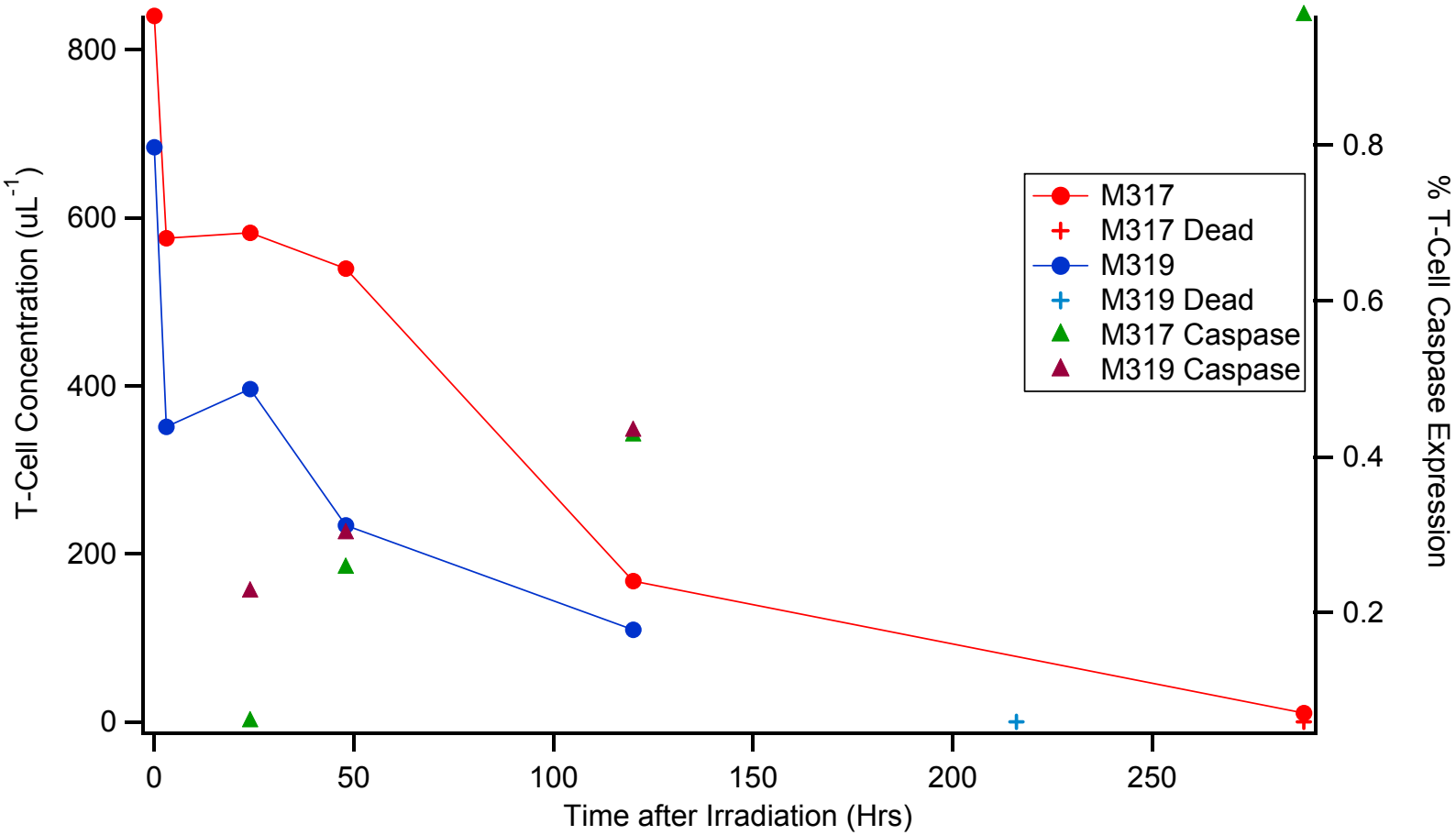

Figure 7.2 Simultaneous monitoring of T-lymphocyte depletion and changes in intracellular caspase expression after exposure to TBI.

7.7 References

(1) Adams, A. A.; Okagbare, P. I.; Feng, J.; Hupert, M. L.; Patterson, D.; Gottert, J.; McCarley, R. L.; Nikitopoulos, D.; Murphy, M. C.; Soper, S. A. *Journal of the American Chemical Society* **2008**, *130*, 8633-8641.

(2) Nagrath, S.; Sequist, L. V.; Maheswaran, S.; Bell, D. W.; Irimia, D.; Ulkus, L.; Smith, M. R.; Kwak, E. L.; Digumarthy, S.; Muzikansky, A.; Ryan, P.; Balis, U. J.; Tompkins, R. G.; Haber, D. A.; Toner, M. *Nature* **2007**, *450*, 1235-U1210.

(3) Hedley, D. W.; Friedlander, M. L.; Taylor, I. W.; Rugg, C. A.; Musgrove, E. A. *Journal of Histochemistry & Cytochemistry* **1983**, *31*, 1333-1335.

(4) Hedley, D. W.; Philips, J.; Rugg, C. A.; Taylor, I. W. *European Journal of Cancer & Clinical Oncology* **1984**, *20*, 749-752.

(5) Dolezel, J.; Bartos, J. *Annals of Botany* **2005**, *95*, 99-110.

(6) Dolezel, J.; Bartos, J.; Voglmayr, H.; Greilhuber, J. *Cytometry Part A* **2003**, *51A*, 127-128.

(7) Krutzik, P. O.; Nolan, G. P. *Cytometry Part A* **2003**, *55A*, 61-70.

(8) Krutzik, P. O.; Irish, J. M.; Nolan, G. P.; Perez, O. D. *Clinical Immunology* **2004**, *110*, 206-221.

(9) Krutzik, P. O.; Hale, M. B.; Nolan, G. P. *Journal of Immunology* **2005**, *175*, 2366-2373.

(10) Krutzik, P. O.; Crane, J. M.; Clutter, M. R.; Nolan, G. P. *Nature Chemical Biology* **2008**, *4*, 132-142.

(11) Krutzik, P. O.; Clutter, M. R.; Nolan, G. P. *Journal of Immunology* **2005**, *175*, 2357-2365.

(12) Weaver, J. L.; Broud, D. D.; McKinnon, K.; Germolec, D. R. *Toxicology Mechanisms and Methods* **2002**, *12*, 95-118.

(13) Michelin, S.; Perez, M. D.; Dubner, D.; Gisone, P. *Neurotoxicology* **2004**, *25*, 387-398.

(14) Marshman, E.; Ottewell, P. D.; Potten, C. S.; Watson, A. J. M. *Journal of Pathology* **2001**, *195*, 285-292.

(15) Hur, S. C.; Tse, H. T. K.; Di Carlo, D. *Lab on a Chip* **2010**, *10*, 274-280.

(16) Ateya, D. A.; Erickson, J. S.; Howell, P. B., Jr.; Hilliard, L. R.; Golden, J. P.; Ligler, F. S. *Anal Bioanal Chem* **2008**, *391*, 1485-1498.

(17) Buhlmann, C.; Preckel, T.; Chan, S.; Luedke, G.; Valer, M. *J Biomol Tech* **2003**, *14*, 119-127.

(18) Dittrich, P. S.; Schwille, P. *Analytical Chemistry* **2003**, *75*, 5767-5774.

(19) Fu, A. Y.; Chou, H. P.; Spence, C.; Arnold, F. H.; Quake, S. R. *Anal Chem* **2002**, *74*, 2451-2457.

(20) Fu, A. Y.; Spence, C.; Scherer, A.; Arnold, F. H.; Quake, S. R. *Nat Biotechnol* **1999**, *17*, 1109-1111.

(21) Wolff, A.; Perch-Nielsen, I. R.; Larsen, U. D.; Friis, P.; Goranovic, G.; Poulsen, C. R.; Kutter, J. P.; Telleman, P. *Lab Chip* **2003**, *3*, 22-27.

(22) McClain, M. A.; Culbertson, C. T.; Jacobson, S. C.; Allbritton, N. L.; Sims, C. E.; Ramsey, J. M. *Anal Chem* **2003**, *75*, 5646-5655.

(23) Shapiro, H. M.; Perlmutter, N. G. *Cytometry Part B-Clinical Cytometry* **2008**, *74B*, S152-S164.

APPENDIX A:

LABVIEW SOFTWARE FOR DATA ANALYSIS

Programs were developed using LabVIEW to analyze raw data from PMT current outputs and extract important peak information for detected events. Data acquired using a 16-bit data acquisition card (NI PCI-5122) and a modified Ramsey group data acquisition program was imported to the program named Josh Mach VIII, and a screen capture of the program is shown in Figure A.1. This figure shows the peak extraction portion of the program where the top graph plots the raw PMT outputs from both channels, while the bottom two graphs plot single channel peak intensity histograms.

This program was developed in order to detect peaks from two individual channels above user defined or calculated threshold values. Threshold values were normally set at 5 times the signal to noise ratio. The program extracts a peak intensity and time stamp from each detected event. Histograms are plotted for each individual channel, and the timestamps for events are used to correlate signals in both channels to plot two-dimensional histograms. The LabVIEW program also can export both the single channel and dual channel histograms as spreadsheet files to facilitate further data analysis.

Standard operating parameters for this program were to run 30 second acquisitions with resulting data files having 2 channels of data. Since the standard data acquisition program saves every data point, and files were acquired at rates of 50 – 100 kHz, large data files resulted. Attempting to analyze data sets longer than 30 seconds

resulted in LabVIEW crashing and large data files had to be split up before analyzing with the Josh Mach VIII program.

The limitations in data acquisition and analysis with the PCI-6251 hardware and Josh Mach VIII software led to the acquisition of a 14-bit high-speed data acquisition card (NI PXI-5122). This use of 2 of these cards facilitated use for extended experimental acquisitions of data in up to four separate channels at acquisition rates up to 10 MHz per channel. A separate acquisition program was developed to use with these cards, and peak extraction was written into the acquisition program. Using this program, only when the PMT output rises above a defined threshold value is data saved, and subsequently analyzed to extract a peak intensity and area for every detected event. In this manner, this software could easily handle experimental acquisitions for many minutes.

A screen capture of the front panel from the program titled “Peak Capture” is shown in Figure A.2. The front panel shows the raw PMT data in the center graph and a two channel histogram on the right that are both updated in real-time. The left side of the front panel are settings for which channels to acquire data from, data acquisition rate (usually 1 MHz per channel), and threshold levels. This program allows for data to be saved, or thrown out at any time, and all data is saved to a spreadsheet file containing all important program settings and information about each individual event detected.

For certain applications, it is desirable to extract information about a specific subset of data acquired, known as gating. To do this analysis using LabVIEW, the program titled “Peak Analysis” was developed. A screen capture of the front panel of

this program is shown in Figure A.3. This program accepts spreadsheet files from the "Peak Capture" program as inputs, and displays the imported two channel histogram on the top left graph. The cursor is used to draw a box around a specific population of cells or events of interest, and then pressing the update sub-array button displays only the selected region in the top right graph. This action also extracts all of the peak data from only the selected region, and plots single channel histograms for peak intensity and peak area for each channel. The data from the selected region can then be saved along with corresponding gating information.

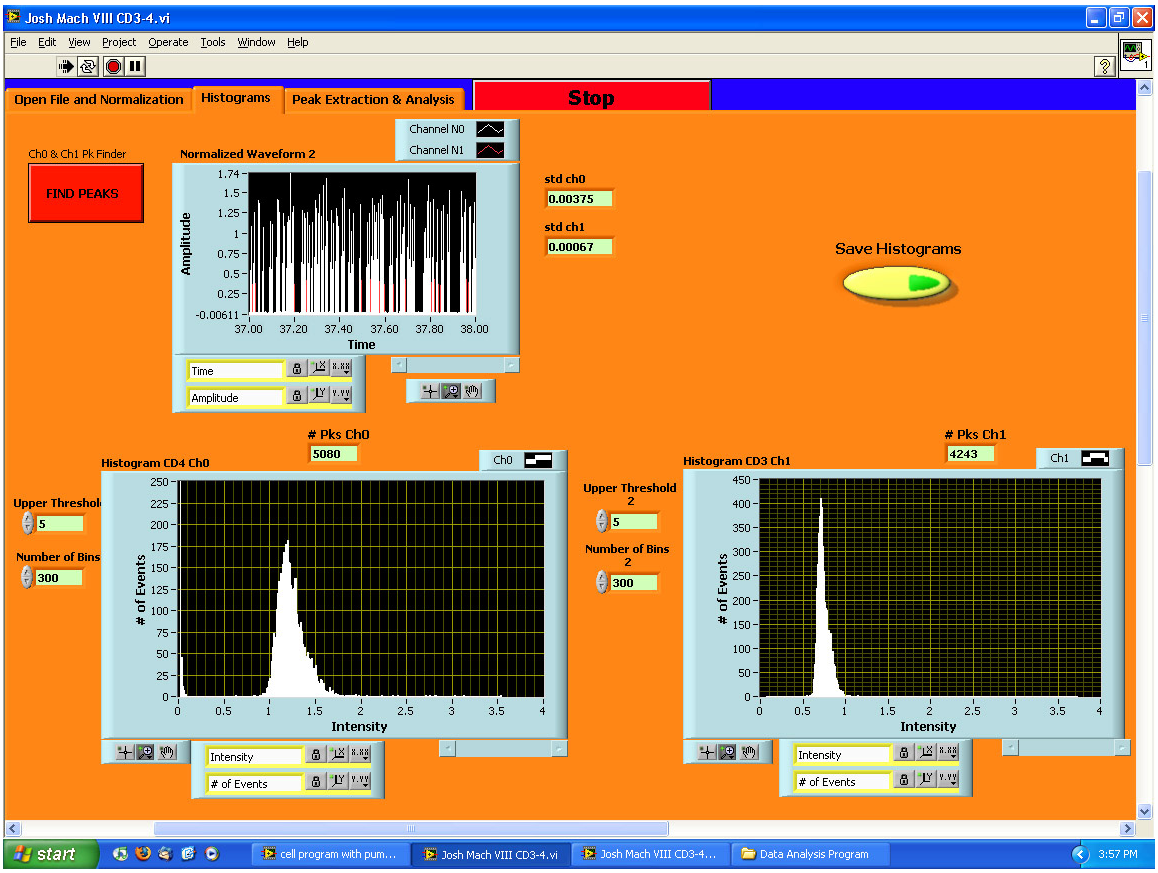

Figure A.1 Screen capture of the front panel of the "Josh Mach VIII" program developed for the analysis of raw data acquired using the PCI-6251 data acquisition card.

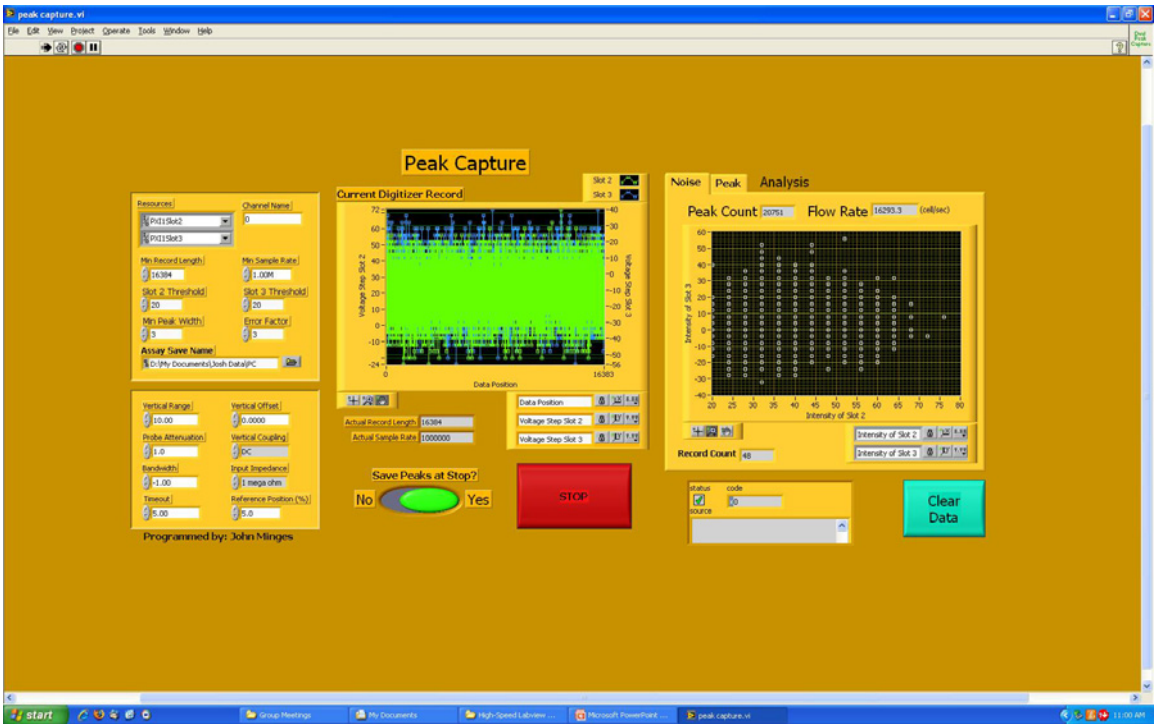

Figure A.2 Screen capture of the front panel of the "Peak Capture" program developed for use with the PXI-5122 high-speed data acquisition cards.

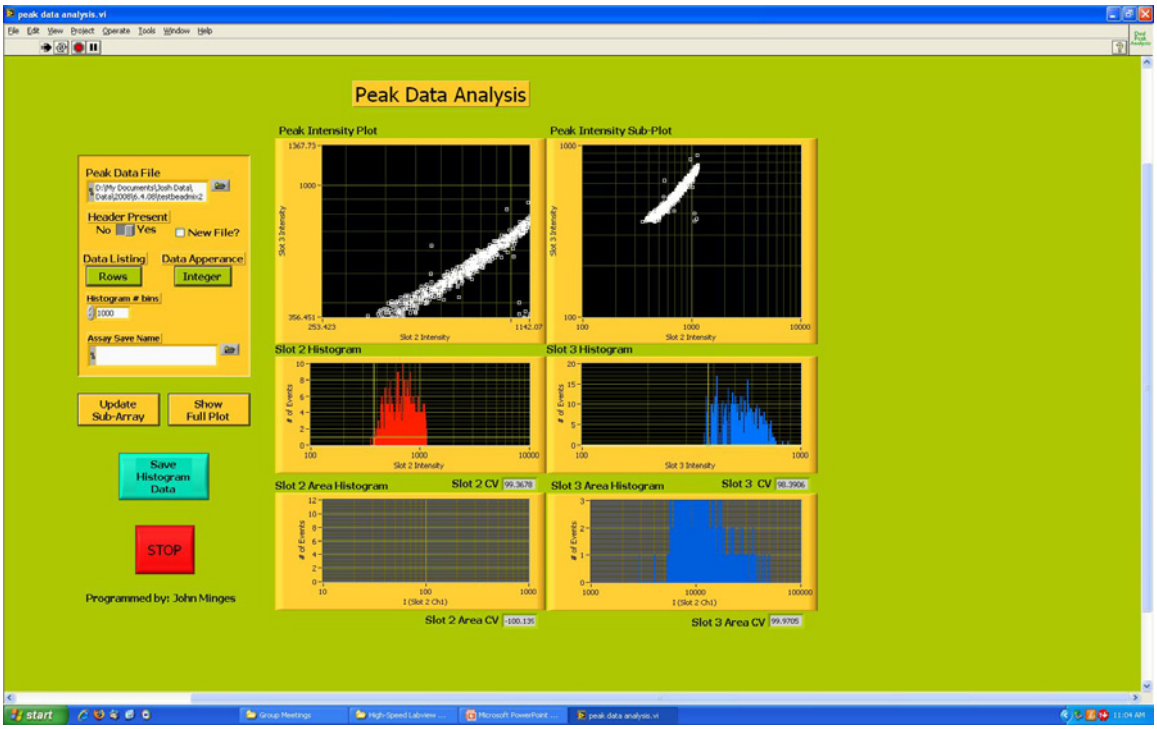

Figure A.3 Screen capture of the front panel of the "Peak Analysis" program developed for analyzing gated subsets of data acquired using the PXI-5122 high-speed data acquisition cards and the "Peak Capture" program.

APPENDIX B:

SIGNAL PROCESSING HARDWARE

Experiments requiring extended acquisition times at very high event rates have proven problematic for LabVIEW processing with current programs. Although efforts were made to optimize the programs discussed in Appendix A, it was determined that another strategy for the extraction of peak information may be preferable. With the assistance of the UNC Chemistry Electronics Facility, we developed and performed some initial tests on a hardware based peak detector and integrator. The idea for this circuit is based on cytometry electronics from years ago.

The circuit developed is meant to work with LabVIEW, but can significantly reduce the software processing requirements since all of the peak extraction will be done using hardware. The result is that only peak intensity and peak area values are sent to the software for each detected event. The circuit is designed to work as follows; first, the raw PMT output from a detector channel (normally forward scatter) is compared to a defined threshold. If the scatter signal is above the threshold, the peak detector and integrator circuits for each channel are initialized for a specific duration. At the end of this "detection window," a pulse is sent to the data acquisition card to alert the software to measure the peak intensities and areas from each card. After this "sampling window" a pulse is send to each peak detector and integrator to reset them in order to sample the next event.

A peak detecting and integrating circuit was developed and fabricated on a printed circuit board. Three of these boards were built; one for the forward scatter signal, and two for fluorescence channels. The circuit diagram for the peak detector and integrator is shown in Figure B.1. The top half of the circuit is the peak detector, consisting of a half-wave rectifier followed by an integrator. This circuit charges a capacitor to a charge proportional to the intensity of the detected peak for that channel. On the bottom of the circuit is the integrator, which charges another capacitor to a value proportional to the area of each detected peak. A photograph of the assembled circuit is shown in Figure B.2.

A digital control circuit was also assembled in order to control the timing of the signal processing. A schematic of the digital control circuit is shown in Figure B.3, and a photograph of this circuit is shown in Figure B.4. This circuit utilizes a series of monostables and flip-flops to control the peak sampling duration, and also controls the initialization of the individual peak detector and integrator circuits based on the threshold value input. Additionally, trigger pulses for software initialization and reset pulses are sent out from this circuit.

Photographs of the entire peak detector and integrator circuit are shown in Figures B.5 and B.6. Initial testing was done using the assembled circuit by analyzing fluorescently labeled polystyrene beads on-chip, and monitoring the output from the peak detector and integrator using an oscilloscope. A representative result from these tests is shown in Figure B.7. The top trace shows the input peak signal obtained from the detection of a single fluorescent microbead. The center trace shows the output signal from the peak detector circuit. The amplitude of this peak is a measure of the detected

bead peak intensity, and a trigger pulse will be sent to the ADC to initialize sampling of the value of this peak in the last 50 µs of the pulse. The bottom trace shows the output signal from the integrating circuit. Similarly, the amplitude of this peak is a measure of the detected bead peak area, and the same trigger pulse is sent to the ADC to initialize sampling of the value of this peak in the last 50 µs of the pulse. The peak detector and integrator signals simultaneously return to baseline after the ADC "sampling window" because each receive a reset pulse from the digital control circuit which discharges the capacitors in the circuits to prepare for the next event.

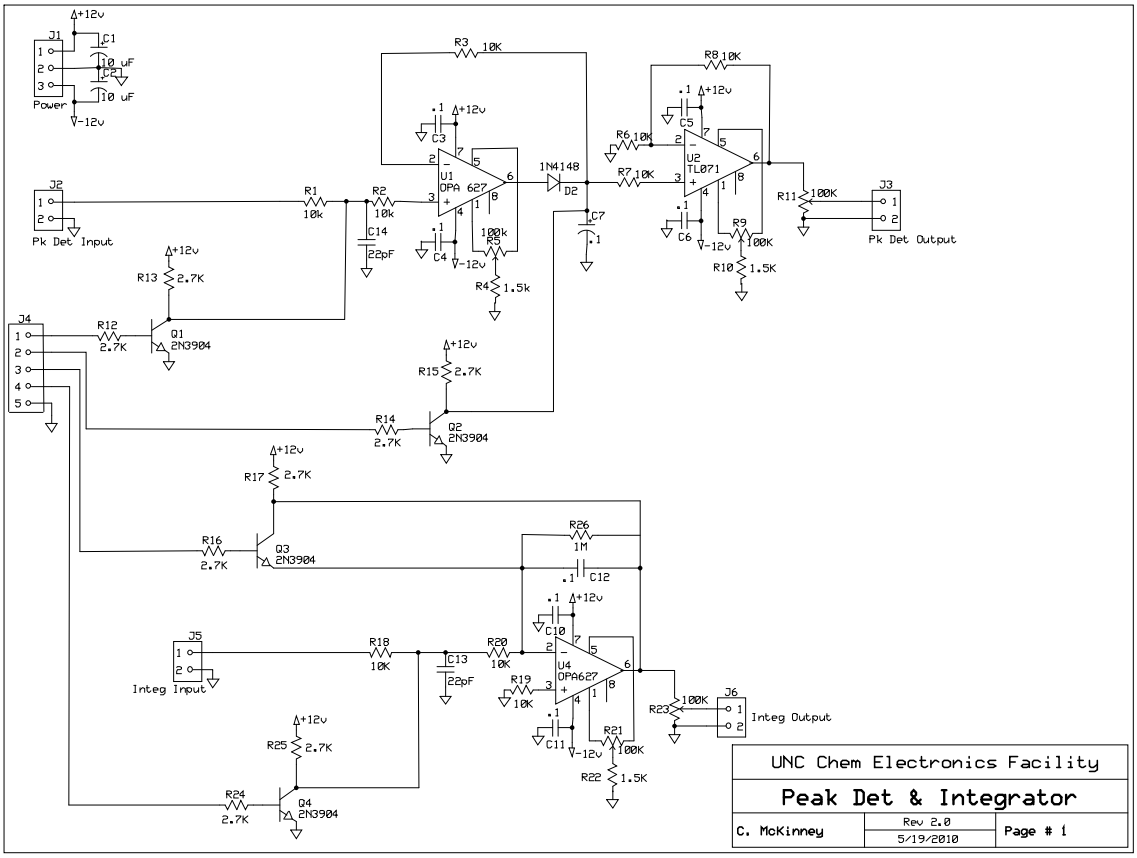

Figure B.1 Circuit diagram for the peak detector and integrator.

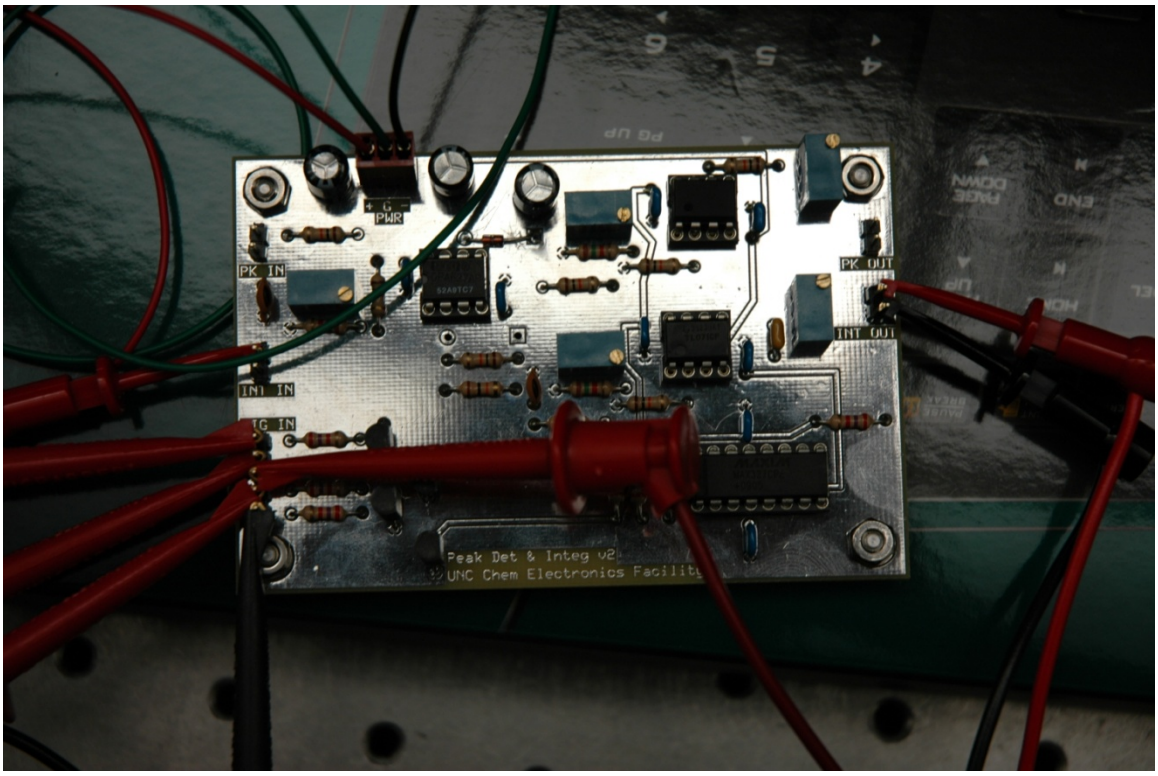

Figure B.2 Photograph of the peak detector and integrator circuit.

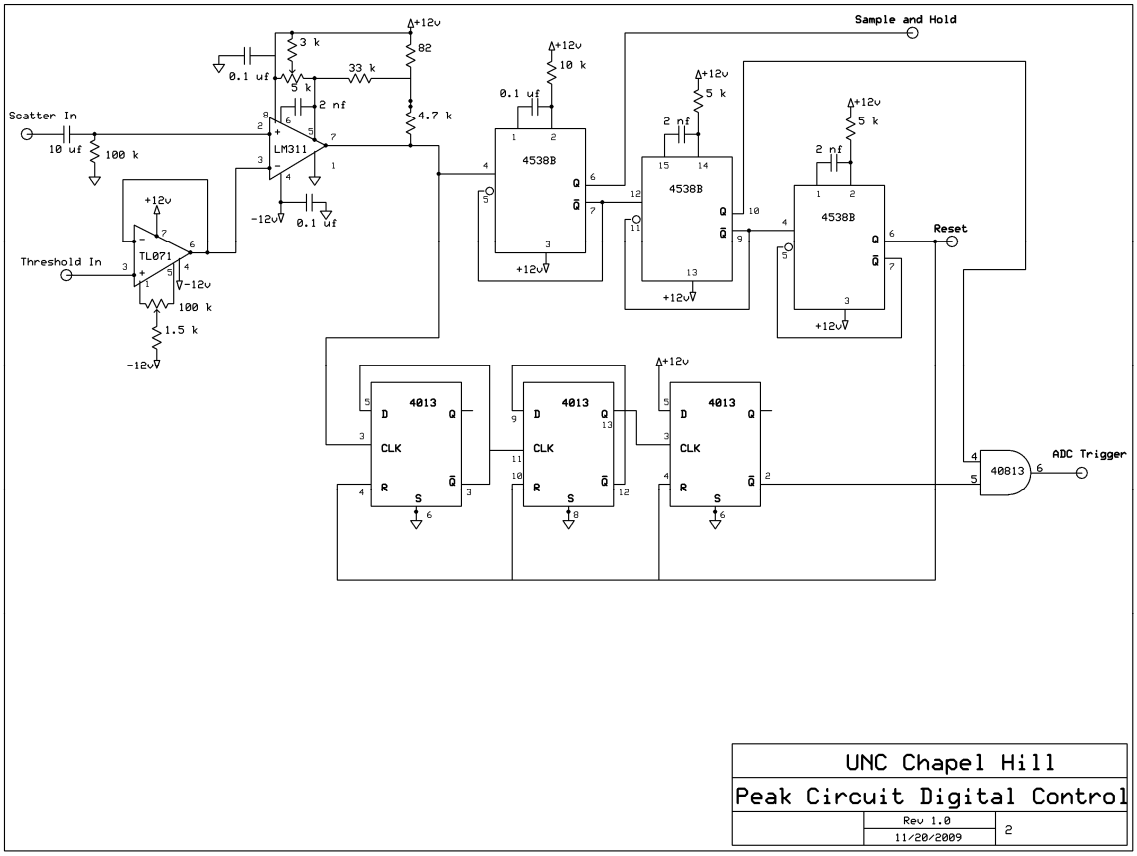

Figure B.3 Diagram for the digital circuit used to control timing of the peak detector and integrator.

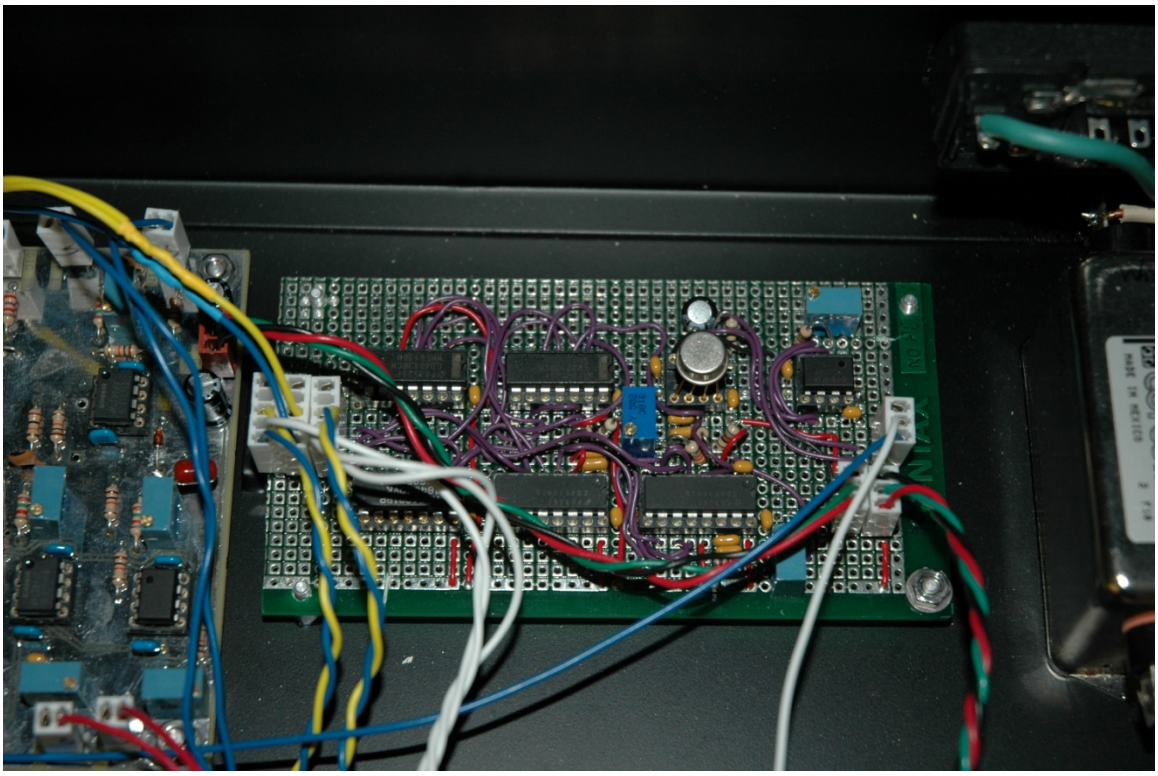

Figure B.4 Photograph of the installed digital control circuit.

Figure B.5 Photograph of the front panel of the assembled peak detector and integrator.

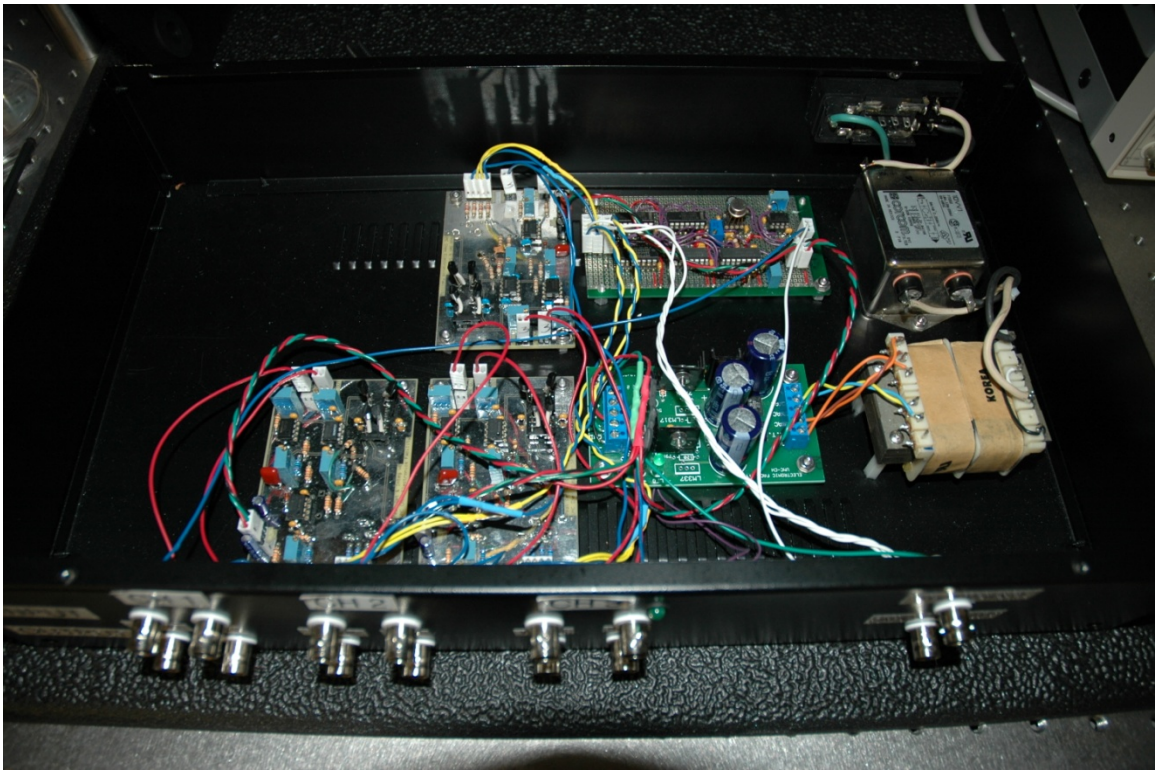

Figure B.6 Photograph of the interior of the assembled peak detector and integrator with all boards mounted and a power supply installed.

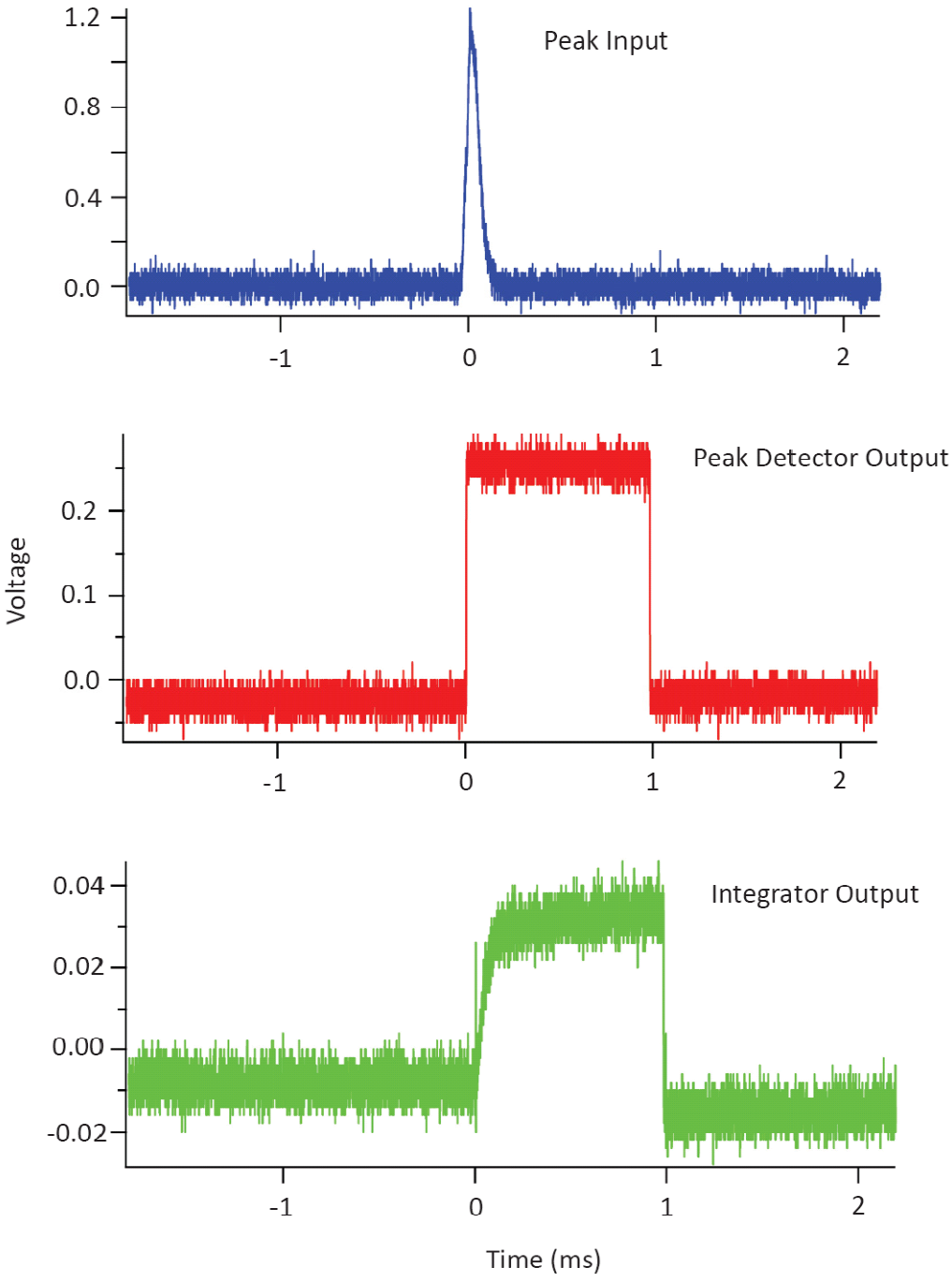

Figure B.7 Result from the initial testing of the peak detector and integrator circuits showing the detection of a single event in the top blue trace, and the peak detector and integrator output signals in the center red and bottom green traces, respectively.